CODEN:LUTEDX/(TEIE-5455)/1-117(2021)

Industrial Electrical Engineering and Automation

Dynamic Torque Modeling of a Wet Lamella Clutch Pack

Johan Appelros
Jacob Wallersköld

Division of Industrial Electrical Engineering and Automation
Faculty of Engineering, Lund University

Dynamic Torque Modeling of a Wet Lamella Clutch Pack

Johan Appelros
ine14jap@student.lu.se

Jacob Wallersköld
mas14jw1@student.lu.se

February 18, 2021

LUND
UNIVERSITY

This thesis is a Master's Thesis towards the degree of Master of Science in Mechanical Engineering, Faculty of Engineering, Lund University.

It was conducted at the Division of Industrial Electrical Engineering and Automation, Faculty of Engineering, Lund University in collaboration with BorgWarner Sweden AB.

Supervised by Fredrik Salbrink and Daniel Blom from BorgWarner Sweden AB.
Supervised by PhD-student Anton Karlsson from the Faculty of Engineering.
Examined by Assoc. Prof. Gunnar Lindstedt from the Faculty of Engineering.

The division of labor was evenly distributed between the two authors.

Division of Industrial Electrical Engineering and Automation.
Box 118, 221 00 Lund
Sweden
www.iea.lth.se

Abstract

Wet lamella clutches are used in the automotive industry to enable all-wheel drive and thereby increase acceleration, handling and safety of cars. The clutches work by transmitting torque from an incoming- to an outgoing shaft through a series of lamella - steel-disc friction surfaces (lamella pack), lubricated by an oil. Based on temperature- and wheel-speed measurements, a mathematical model of the clutch is used by the software to calculate the appropriate actuation of applied pressure to match a desired torque output.

The primary goal of the thesis was to identify the dynamic behavior of the clutch in order to increase torque accuracy in the torque estimation model. This was done by first analysing previously collected data from tests in rigs and cars and thereby form two hypotheses. Hypothesis 1 was related to spline friction losses within the lamella pack and Hypothesis 2 was related to oil film reduction and an increase in friction coefficient.

In an attempt to prove the hypotheses, rig tests were performed where dynamic torque responses were provoked. A novel measurement technique was introduced comprising of four thin force-measuring sensors being placed at the front and rear lamellas in the pack respectively in an attempt to measure variations of force. As some sensors were damaged during the tests it was not possible to get an absolute measurement of force, but by making relative comparisons as well as motivated assumptions, some indications related towards Hypothesis 1 could be observed.

Two versions of a mathematical model assuming each lamella to be affected by a spring force, a damping force and a spline friction force acting on its body were suggested. Both of these versions were shown to increase torque accuracy on tested data.

Keywords: wet lamella clutch, friction modeling, torque modeling, torque accuracy, force measurements, system identification, grey-box modeling

Sammanfattning

Våtlamellkopplingar används i fordonsindustrin för att möjliggöra fyrhjulsdrift och därmed ge ökad accelerationsförmåga, styrbarhetsförmåga och säkerhet i bilar. Kopplingarna fungerar genom att överföra moment från en ingående- till en utgående axel genom en uppsättning friktionsytor mellan lamell och stålskiva (lamellpaket), smörjt av en olja. Baserat på temperatur- och hjulhastighetsavläsningar används en matematisk modell på kopplingen av mjukvaran för att beräkna lämpligt aktuatortryck för att matcha begärt moment.

Det primära målet med denna uppsats är att identifiera dynamiska egenskaper i kopplingen för att förbättra momentnoggranheten i momentestimeringsmodellen. Detta gjordes genom att först analysera tidigare samlad data från tester i rigg och bil och därigenom formulera två hypoteser. Hypotes 1 var kopplad till spårfriktionsförluster inom lamellpaketet och Hypotes 2 var kopplad till oljefilmsreduktion och en ökning av friktionskoefficient.

I ett försök att bevisa dessa hypoteser utfördes riggtester där dynamiska momentsvar provocerades fram. En nymodig mätmetod introducerades bestående av fyra tunna kraftmätande sensorer som placerades på den främsta och bakersta lemellen i paketet i ett försök att mäta kraftvariationer. Då några sensorer skadades under testerna var det ej möjligt att ge en absolut kraftmätning, men genom relativa jämförelser och motiverade antaganden kunde indikationer mot Hypotes 1 observeras.

Två versioner av en matematisk modell som antar att varje lamell påverkas av en fjäderkraft, en dämpande kraft och en spårfriktionskraft föreslogs. Båda dessa versioner visades öka momentnoggrannheten på testdatan.

Nyckelord: våtlamellkoppling, friktionsmodellering, momentmodellering, momentnoggrannhet, kraftmätning, systemidentifiering, gråbox-modellering

Acknowledgements

Throughout the course of this project, we have received input and support from several people at BorgWarner and the Faculty of Engineering at Lund University. They have all made our work more fun and helped elevate the quality of this thesis.

First and foremost, we would like to direct our gratitude toward our supervisors at BorgWarner - Fredrik Salbrink and Daniel Blom. Fredrik, with his child-like curiosity and seemingly endless knowledge in automotive engineering has both challenged our ideas and helped directing our focus towards where it belonged. Daniel, being the team leader at Vehicle Dynamics and Simulations has been invaluable in finding the right connections within the company as well as making sure that the project stays on course with company goals.

We would also like to thank our supervisor at the Faculty of Engineering - Anton Karlsson. When stuck, his guidance ensured that progress could be maintained.

Furthermore, we would like to thank Johan Björnstedt, Getachew Darge and Jonas Engqvist at the Faculty of Engineering for their contributions. Johan, for his unmatched skills in electrical components and troubleshooting, Getachew for providing us with the AD820AN OP-amp and Jonas for helping us with the calibration tests.

We would also like to direct our gratitude towards some colleagues at BorgWarner, namely Pierre Pettersson, Ola Nicklasson and Ola Nockhammar. Pierre for his good company in the office, Ola Nicklasson for his passion and knowledge in cars and vehicle dynamics, and Ola Nockhammar for answering all of our difficult questions regarding modeling.

Last but not least we would like to thank our fellow Master's Thesis colleagues at BorgWarner; Edvin Malm and August Wahlberg. With their good company and many challenging discussions they elevated our time at the company immensely.

Once again, thank you all!

Contents

List of Figures

List of Tables

List of Acronyms

- **AT** - Automatic Transmission.
- **AWD** - All-Wheel Drive.
- **cDAQ** - Compact Data Acquisition Systems.
- **DAQ** - Data Acquisition Systems.
- **DBP** - Delta Before Pressure.
- **ECU** - Electronic Control Unit.
- **FF** - FlexiForce.
- **IC** - Integrated Circuit.
- **MISO** - Multiple Inputs - Single Output.
- **NVH** - Noise, Vibration and Harshness.
- **OP-amp** - Operational Amplifier.
- **PBD** - Pressure Before Delta.
- **PCB** - Printed Circuit Board.
- **RMSE** - Root Mean Square Error.
- **rpm** - Revolutions Per Minute.

List of Definitions

- **Base Omega** - The rotational speed of the incoming or outgoing shaft with the lowest speed. Also denoted ω_{base}.
- **Diff Omega** - (Rotational speed of the incoming shaft) - (Rotation Speed of the outgoing shaft). Also denoted ω_{diff}.
- **Effective (lamella) Radius** - Average of the inner lamella radius (R_i) and outer lamella radius (R_o) according to $\frac{R_i+R_o}{2}$. Also denoted R_e.
- **Lamella Pressure Difference** - (Total pressure on front lamella) - (Total pressure on rear lamella). Also denoted P_{diff}.
- **Torque Accuracy** - (Measured Torque) / (Reference Torque).
- **Torque Overshoot** - A Torque Accuracy above 1.1.
- **Torque Undershoot** - A Torque Accuracy lower than 0.9.

1 Background

1.1 BorgWarner and All Wheel Drive

BorgWarner is a multinational company which develops various kinds of automotive drive modules and power transfer devices. At their site in Landskrona a large part of their development is focused towards all-wheel drive (AWD) systems for combustion vehicles, amongst other products such as various drive modules towards electric and hybrid vehicles. With AWD, one can utilize the grip of every wheel by distributing the torque depending on traction. By doing this, the safety, acceleration and handling of the vehicle can be improved. A number of studies have shown the benefits to vehicle dynamics of all wheel drive systems compared to traditional two wheel drive systems, such as [3, 4, 5]. The AWD system is either engaged by switching on a manual setting from the driver, or automatically when the system detects the need to engage AWD to improve the vehicle's performance on criteria such as mentioned above.

In traditional all wheel drive systems, a viscous coupling is commonly installed on the propeller shaft in order to transmit torque while still allowing some difference in rotational speeds between front and rear axle. The function of a viscous coupling has been subjected to extensive research for quite some time [6]. One drawback with a viscous coupling is that it is not controllable during operation and therefore does not work well with electronic driving aid systems such as electronic stability programs and traction control systems [1].

Instead, the AWD systems developed by BorgWarner comprise of a clutch which controls torque distribution between the front and rear axle as well as one differential for each axle which governs left/right torque distribution. The clutch can therefore be considered an "intelligent" differential which is controlled electronically. When taken into consideration whether the primarily driven axle is the front or rear axle as well as the placement of the clutch, the engine and the gearbox, several different drivetrain configurations are possible. The purpose of the clutch in these applications, however, is always the same; to control torque distribution between front and rear. In BorgWarner's products, this is done using an open control loop. As it is more common that the AWD-vehicles are primarily front-wheel driven (called hang-on to rear), this configuration is used in all examples in this report. Some AWD configurations used by BorgWarner can be seen in Figure 1.

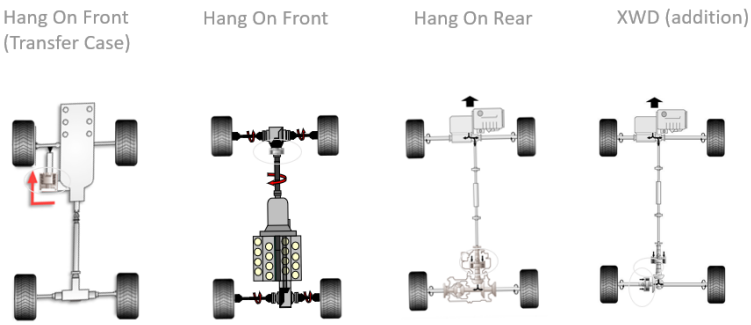

Figure 1: AWD configurations used by BorgWarner.

1.2 Problem Formulation

Assuming hang-on to rear, the torque distribution between the front and rear axle is requested by demanding a certain torque at the rear axle. As a measurement of how well this request is matched by the clutch, a number called the Torque Accuracy = (Measured Torque) / (Reference Torque), is considered. It then follows that a Torque Accuracy of 1 means perfect reference following. Within this thesis, a Torque Accuracy of $0.9 \leq$ Torque Accuracy ≤ 1.1 was considered good and within the accepted range. This is equivalent to the outputted torque being within $\pm 10\%$ of the requested torque. This boundary was set in collaboration with BorgWarner.

A Torque Accuracy of less than 0.9 was in this thesis considered a Torque Undershoot and a Torque Accuracy above 1.1 was considered a Torque Overshoot. Although both Torque Overshoot and Torque Undershoot happen to occur, the consequences related to Torque Overshoot are greater as it runs the risk of leading to the exceeding of dimensioned forces of components in the rear half of the drivetrain (behind the clutch). The front half is typically dimensioned for higher loads as the front axle is sometimes used as the only driven axle and Torque Undershoot is thus not as problematic.

BorgWarner have identified some "extreme" driving conditions (which will be discussed later in the report) where it is desired to increase the Torque Accuracy. These are often highly dynamic cases with a high relative rotational speed of the wheels and dynamic changes in input variables to the model. This sometimes leads to transient torque outputs which are difficult to stabilize. This sort of behavior in the Torque Accuracy has also been able to be provoked in isolated rig tests.

1.3 Thesis Purpose

The purpose of this thesis is therefore to gain an increased understanding of the physical properties of the clutch and how these are related to the dynamic torque responses. As the problems related to Torque Overshoot are greater than Torque Undershoot, these issues were mainly considered. The following goals were defined, in a decreasing degree of priority:

1. The first goal was to identify the dynamic behavior of the lamella pack and its correlation towards the torque output of the clutch. This was the primary goal of the thesis as it would lead to a greater understanding of the product at a mechanical degree.
2. The second goal was to propose a model which based on physical characteristics describes the found dynamics of the clutch. This was considered a desired but not critical goal since modeling is a work process which takes time to tune and incorporate in the product software in a desirable manner.
3. The third goal was to implement the model in the control algorithm and validate it in car and rig. This was the final goal which was considered very ambitious and unlikely to be realized due to the time constraints of the project.

1.4 Methodology

The project was conducted by first studying some literature related to the topics at hand. This, in order to develop an understanding of the theory related to the working principles of wet lamella clutches, what factors affect the torque output and possible modeling techniques.

Then, some internal material at BorgWarner was studied, such as collected clutch data and previously conducted tests. This was done to further the understanding of wet lamella clutches, hypothesis formulation and as inspiration toward formulation of test plan.

After that, testing was performed and data was collected. This was then analyzed with the goal of finding indications toward physical characteristics related to dynamic behavior of the clutch.

Lastly, system identification and modeling techniques were applied to propose a model related to found dynamics. This was validated based on collected data.

Throughout the thesis project, all researched, collected and developed data, theories and models were critically reviewed, partly with the help of supervisors and colleagues at BorgWarner.

2 Theory

2.1 Wet Lamella Clutches

As described above, lamella clutches are mechanical devices which are used to transfer a desired amount of torque from an incoming to an outgoing shaft. A wet clutch is a clutch working under lubricated conditions and the lubricating transmission fluid used is commonly simply referred to as the oil. By using a wet clutch, the control of torque transfer, cooling rate as well as clutch durability can be improved [1].

The clutch used by BorgWarner in Landskrona utilize multiple lamella discs connected by inner splines to the incoming shaft, while separating steel discs are connected by outer splines to the outgoing shaft. The clutch is engaged by applying a normal force from the hydraulic piston pump seen in Figure 2 to this "pack" of alternating sinter and steel discs. By doing so, the discs are pressed together and torque can be transferred by the friction in this interface.

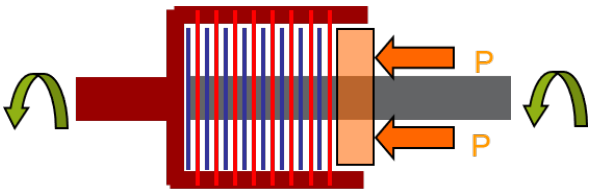

Figure 2: Generic clutch schematics.

Wet clutches can be used in various applications where a controllable amount of torque output is desired. These applications include automatic transmissions, wet brakes, lock-up clutches, launch control clutches and limited slip differentials to mention some [1, 7]. Most commonly, wet clutches operate during very short times of engagement. Such is the case in automatic transmissions, where wet clutches are used to couple the relative speeds of two rotating shafts during small periods of time (usually fractions of a second). In the case of AWD clutches, however, the wet clutches are operating under a small/limited amount of slip over a longer period of time without reaching a locked state. During this kind of applications, much heat can be generated [7]. See Figure 3 for an exploded view of the BorgWarner clutch.

See Figure 4 for a sectioned view of the BorgWarner clutch including arrows indicating the oil flow. Note that there are two separate oil systems in the clutch:

1. The red arrows show where the pump controls the actuating oil pressure which applies a normal force which compresses the lamella pack.
2. The green arrows show where the oil flows between the discs in the lamella pack. This serves the purpose of producing a thin oil film and cooling the discs which helps keeping the friction coefficient well-defined. This is discussed in detail in Section 2.1.1.

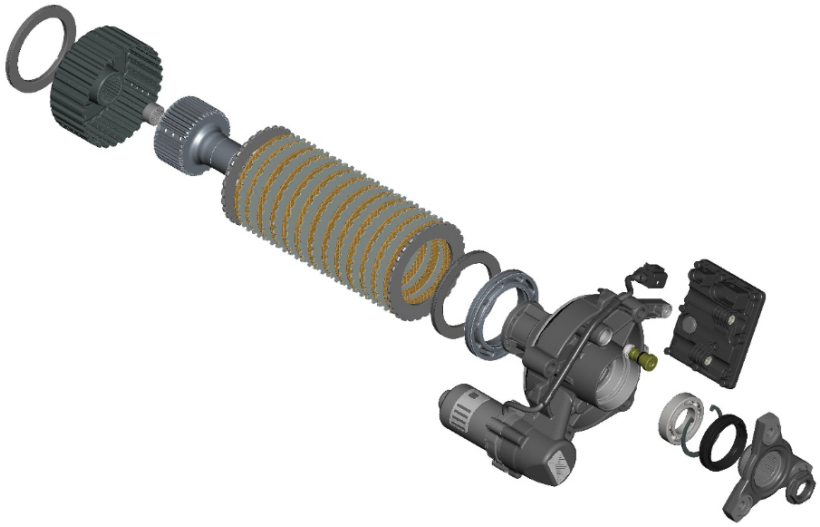

Figure 3: Exploded view of the BorgWarner clutch.

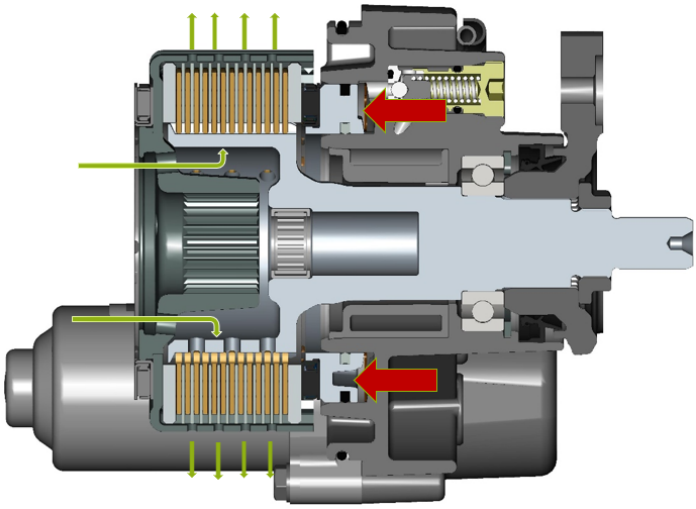

Figure 4: Sectioned view and oil flow.

In steady state, the clutch can be thought of to be operating in one of three states:

1. **Disengaged/open** - When there is no actuating pressure applied, only a small (usually negligible) amount of torque is transferred due to drag in viscous effects through the oil [1].
2. **Slipping** - When the actuating pressure is high enough for the secondary shaft to transmit some but not all of the incoming power (i.e. speed and torque). When an actuating pressure is applied (but not enough for the shafts to lock together), the shafts are rotating with a difference in speed (Diff Omega = ω_{diff}). The clutch is then said to be operating in a slipping state.
3. **Fully engaged/locked** - When the actuating pressure is high enough for the incoming and outgoing shafts to lock together, their speeds match. The incoming and outgoing shaft will behave as if they were one shaft where torque can get transferred "freely".

By having an accurate model of the friction in each of the surface interfaces between the lamella and steel discs, one can apply the appropriate piston pressure to output a desired amount of torque on the rear axle. As will be discussed later in the report, the current clutch model assumes a time-invariant uniform normal force on every lamella in the pack. Given a known force, the problem of modeling torque is then equivalent to the problem of modeling friction.

2.1.1 Friction of Wet Lamella Clutches

In a lot of other applications such as bearings, the reduction of friction is desired, whereas in the case of wet lamella clutches, a high and well-defined friction is of interest [1]. In wet lamella clutches, friction is not a side-product, but rather the means by which it achieves its purpose. There are several factors that can be investigated to have an affect on friction, most notable are the following:

1. **Lamella material** - The material of the lamellas has been found to have a significant affect on friction. The largest type of friction materials used for wet clutches are organic materials which comprise of paper-based materials such as cotton linters or cellulose fibers [7]. As a result, almost all research which has been done on clutches have been conducted on paper-based friction materials. At BorgWarner in Landskrona, however, the lamellas are made using sintered brass based friction material between the separating steel discs, with the main advantage of having a higher stress and temperature capabilities [1]. However, they still use organic lamellas in research for comparison purposes and to further their product understanding. The brass based sintered lamellas can be seen in Figure 5.

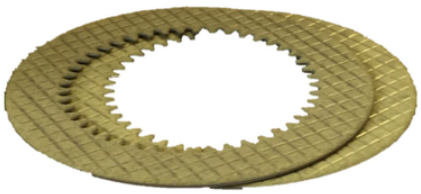

Figure 5: Brass based sintered lamellas used by BorgWarner in Landskrona.

2. **Permeability** - The permeability of the lamellas is the ability for lubricating oil to flow inside the friction material. It has been found that the friction can be influenced by the permeability of the material. The permeability can also affect the engagement time of the clutch [7].
3. **Lamella Groove pattern** - The "waffle-like" groove pattern can be seen in Figure 5. Its purpose is to quickly lead the oil towards and from the surface during engagement/disengagement and thus reducing the time of engagement. Its purpose is also to ensure an even distribution of oil throughout the entire surface as well as cooling of the plates. [7].

4. **Oil viscosity** - This has been found not to have a significant influence on friction [1]. It may have other effects such as flow rate and thereby lubrication of lamellas, lamella cooling rate and damping properties of a lamella pack. These effects can also be expected to be temperature dependent since it has been shown that the oil viscosity decreases with temperature [8].
5. **Oil additives** - Various kinds of additives are commonly known to be mixed with the base oil to improve oil characteristics such as friction, viscosity, anti-wear properties, rust prevention, anti-foaming and more. These have been found to have a significant influence on friction [7]. The rate of change in friction can be altered by using different additive combinations, which can be seen in Figure 6 shown by [1].

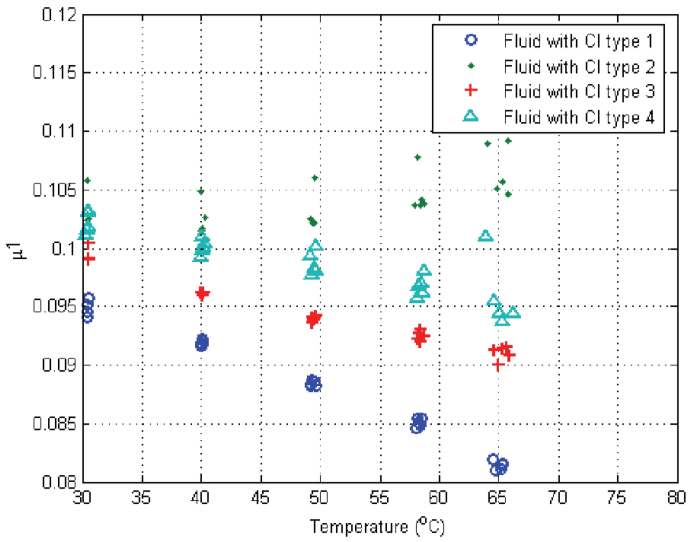

Figure 6: Friction with respect to temperature and oil additives as shown by [1].

6. **Temperature** - The lamella temperature has a significant influence on friction. An increase in temperature leads to an increase in the formation of so-called tribolayers in the oil, which are surface active layers where the oil additives are more prevalent. As a result, temperature rise tends to lead to a decrease in friction. It was shown by [1] that generally, a linearly decreasing friction with respect to temperature is a good estimation, as can be seen in Figure 7. However, it was also shown by [1] that this is not always the case, since oil additives and Diff Omega may alter the temperature dependency, see Figure 6 and 8.

   A higher oil temperature also results in a lower oil viscosity. The main rise in temperature of the oil occurs near the friction surface, due the oil film generally being very thin. Subsequently, at least within the scope of this thesis, the temperature of the oil at the friction surface is considered to equal that of the lamella. In contrast, due to its comparatively large volume, the oil sump temperature has a much slower dynamic. The lamella temperature is mainly governed by the power input through the clutch (ω_{diff} and transmitted torque) as well as heat dissipation, mainly through the oil. The temperature of the oil and lamellas are also a function of the heat transfer from adjacent systems in the vehicle (or

equivalent operating application). The temperature of the lamella can either be found experimentally or through modeling such as suggested by [9].

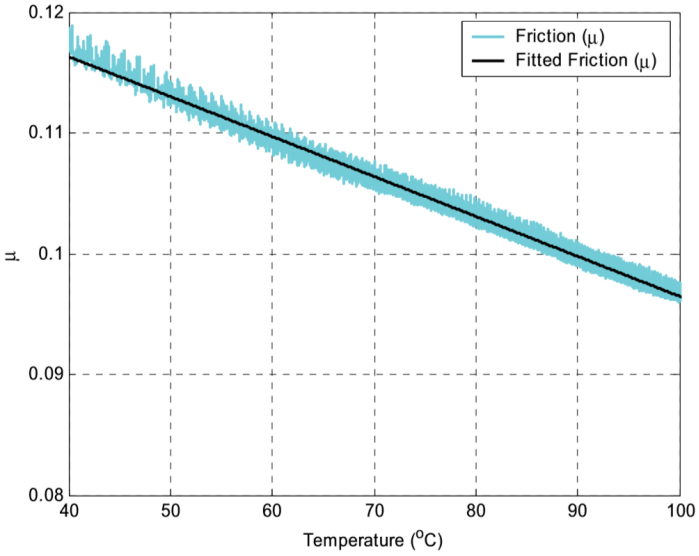

Figure 7: Friction with respect to temperature as shown by [1].

7. **Base Omega** - Base Omega, or ω_{base} (≥ 0), is here defined as the rotational speed of the incoming or outgoing shaft with the lowest speed. The speed of the other shaft thus becomes $\omega_{base} + |\omega_{diff}|$. Although the relative speed between the plates, i.e. ω_{diff} (see below), is the only speed which is experienced by the interface, ω_{base} also has an influence on the friction of the system due to its correlation to oil flow. This is because the oil is inserted into the pack from the inner drum spline (connected to the incoming shaft), forced radially outward through the surface interfaces by centrifugal force, and finally exited through holes in the outer drum splines (connected to the outgoing shaft). See figure 3 and 4. Therefore, oil flow and subsequent friction coefficient is dependent on a rotational speed of both the incoming and outgoing shaft. The lowest of these speeds is the more limiting factor, and this is described by ω_{base}.
8. **Diff Omega** - Diff Omega, or ω_{diff}, is the rotational speed of the incoming shaft minus the rotational speed of the outgoing shaft of the clutch. As the lamella pack is rotationally symmetric with itself and itself transposed, it is (at least within the scope of this thesis) assumed that the friction is independent on direction of rotation. ω_{diff} has a significant influence on friction. However, there is no general answer as to how the friction will depend on ω_{diff} since this relationship will vary depending on fluid formulation, lamella material and temperature [1]. Generally, it is desired to have a mechanical design which makes the friction increase with respect to ω_{diff} since this will reduce the risk of a phenomenon in the clutch called stick-slip which in turn may cause NVH (Noise, Vibration, Harshness), which is a collected description of irregular movements in the clutch and/or drivetrain which may cause excessive wear of components as well as a rough driving experience [10].

It also needs to be addressed that no Diff Omega (equivalent to no relative speed between the clutch shafts, i.e. locked clutch) leads to a static coefficient of friction, which is higher than the kinetic one, both in dry and lubricated conditions (where lubricated friction is generally lower than the dry one) [11]. This can be explained by the fact that the surface grooves dig deeper into each other. The exact correlation in wet clutch applications is difficult to predict due to oil film interaction, but one theory[1] is that no Diff Omega leads to no oil lubrication from the lamella grooves to the friction surface interface, which results in a higher friction coefficient. More on friction modeling related to Diff Omega is discussed in Section 2.2.3. Some examples of how Diff Omega may affect friction can be seen in Figure 8 as shown by [1].

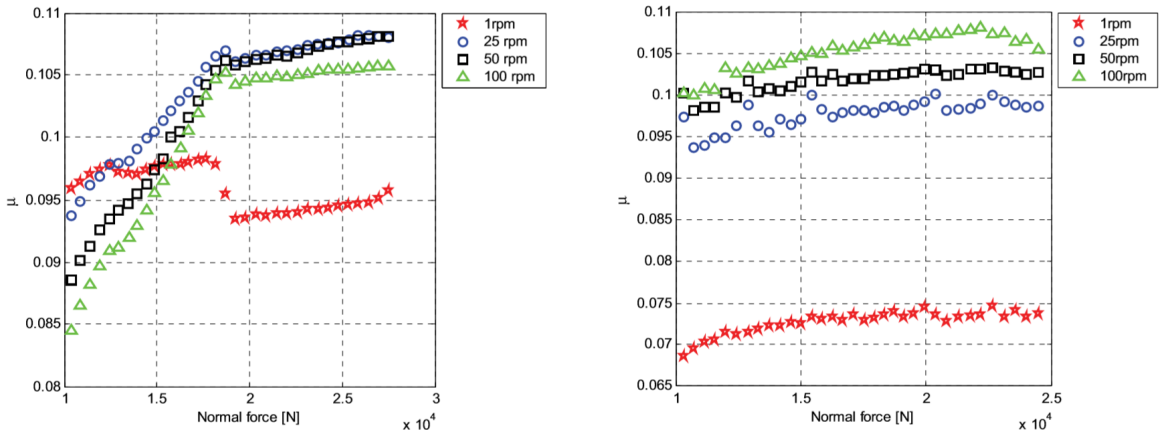

(a) 20°C (b) 50°C

Figure 8: Friction vs ω_{diff}, force and temperature as shown by [1].

9. **Normal Force** - In general, the normal force influence on friction coefficient is quite moderate (typically positive/increasing correlation, but not more than 5%) [1]. In turn, this means that the output torque is relatively linear with respect to normal force (according to Equation 1, which is desirable [12]. At low temperatures and low loads, however, the friction may become dependent on normal load, as suggested by [1], see Figure 8.
10. **Lamella wear** - As the clutch is utilized, the lamellas surfaces are worn down and friction tends to decrease.
11. **Lamella radius and surface area** - As the lamella surface area increases, the maximum amount of transferable torque increases in a linear fashion. The average of the inner and outer lamella radii is called the effective radius, $R_e = \frac{R_i+R_o}{2}$. The effective radius can be used to describe the total outputted torque according to equation 1.
12. **Number of lamellas** - Some clutches only use a single lamella, but due to the high amounts of torque being transfered in the AWD applications (as described in Section 1.1), BorgWarner use several lamellas (multi-plate clutch). As the number of lamellas (denoted N) increase, the total available friction surface in-

[1]According to BorgWarner internal material

creases in a linear fashion (assuming same/constant lamella areas) with the factor 2. Again, assuming a time-invariant uniform normal force on every lamella, the total torque output therefore also increases linearly with an increased number of lamellas, according to equation 1.

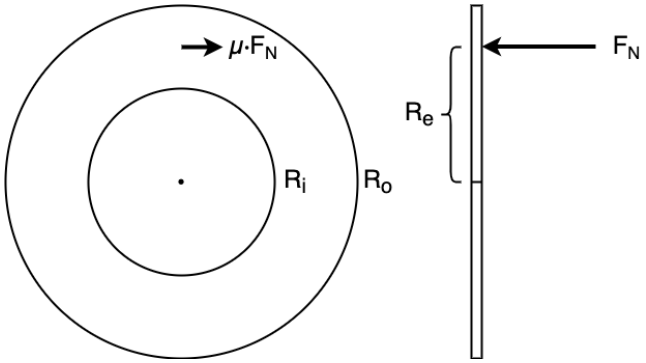

Figure 9: Normal force, lamella radii and friction coefficient.

It is clear that there are several factors which affect friction. Several of these are also interacting with each other and must therefore be studied simultaneously for a complete understanding [13]. On top of this, tribology is a complicated field since it consists of several other sciences such as solid mechanics, contact mechanics, fluid mechanics, thermodynamics, chemistry, material sciences and physics. This makes tribological simulations very complicated and the tribological contact difficult to model. These tribology investigations therefore often involve more testing and less modeling [7]. This also makes the design harder in terms of Torque Accuracy.

A common model of a wet lamella clutch (currently used by BorgWarner) is to assume a time-invariant uniform normal force on each lamella, where the total outputted torque can be described according to Equation 1, where R_e is the effective radius, is the friction coefficient, F_N is the normal force and N is the number of lamellas. The 2 in the equation comes from each lamella having two friction surfaces.

$$T_{out} = 2 \cdot R_e \cdot \mu \cdot F_N \cdot N \tag{1}$$

Any factor affecting torque can then be accounted for by adjusting the assumed friction coefficient and/or normal force.

As mentioned, the first and foremost goal of this thesis was to investigate dynamic properties of a wet lamella pack and its correlation to torque output. Within the scope of the thesis, however, all hardware oriented factors were considered fix in terms of freedom in design. The only variable to be altered was actuation of the Clamp Force through the software.

2.1.2 Dynamic Properties of a Lamella Pack

The dynamic properties of a lamella pack is considered the main properties that can influence the axial movement of lamellas inside a clutch.

- **Axial Lamella Spring Constant** - BorgWarner internal measurements of spring constants of lamella packages indicates an increased spring constant for increased actuating forces. This is believed[2] to be a result of not perfectly flat lamellas. Thus the spring constant is also stabilized for high actuating pressures when the irregularities are flattened out.
- **Axial Lamella Damping Coefficient** - The axial damping coefficient of a lamella pack is believed [3] to mainly be a function of viscous effects. When a lamella pack is compressed, the oil in between the lamellas and the steel plates will be forced aside as the actuating pressure increases. Since the clutch house is not pressurized and the spline drum is constructed with several flow venting holes, the oil flow has little resistance when being pushed aside and thus the damping effects are believed to be low.

2.2 Modeling

Models are used within several fields and areas and thus have many interpretations. People create mental models to learn how to drive a car or a bike, artists uses physical models to test aesthetic properties and economists use models in an attempt to predict market trends. In general, models serve as a tool to give answers to questions of a system without performing experiments. The actual word originates from latin and means mold or pattern. In other words one could say that a model is intended to serve as an imitation and follow the laws of something. The focus in this thesis will be yet another type of model: mathematical models. Mathematical models describes relations of quantities [14]. For example the relation between force, mass and acceleration described by Newtons second law of motion [15] or the relation between resistance, voltage and current described by Ohms law [16]. One can thus imagine how mathematical models are certainly useful within engineering to describe physical behavior of systems or as in this case: the torque behavior of a clutch.

Before immersing into technicalities, a famous quote in the realm of modeling which is good to keep in mind is that of George Box, which goes: "All models are wrong, but some are useful" [17]. This certainly applies in this case.

2.2.1 Modeling Techniques

According to Ljung [18], there are two basic principles of modeling:

- **Physical modeling** - By using the physical laws of nature, the quantities of a system or subsystem can be described with mathematical equations. This

[2]According to BorgWarner internal material
[3]According to BorgWarner internal material

requires that the physical laws of the system are known and mathematically describable.

- **Identification** - With identification methods, observations of the system can be used to fit the model properties. Identification can either be done as a complement of Physical modeling (grey box modeling), or without any prior knowledge of the physic laws (black box modeling).

The difficulties within modeling is not building them, it is to make them accurate and reliable. Thus all models should be verified or validated. A suggested method according to Ljung is residual analysis [18]. A residual is mathematically defined according to Equation 2, where ϵ is the residual, y is the system output and $\widehat{y}(t)$ is the estimated output by the model.

$$\epsilon(t) = y(t) - \widehat{y}(t) \tag{2}$$

The residuals can be used for several validation purposes. The first to be considered is Root Mean Square Error (RMSE in short). In this context, the error equals the residuals. A small RMSE-value indicates a high correlation between the model and the actual system. Thus, by minimizing the RMSE, the model can be optimized towards the system. Another useful analysis of the residuals is its correlation to the input. The residuals are ideally independent from the input. If not, it is likely that there are dynamics not fully covered by the model. This can be validated through a cross correlation analysis. To test the cross correlation between an input and the residuals R, Equation 3 will be used, where N is number of samples, τ is the sliding window constant and u is the input to the system.

$$R = \frac{1}{N}\sum_{t=1}^{N} \epsilon(t+\tau)u(t) \tag{3}$$

For a large amount of samples (i.e. a large N), Equation 3 should be normally distributed with mean zero for low cross correlation [18].

It is also important to understand the fundamental limitations and the domain of validity of different models. For example, the acceleration of a body receiving a force can be computed using Newton's laws of motion [15]. For a lamella in a clutch, these laws of motion would be valid but for bodies with velocities close to the speed of light they would not [14]. Determining the domain of validity is also a question of computing power. For instance, one needs to consider whether the model computations are to be made in real-time by a microprocessor. If this is the case, the computation time will limit the possible sampling rate and therefore the calculation accuracy. Choosing a high level domain of validity may therefore be beneficial for fast sampling systems.

2.2.2 BorgWarner Torque Model

The following section briefly describes the principles of the current friction model used by BorgWarner. Due to confidentiality, not all details of the model will be presented. However, in order to identify what dynamics that currently are not covered by BorgWarner's friction model, a brief explanation is still considered necessary.

First of all, the control fundamentals of the clutch (or mathematically speaking: system) will be explained briefly. This will hopefully give an insight to why a model based control system is used in the BorgWarner clutch when there are numerous of ways to control a system in general. The BorgWarner clutch is controlled electronically using an electronic control unit (ECU in short). A simple pseudo description of the system in action would be: the ECU gathers information of the vehicle states through sensors, processes the information of the states and orders the pump to apply an actuating pressure on the lamellas which will initiate a torque transfer from the incoming to the outgoing driveshaft. Figure 10 illustrates the flow of input and outputs of this system.

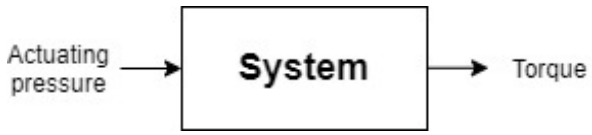

Figure 10: Block diagram of input and output of the system with no control.

So far no control takes place at system level. An actuating pressure is applied which results in a torque output. In a vehicle however, it is not of interest to simply apply a torque, but instead to apply a certain amount of torque. Skogestad defines the objective of a control system to make the output behave in a desired way by manipulating the input. Further, he defines the servo problem as to manipulate the input to keep the output close to a reference signal. As "close to" is a rather vague term it might instead better be defined mathematically as: minimising the control error $e = r - y$, where r is the reference signal and y is the output of the system [19]. Computing the control error e is consequently a function of the reference signal and the output signal. In terms of a BorgWarner clutch the reference signal is computed at vehicle level and fed to the clutch ECU as a torque request while the output signal in this case is the torque output. It is by now obvious that the torque must be measured somehow in order to compute the control error. However, as of now, no measurements of torque takes place in BorgWarner's clutch systems (except sometimes in testing and validation purposes). Why is not a question to be answered in this thesis but general implications of added sensors could be increased costs, increased hardware complexity and added control complexity due to dynamics from the sensor itself. So instead of measuring the torque, a model that estimates the torque output is used as a basis to regulate the actuating pressure. Therefore, an accurate model is of great importance in order to control the torque transfer to the rear axle, and ultimately the AWD performance.

The current friction model is considered a Multiple Input Single Output-system (MISO) with three inputs and one output. The input variables are actuating pressure, lamella temperature and Diff Omega and the output is the computed friction coefficient, see

Figure 11. Even though the lamella pack consists of multiple lamellas which in theory could experience different temperatures and contact forces, the model assumes a one unit, time invariant pack of lamellas, as described by Figure 9 and Equation 1. Thus, eventual losses along the pack are modelled to scale the average normal force of the entire pack, not for each lamella individually. This is the denoted F_N in Equation 1. The same applies for the friction coefficient μ that represents the average friction coefficient in the entire lamella pack.

Figure 11: BorgWarner MISO friction model.

The inputs to the model are both measured and estimated values.

- No measurement of pump pressure takes place in the clutch. Instead the actuating pressure is estimated based on pump dynamics.
- The temperature measurement takes place in the pump ECU rather than the actual lamella. However, since the oil is actively being circulated around the housing and into the lamellas, an accurate estimation can be done with knowledge of ambient temperature and surrounding energy sources.
- ω_{diff} is measured with wheel speed sensors and computed according to Equation 4, where ω_{FR} is the speed of the front right wheel, ω_{FL} is the speed of the front left wheel, ω_{RR} is the speed of the rear right wheel and ω_{RL} is the speed of the rear left wheel.

$$\omega_{diff} = \omega_{front} - \omega_{rear} = \frac{\omega_{FR} + \omega_{FL}}{2} - \frac{\omega_{RR} + \omega_{RL}}{2} \tag{4}$$

As highlighted in Section 2.1.1, the friction coefficient of a lamella depends on several factors. Multiple tests have been done with single lamellas to measure the correlation between friction and these variables. For example, the correlation between friction and-actuating pressure, temperature and ω_{diff} are all well mapped. With this knowledge as a basis, BorgWarner have been able to extract accurate steady state models for different types of lamella packages; i.e. a form of grey box modeling where physical knowledge was used as a model structure and thereafter optimized for individual clutch models. Once a friction coefficient is estimated, the torque can be computed according to Equation 1.

What is presented above is what can be considered the main torque-model. However, on top of this model, some additional functions have also been included in the software with the purpose of detecting specific driving conditions where torque overshoot is likely to arise (but it is not fully known why) and adjust for this. In this report,

these functions are referred to as "add-on functions". The main issue of the add-on functions is the fact that they do not describe the physical characteristics of the clutch, but rather adjusts for the discoverance of torque overshoot scenarios. If a model would be developed which in perfect detail describes every physical property of the clutch and results in a perfect Torque Accuracy (= 1), along with being able to be implemented in the software. Therefore, in a sense, the modeling goal was to partly to render the add-on functions obsolete. As a result, the add-on functions were not considered when analysing the torque outputs in specific tests, but these functions were however analyzed with the purpose of gaining an increased knowledge in terms of when and how the torque inaccuracies tend to arise.

2.2.3 Modeling of Friction

Modeling friction is usually difficult due to discontinuous frictional force characteristics at zero velocity. The discontinuous characteristics of force (also referred to as breakaway force) results in large differences in computed force for a small difference in velocity and by setting inappropriate thresholds, energy generating friction forces can be provoked [2]. To illustrate, three well known models are presented in Figure 12.

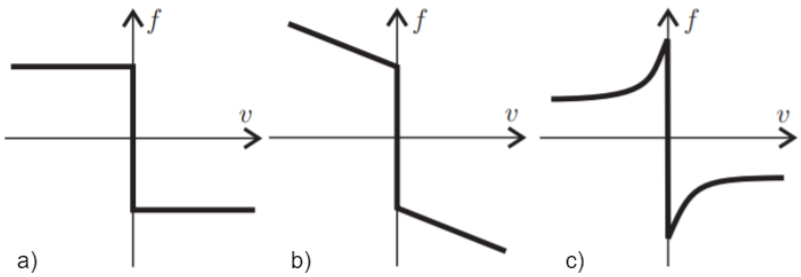

Figure 12: Discontinuous frictional force models: a) Coulomb friction, b) Coulomb viscous friction, and c) Coulomb friction with Stribeck effect. Shown by [2]

The Coulomb friction model (Figure 12 a)) is often considered as a dry friction model. As it however results in a nonlinear dynamics of motion, another model, the Viscous friction model (not in figure) is often used instead. In the Viscous model, the friction force is a linear function of sliding speed. The Coulomb- and the Viscous model can also be combined into a Coulomb viscous model (Figure 12 b)). For lubricated contact surfaces the Coulomb friction model with Stribeck effect (Figure 12 c)) is instead considered most accurate. Stribeck showed that in lubricated contacts the frictional force decreases until a full film is obtained. Thereafter the frictional force can both increase or decrease depending on thermal and viscous effects [11].

3 Analysis of Previous Tests

BorgWarner possess an in-house test department where clutches continuously are being tested and over the years a database from various tests have been saved. As a part of the research in this thesis, some of this data has been analyzed with the purpose of gaining an increased knowledge of clutch behavior and as a basis of formulation of hypotheses. Two of these tests were considered especially relevant for this project and are therefore discussed below. In this report they are referred to as Test A and Test B, due to confidentiality. To clarify, the data in the following subsections is not gathered during this thesis but rather from BorgWarner's test department. However, conclusions, discussions and hypotheses presented are a result from thesis analysis.

Since BorgWarner customizes clutches for each vehicle model with respect to vehicle specifications, properties such as number of lamellas or oil type can differentiate between clutch models. In Table 1, the most important clutch properties of the analyzed tests are listed.

Table 1: Tested clutch properties.

Test	A	B
Clutch generation	Gen VI	Gen VI
Lamella type	Organic	Sintered
Friction surfaces	26	20
Setup	Driveshafts in rig	In vehicle

3.1 Test A

Test A performed by BorgWarner on a GenVI (currently, the latest version of their clutch) with organic lamellas in 2017 was used as one basis to form hypotheses for the root cause of the Torque Accuracy issues. For this test, a full clutch and differential setup with one incoming shaft and two outgoing axles was used, as shown in Figure 13. In this setup, the speed of the outgoing axles from the differential are controllable by electric motors. The lamella pack used included 13 organic lamellas, i.e. 26 friction surfaces.

Figure 13: A full clutch and differential test setup.

In Figure 14 and 15, the torque response and the Torque Accuracy for a decremented step actuating pressure input is plotted for different ω_{diff}. As mentioned in Section 1.2, the Torque Accuracy is a measurement to illustrate how well the model can estimate the torque transfer. The Figure especially illustrates how ω_{diff} can influence the torque-transfer and accuracy.

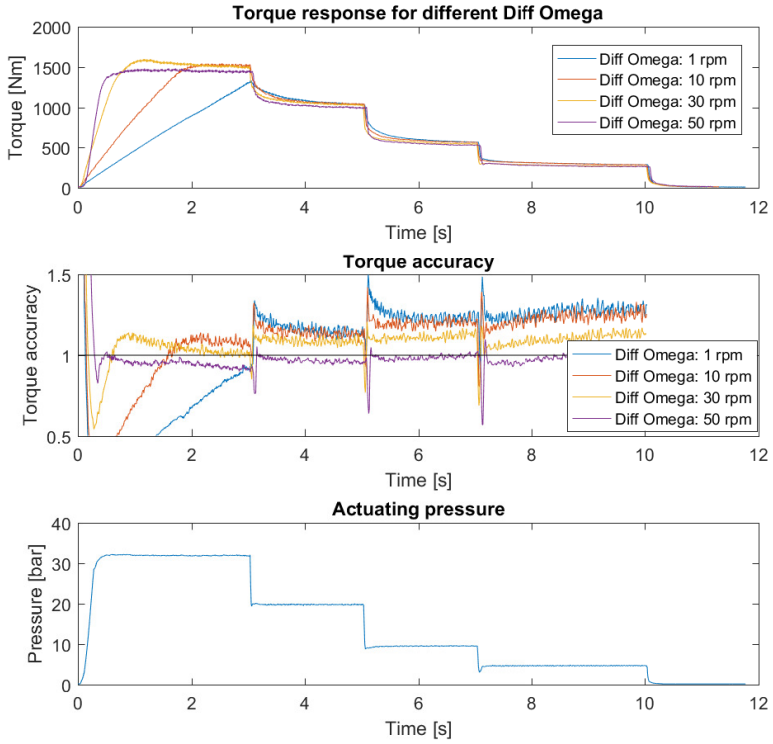

Figure 14: Comparison of torque and Torque Accuracy for different values of ω_{diff} for incremented steps of actuating pressure.

An obvious phenomenon is the time linear elastic behavior that can be seen in the torque response at increased actuating pressure. For low ω_{diff} the torque builds up slowly, while for high ω_{diff} the torque rapidly reaches max torque. It can be shown that the torque rise approximately is proportional to ω_{diff} which indicates that the behavior is a result of driveshafts of soft torsional properties. The fact that a soft drivetrain was used in the test was also confirmed by the test report. Elasticity in the drivetrain means that the ω_{diff} perceived by the clutch may be different than the ω_{diff} measured by the wheel speed sensors. This leads to difficulties in the torque estimation process which will be discussed further in the report. For example, during an increase in actuating pressure, the torque will initially build up tension in the driveshaft before a resulting torque is generated at the wheels. As a result, an elastic drivetrain induces a time delay at the ω_{diff} input. For this specific test, a time delay of as much as 3-4 seconds was observed for the lowest tested ω_{diff}.

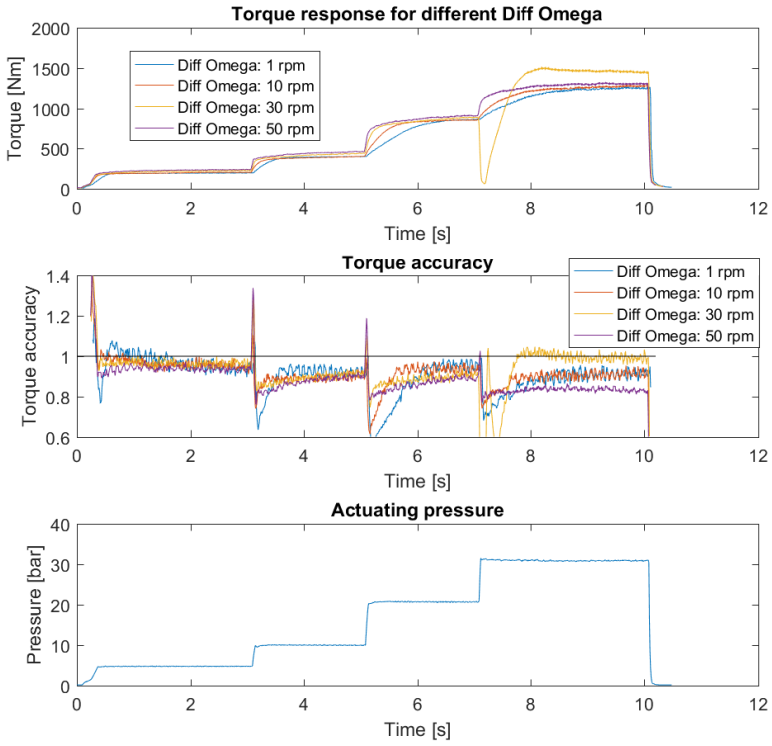

Figure 15: Comparison of torque and Torque Accuracy for different values of ω_{diff} for incremented steps of actuating pressure.

Another potential consequence of the elasticity and the time delay is the so called "Pressure Before Delta"-phenomenon (or PBD in short). In most dynamic driving scenarios, ω_{diff} is non zero and the actuating pressure is used to control the torque transfer thereafter. If an infinitely stiff drivetrain is imagined, one can see how an increase in actuating pressure would result in a compression of the lamellas and larger friction forces instantly being transferred to the wheels. This also means an instant reacting torque from the wheels and if the actuating pressure is not high enough to

lock the lamella pack, the reacting torque keeps ω_{diff} from zero. If instead a highly elastic driveshaft is considered, an increase in actuating pressure would compress the lamellas which would start to transfer torque towards the rear wheels. However, the reacting force from the wheels will have a ramp response characteristics due to the time it takes to tension the shafts, and as described in Section 2.2, the measurement of ω_{diff} takes place at the wheels of the vehicle. As a result, there is a risk that the actual ω_{diff} is reduced, possibly even a locking of the lamella pack takes place during the torque build up time while the measured ω_{diff} is increased; hence, in practice a PBD scenario, even though it is not observable for the system.

PBD can also occur in scenarios such as launch starts for certain vehicle models that uses pre-locking of the clutch in order to maximize the potential torque transfer to the rear wheels at start (assuming hang-on to rear configuration as described in Section 1). However, this can more easily be handled by the system since it is observable from sensor measurements.

Dynamic properties regarding PBD can further be split into two subcategories. First of all, a non zero ω_{diff} is necessary to fully lubricate the lamella to steel plate interface as described in Section 2.1.1. Since the oil in the lamella drum is not pressurized, the lubrication oil of the lamellas has theoretically zero bearing capacity and is thus also theoretically pushed away rapidly from the lamella to steel disc interface. Therefore, in order to keep the lubrication active, a relative motion (i.e. a nonzero ω_{diff}) is needed between lamella and steel disc for the oil to be able to spread at the steel surface. This could potentially increase the friction coefficient according to the theory presented in Section 4.1.1.

Secondly, PBD allows for different compression and rebound characteristics compared to DBP. When a torque is being transferred through a lamella pack, the lamella splines will be loaded with forces from the spline drum reacting to the frictional forces. The spline forces will not only transfer the torque through the drum to the outgoing shaft, but also enable for a frictional axial force on the lamella in the spline interface. Hence, theoretically, a clutch transferring high torque will require a larger actuating pressure to compress the lamellas axially than a clutch transferring low torque. The same would theoretically be true for the rebound movement where the lamellas natural rebound movement(due to spring effects of lamellas) would be obstructed from the spline frictional forces. Since this kind of dynamics theoretically is a function of torque, it is also applicable during all scenarios. To conclude: if axial loads are carried by the spline drum, it means that there would be a difference in normal force on the lamella friction surfaces compared to if all axial loads went through the lamellas. Since the frictional forces are a function of normal load, this ultimately also would result in differences in torque output. This effect is believed to be seen in Figure 16 where the same actuating pressure results in different torque outputs depending on the previous state of torque.

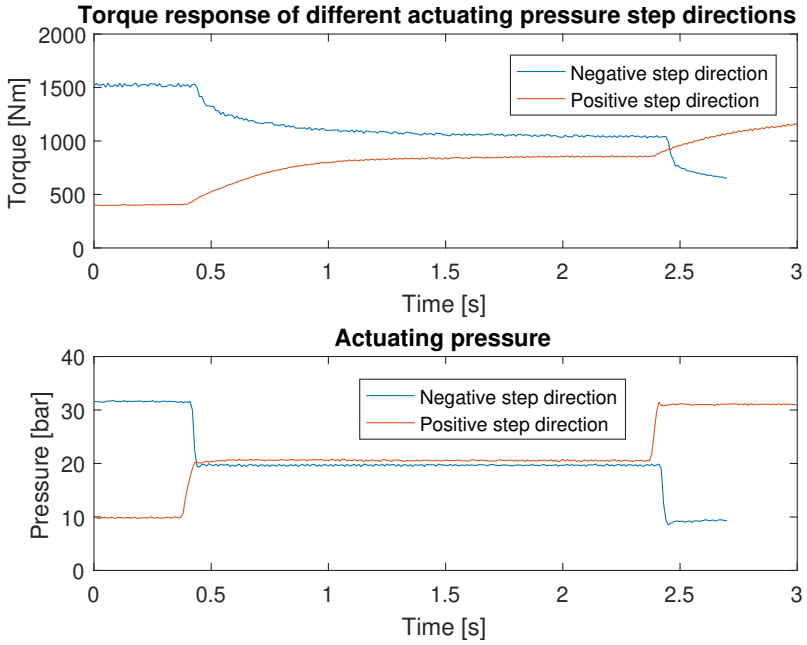

Figure 16: Comparison of different actuating pressure step directions shows hysteresis torque output.

Another effect to be considered is how the relation between elastic drivetrains and spline friction forces can affect lamella movement. As described before, an elastic drivetrain is considered to transfer the torque in a linear elastic fashion. Thus, if the clutch for example is connected to a high elasticity drivetrain, the compression of lamellas due to the actuating pressure can take place during the linear elastic torque rise. Since the spline friction forces theoretically are a function of torque, less axial losses and higher torque can thus be expected for these scenarios.

3.2 Test B

While test A was performed in a test rig, test B was instead performed in a vehicle. It also used the standard sintered lamellas instead of organic ones. Even though a test rig is most often used to test the dynamics of the clutch, it can never truly represent real conditions in terms of loads, vibrations and gravitational forces, but also human factors such as how steering angles and the throttle is applied. Another benefit from in vehicle tests is the driver feedback of handling capabilities; often in terms of tendency of understeer or oversteer.

There are several different kinds of in-vehicle AWD tests performed by BorgWarner. One should note that these are often extreme cases in terms of mechanically stressing the vehicle and clutch as well as not being especially representative of typical operational scenarios for every-day usage. However, when testing the system capabilities it is important to cover the most demanding test cases. If the system can handle these, it is likely that it can handle most encountered scenarios.

Test B contains data from one such test, called µ-jump, where the vehicle is placed on a high friction surface (such as tarmac) with a low friction surface (such as ice) ahead. As the vehicle is accelerating (often during high torque requests), first the front wheels enter the low friction surface after which the rear wheels enter the low friction area. This is called a µ-jump test since the change from high to low friction is very sudden.

Test B consists of data from seven runs of µ-jump. To get a comparative overview of the runs, the data files from all runs were merged, see Figure 17. For detailed analysis, they were also studied individually, which is discussed more below. For all runs, the torque requests were capped at 1440 Nm which is also the requested value for most of the time during the runs. The top subplots illustrate the torque request, the measured torque output (on the rear axle), the pump ECU current and the filtered (estimated) Diff Omega. It also includes horizontal dotted lines which indicate the desired Torque Accuracy margin of ±10% for torque requests of 1440 Nm. These are also the limits for Torque Overshoot and Torque Undershoot. The second subplot shows the engine rpm, the speeds of the front and rear axles (ω_{front} and ω_{rear}), the unfiltered (UF) Diff Omega (according to equation 4) and a filtered (F) Diff Omega. In this analysis we are not interested in the absolute values of the speeds, but rather the relative comparisons. Therefore, ω_{front} and ω_{rear} are both scaled by the same factor so that one of them peaks at 1. Similarly, both the F- and UF Diff Omega are scaled to peak at 1 respectively.

It is worth noting that it is the filtered Diff Omega which is used as input in the friction model and that the reason why Diff Omega is filtered is due to elasticity and inertia of the drivetrain. This means that the actual Diff Omega perceived by the clutch is dampened in relation to the immediately measured Diff Omega based on wheel measurements. Note the difference between the unfiltered and filtered Diff Omega in Figures 18 and 19. The reason why the unfiltered Diff Omega is also included in these graphs is to highlight the affect of the filtering. This is done because it is not evident how to filter Diff Omega most accurately and because the way Diff Omega is filtered will affect the modeled torque.

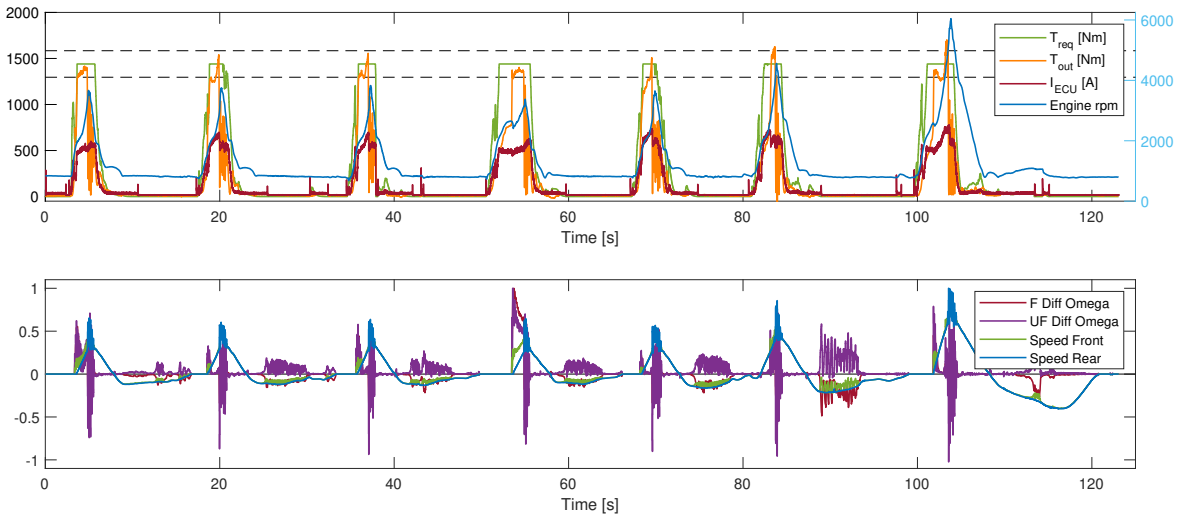

Figure 17: Test B - all data.

When considering Figure 17 (and Figures 18 and 19), a few points are worth noting:

- Even though the same torque is requested in all runs, different outputs are received. This is because other variables such as Diff Omega and engine rpm are different between runs. This fact can be used to analyze when and why Torque inaccuracies may occur.
- Not only does one need to be concerned with Torque Overshoot, but also Torque Undershoot. Although the issue of Torque Overshoot has been focused on in this analysis, it goes to show that Torque Accuracy need to be addressed in general. This fact makes the issue of Torque Overshoot more difficult to handle since it means that increasing the modeled torque (and subsequently reducing the actuating pressure) for any instance where the actual torque output is below requested torque would decrease the Torque Accuracy and possibly increase the issues of Torque Undershoot. This illustrates that the modeling is a trade-off between running the risk of giving a too high vs too low torque output.
- The values for the torque output (and other variables) are not behaving in a uniformly changing manner, i.e. it is not following a trend which can be explained by a simple function. This is simply because there are more factors at play in real driving scenarios compared to isolated rig tests. These real-life factors are often harder to measure and predict. This is also important to keep in mind when considering data from rig-tests. Furthermore, it also means that rig-tests have the benefit of being more repeatable and adjustable for individual factors.

To highlight some of the more specific behavior, the runs 2 and 7 are illustrated below in detail in Figures 18 and 19. A detailed view of all runs can be seen in the Appendix, Section 8.1.

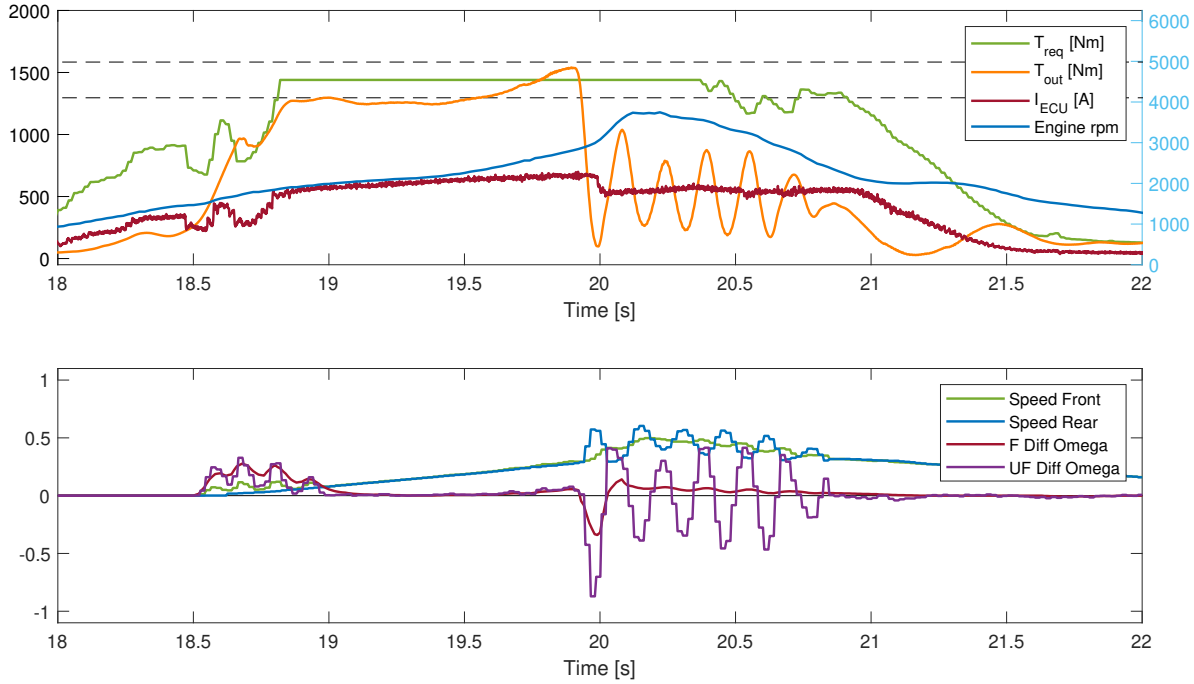

Figure 18: Test B - run 2.

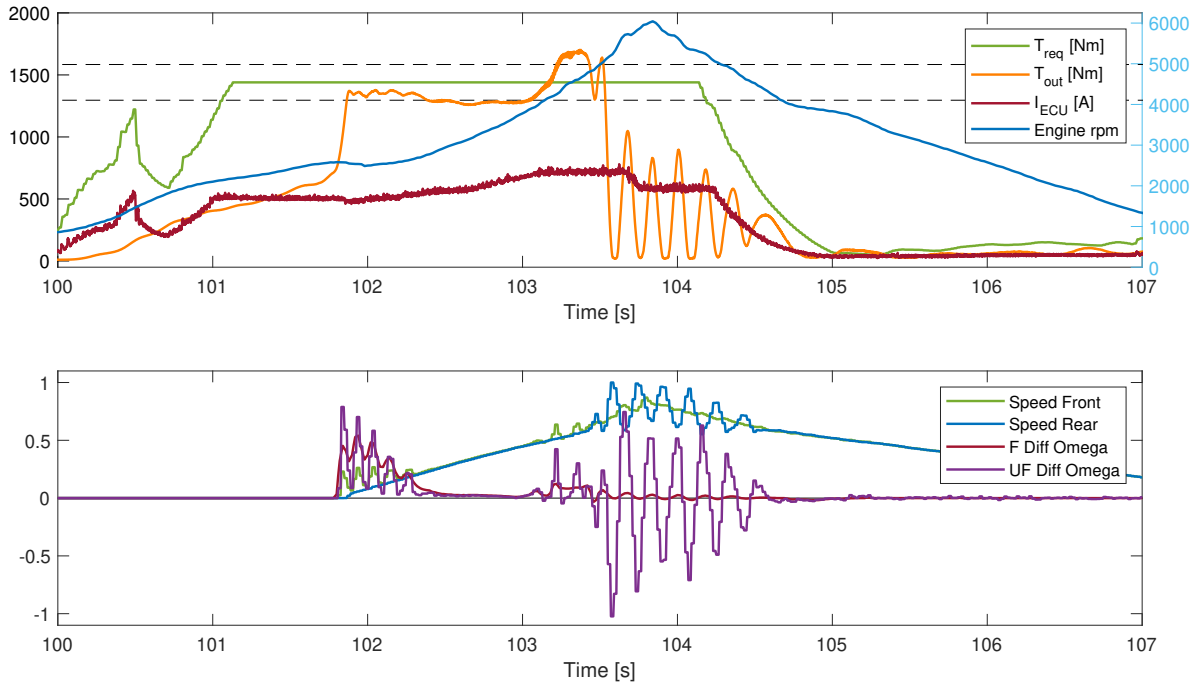

Figure 19: Test B - run 7.

In the graphs, some aspects worth pointing out are:

- The oscillating behavior first of the front axle (ω_{front}) as it enters the low-µ area, and then of the rear axle (ω_{rear}) as it enters low-µ. As the front axle starts oscillating, T_{out} seems to increase. Then, as the front axle stabilizes, torque tends to decrease. During the jumps in wheel friction, and especially as the rear enters low-µ, one can also note the oscillations of T_{out}. It is believed that the reason for these oscillations is that before an axle enters low-µ, it is tensed, then as it enters low-µ, all of a sudden it loses all reactive forces from the wheels and lets go in a spring-like manner. The other axle then experiences higher torque which appear in the form of impulses due to oscillations in tensioning of the drivetrain, which also causes oscillations in torque.

  One can note that the filtered Diff Omega dampens out the oscillations very quickly, even when the unfiltered Diff Omega is oscillating between positive and negative. If one compares these both curves with the torque output, it seems that T_{out} has a stronger correlation towards the unfiltered rather than the filtered Diff Omega during the oscillations. This suggests that (at least for these kinds of oscillations) there may be some dynamics which are uncaught by the model or filtering of ω_{diff}.

  However, as mentioned above, these are extreme cases where it is highly difficult to achieve a perfect reference following of torque. The fact that all wheels are now on low-µ and because outputted torque oscillations are always below the reference torque (no Torque Overshoot), the Torque Accuracy for these instances was not investigated further as it was considered outside the scope of this thesis.
- A common factor of both runs is that the tendency of torque overshoot occurs right after ω_{diff} has been zero, suggesting a locked clutch. What seems to initiate the overshoot is a small and slow rise of w_{diff}. A theory of what happens during this time interval is that the actual ω_{diff} is zero, but that elasticity in the drivetrain causes estimation errors for ω_{diff}. As described in Section 2.1.1, in general, a zero ω_{diff} can result in a higher friction coefficient and thereby a higher torque output. This theory suggests that the model is sensitive to drivetrain elasticity and ω_{diff} estimation errors. These issues are generally more difficult to demonstrate in rig-tests due to stiffer axles and more isolated behavior.
- Run 7 is where the biggest Torque Overshoots occur. The most notable difference between this and other runs is that in run 7, the motor was running at a substantially higher rpm. This suggests that there may be a correlation between high engine rpm and torque overshoot (at least for these kinds of driving scenarios).

3.3 Summary of Hypotheses

The results from previous rig- and in-vehicle tests as well as meetings with involved employees at BorgWarner were used as a basis to form hypotheses of what dynamics could be missed or not fully covered with the current friction model. The two following hypotheses were concluded to be the most likely causes of the friction inaccuracies:

1. **Spline friction losses** - Frictional forces in the lamella splines causes a varying normal force and subsequent torque-transfer from one lamella to the next in the clutch pack during compression and rebound. This splines friction varies depending on torque transmitted which causes varying losses through the lamella pack, which needs to be taken into account by the model. This results in a variation of torque output for similar actuating pressure. I.e. the assumption of a time-invariant uniform normal force on every lamella in the pack is invalid.

   To evaluate Hypothesis 1, a value called P_{diff} is defined and considered. It is defined as the estimated pressure ($\propto$ force) of the front lamella minus the estimated pressure of the rear lamella ($P_{diff} = P_{front} - P_{rear}$), see figure 20.

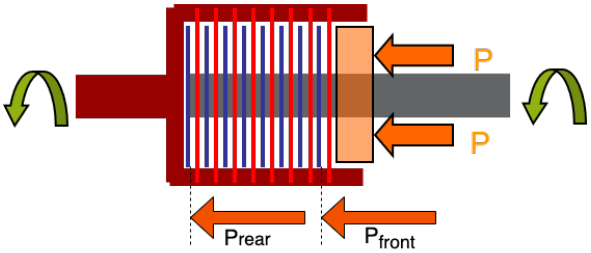

Figure 20: $P_{diff} = P_{front} - P_{rear}$.

   More specifically, assuming incoming and outgoing shafts with elastic properties, the following behavior is expected:

   (a) At low ω_{diff} before positive pressure transients: Low spline friction losses since lamellas can compress before torque builds up. The normal force acting on the rear lamellas in the lamella pack is similar to that of the front lamella. This results in a higher torque output than in case 1 (b).

   (b) At high ω_{diff} before positive pressure transients: High spline friction losses since torque builds up quickly and prevents compression. The normal force acting on the rear lamellas in the lamella pack is noticeable lower than that of the front lamella. This results in a lower torque output than in case 1 (a).

   (c) At negative pressure transients: High spline friction losses during rebound from a compressed state, thus resulting in the lamella pack getting stuck at a more compressed state than expected for a given pressure. This results in an increased friction and subsequent torque. The normal force acting on the rear lamellas may even be higher than that of the front lamella.

2. **Oil film reduction** - At low ω_{diff}, i.e. at relative speeds close to zero in the lamella to steel disc interface, the lubrication effect is deteriorated. This, together with high actuating pressures causes the oil film to be reduced, dry friction occurring and friction surfaces to dig deeper into each to the extent where the friction coefficient is significantly increased. These effects are expected to result in Stribeck friction characteristics, as described in Section 2.2.3. The highly non-linear characteristics around zero velocity in the Stribeck curve makes the velocity estimation extra important. Furthermore, in a vehicle application, Diff Omega is typically derived from wheel speed sensors and in practice a drivetrain both have some degrees of compliance and elastic properties. This results in ω_{diff}-estimation being a non-trivial task. Hypothesis 2 therefore suggests that the accuracy in ω_{diff}-estimation during low Diff Omega - speeds is critical for a precise torque accuracy since small errors in velocity estimation could result in high errors in estimated frictional force. If this hypothesis holds, the friction should quickly reduce as a ω_{diff} is initiated, since the surfaces let go and lubrication effects are restored.

4 Rig Tests and Data Acquisition

To test the hypotheses presented in Section 3.3, tests in rigs at the BorgWarner facility were planned. In order to acquire relevant data from the tests, several kinds of sensors were decided to be installed.

4.1 Sensors

The following sensors were used which have been used before and are common practice during rig tests at the BorgWarner facility:

- **Torque sensor** - All rigs are pre-installed with torque sensors. Measuring torque is important as this is the physical property which is desired to be controlled. The torque measurements will be compared and correlated to other measurements and inputs throughout the consequent data analysis.
- **Motor speed sensor(s)** - These measurements also come pre-installed with the rigs. Motor speed measurements are directly correlated to ω_{diff} (assuming completely torsionally stiff shafts).
- **Thermocouple sensors** - These sensors consist of two thin wires of different kinds of metals and utilize the thermoelectric effect to produce a temperature dependent voltage between the two wires which can be measured. These sensors were used to measure the temperature of the oil sump and chosen lamellas (same as Flexiforce sensors, see below). Since these sensors are thin and fragile, two sensors were used on each location to guarantee proper measurements. Measuring these temperatures was considered important as the current friction model is dependent on temperature. It also facilitated the tests by guaranteeing that a similar starting temperature was used for all tests.
- **Actuating pressure sensor** - A sensor measuring the actuating pressure was included in the test setup. Even though the tests were performed by setting pressure requests, these requests are not followed by the pump 100% accurately. Measuring the actual actuating pressure was deemed important as the pressure is the only controllable variable in the clutch which affects torque.

4.1.1 FlexiForce Sensors

Mainly in order to test Hypothesis 1 presented in Section 3.3 which is related to transient losses of normal force over the clutch pack, the idea was to insert force sensors next to lamellas at both ends of the pack. If a varying force can be detected in the clutch pack, Hypothesis 1 would be confirmed.

For this purpose, a force sensor called FlexiForce (FF in short) was found. These were considered ideal because of their thin and flexible structure, and suitable length availability. The idea was to mount these between the separating discs in a way which forced the entire normal force from one lamella to the next to go through the sensors. By placing the sensors between two separating steel discs, shear forces could be eliminated as the steel discs are connected to the same shaft by the same spline-

profile. Then, by summing up the force measured by each, the total force would be able to be calculated. The extra thickness introduced by this configuration resulted in on lamella - steel-disc pair having to be removed, going from 9 to 8. The choice of this size of lamella-pack was primarily based on availability.

These sensors work by behaving electrically resistive, and more specifically piezo-resistive, meaning that their resistance varies with the load, which can then be used in an electric circuit to measure the variation of force. According to the FF-datasheets, the standard type is guaranteed to measure forces accurately up to about 4500N (1000lbs). This type also has a temperature rating between -40°C and 60°C. There are however different variations of FF sensors available. Another type, called FF HT201, is developed for reliable behavior in high temperature conditions with a temperature rating between -40°C and 204°C. This type can be seen in Figure 21a. However, this sensor is only guaranteed to measure forces accurately up to about 2224N (500lbs). It can however withstand forces of at least 4500N (1000lbs), but only has a linearity up to about 889N (200lbs).

It is also worth mentioning that the manufacturer (Tekscan) has produced several Integration Guides (FlexiForce Design Integration Guide, Best Practices in Mechanical Integration and Best Practices in Electrical Integration) ([20]), which were studied as a complement to the HT201 datasheet ([21]). [20] mentions that the force measurement is somewhat tunable with the use of the recommended inverting amplifier-circuit. This circuit was therefore used and is described below, see Figure 22a. To ensure a complete and an even distribution of the force onto the FF sensing area, so-called "Pucks" or "Load Concentrators" were used, also as recommended by [20], see Figure 21b.

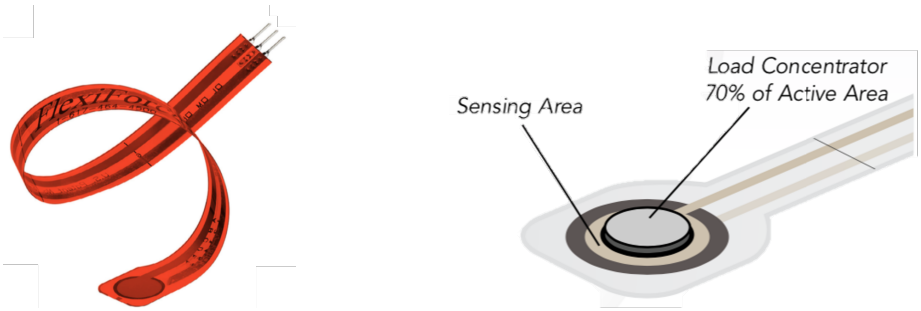

(a) FF HT201 sensor. (b) FF puck (load concentrator).

Figure 21: FlexiForce (FF) sensor.

It had been seen in previous tests such as Test A described in Section 3.1 that the applied force for these kinds of tests would peak at about 15 kN (given 40 bar and an actuating piston area) and that the lamellas may reach temperatures of about 150°C. In order to reduce the force exposure for the sensors, it was decided to mount four sensors on each measured lamella even though theoretically only three would be needed in order to guarantee that the entire normal force was transmitted through the sensors. With four sensors, if the normal force of 15 kN was to be distributed equally during the tests, each sensor would not need to handle a load above 4000N. At the same time, the

option of reducing the applied pressure during the tests to reduce the exposed pressure was outruled since this would be counter-productive in terms of provoking dynamic torque responses in the clutch. Similarly, significantly reducing the ω_{diff} and/or time of exposure during the tests in order to reduce the energy transmitted through the clutch and therefore the losses resulting in temperature development were outruled due to the importance of analyzing the ω_{diff}-dependency as well as the time-dependency for the torque response. It is also worth mentioning that the FF sensors are equipped with a venting function ([20]) in order to prevent built-up of pressure, or "pillowing", of the sensors. It is therefore not recommended to use the FF sensors in liquids or oils as these might enter the sensing area and damage the sensor. This recommendation was however believed to be related to the long-term durability-, rather than the immediate performance of the sensors. Furthermore, as no other viable force-sensing options were found and since the affect was assumed equal for both options of FF sensors, the oil was not decisive when choosing sensor type. However, it did introduce a possible source of error which meant that the sensor quality had to be monitored during testing and that all results had to be critically analyzed. This is discussed further in Section 5.

Ultimately, the choice was made to go for the FF HT201-sensor due to their high heat resistance. The sensor ratings in terms of temperature was considered more important than their force-ratings since exceeding the temperature was believed a more harmful violation in terms of maintaining sensor performance. Since ensuring a temperature under 60°C was deemed impossible while still stressing the clutch, the regular FF sensor was ruled out. Although the sensors were not used in complete accordance with the recommendations from the Design Integration Guides ([20]), they were believed to be the best alternative for the given applications. It did, however, mean that it was unsure how the sensors would handle the heat in combination with the oil and loads. The quality of the sensor responses were therefore evaluated continuously with usage. The sensor quality is discussed in the analysis of the test results and in the discussion of this report, see Section 5 and 7.

Based on values from the FF HT201 datasheet, [21], the typical performance of the FF HT201 sensor is summarized in Table 2. Note that this data was collected using the recommended inverting OP-amp circuit (according to [20], see Figure 22a) which was also used in this thesis.

Table 2: Typical performance of the FF HT201 sensor.

Linearity error (up to 889N)	$< \pm 3\%$ of full scale
Repeatability	$< \pm 3.5\%$
Hysteresis	$< 3.6\%$ of full scale
Drift	$< 3.3\%$ per logarithmic time scale
Response Time	< 5µsec
Operating Temperature	$-40°C - 240°C$
Acceptance Criteria	$\pm 40\%$ sensor-to-sensor variation
Durability	≥ 3 million actuations
Temperature Sensitivity	$0.36\%/°C$

The sensor errors in terms of Linearity, Repeatability, Hysteresis, Drift and Response Time from the datasheet (and as shown in Table 2) were considered very low and therefore neglected in the analysis of the test results. Also, no notable influence of these factors could be remarked during the tests. However, since the sensors were expected to have a sensor-to-sensor variation of ±40% and since they have a nonlinear voltage to force - relationship (see Figure 23), this relationship would need to be calibrated individually for each sensor.

As described above, the sensors themselves are simply a resistance varying based on applied force. In order to measure and log this conveniently with available measurement devices, the sensors needed to be integrated into a circuit which converts the resistance to a measurable voltage. This was done using the manufacturer's recommended inverting amplifier-circuit (as shown by [20]), as seen in Figure 22a. As the circuit is inverting the input, by applying a negative voltage $-V_{ref}$, we get a positive output voltage V_{out}. In the Figure R_S is the variable resistance from the FF sensor.

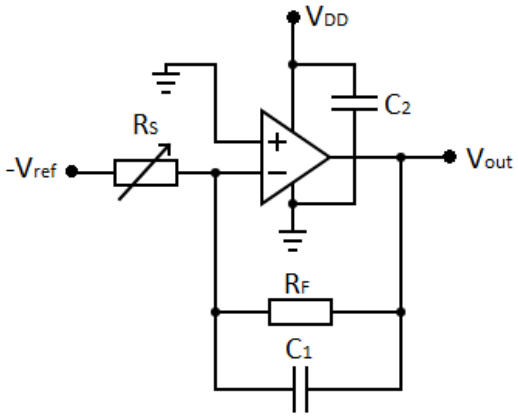

(a) Circuit used for the FF HT201 sensors.

Component	Value
V_{ref}	1V DC
V_{DD}	6V DC
R_F	1kΩ
C_1	100nF
C_2	100nF

(b) Voltages and component values.

Figure 22: HT201 circuit, voltages and component values.

By deriving the output voltage from Figure 22a, we get:

$$V_{out} = V_{ref} \cdot \frac{R_F}{R_S} \tag{5}$$

The reference voltage V_{ref} was set to 1V DC, which is within the OP-amp datasheet specification. Based on the approximate sensor resistance R_S as a function of Force provided by the manufacturer, an approximation of the expected output voltage could be found, see Figure 23. In the figure, $V_{ref} = 1V$, V_{out1} is the output voltage when the feedback resistance $R_F = 1kN$ and V_{out5} is the output voltage when $R_F = 5kN$.

One may note that the capacitors C_1 and C_2 do not have an effect on voltage given the theoretical expression above. However, in practical applications they will affect the output voltage by acting as decoupling capacitors and thus helping by rejecting

disturbances in the circuit. The values of these were based on practical experiments when testing the circuit during prototyping and set to $100nF$.

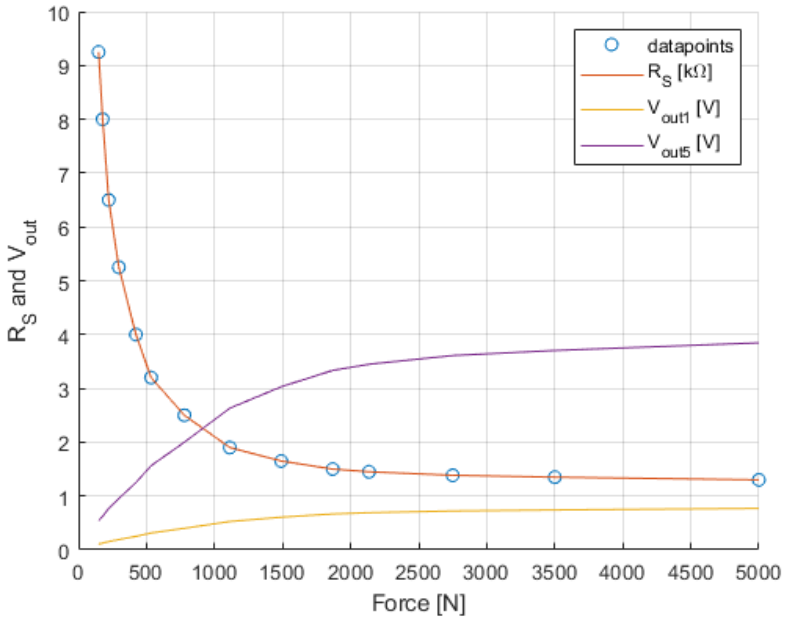

Figure 23: Approximation of resistance and voltage vs applied force.

Since the OP-amp used (MCP6004) has a maximum supply voltage of 6.0V (according to datasheet [22]), the output voltage was not allowed to reach this value as this would lead it to saturate. With that in mind, based on Figure 23, using a feedback resistance of $R_F = 5kN$ was deemed suitable as the output voltage would be well below this limit of 6.0V, including some margin. The complete list of values used in circuit 22a can be see in Table 22b.

The finished installation of the FF sensors and thermocouple sensors at the beginning and end of the lamella pack can be seen in Figure 25. Both of these sensor types were glued to the disc using Loctite 9497 high temperature 2-part adhesive. Although for general usage, it was recommended by [20] to use double-sided tape instead of hard-setting adhesives or epoxies as they may introduce pressure points under the sensor and disrupt the transmission of force to the sensing area, this was still done as it was feared that double-sided tape would not hold in these applications. As recommended by [20], so-called "pucks" (see Figure 21b), were manufactured in aluminum and installed. Although theoretically, there would be no non-normal load and shear stresses of the sensors, it was believed that in practice this would possibly still be the case. Therefore, a surface-sensor-puck configuration recommended by [20] to reduce the effect of shear on the sensor and to concentrate the loads to the sensing area was used, see Figure 24. By cutting out slots in the drum of the clutch, the FF- and thermocouple sensors could be exited straight out, see Figure 25b.

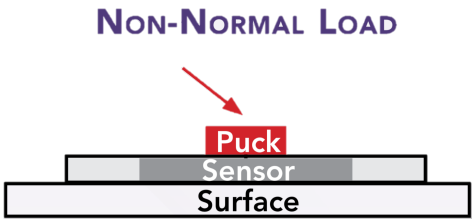

Figure 24: FF HT201 surface-sensor-puck - configuration used.

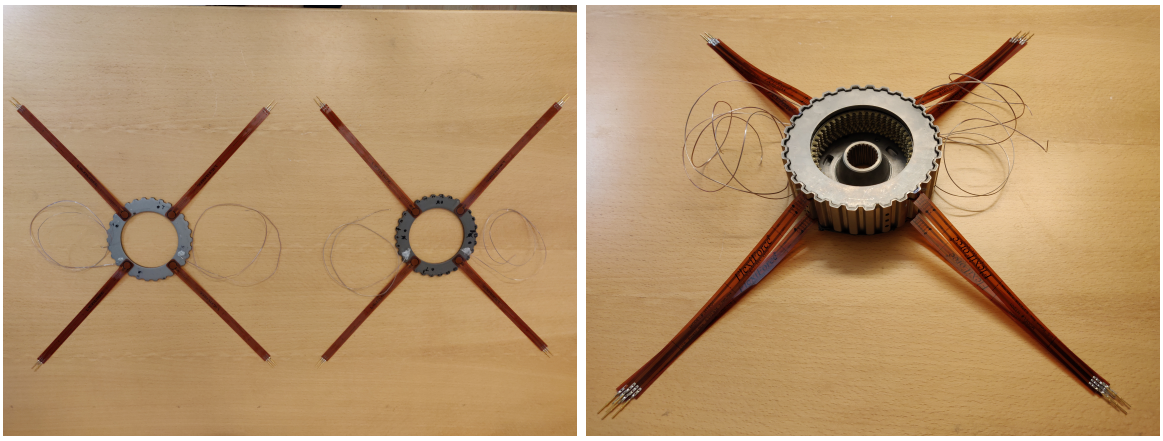

(a) FF sensors mounted on steel discs. (b) FF sensors mounted in clutch.

Figure 25: FF in clutch.

As these sensors introduce a novel measuring method in these applications and since they are one the main tools used to evaluate the hypotheses, their collected data will occupy a significant part of the analysis of the lamella pack dynamics.

4.2 Data Acquisition

The data was collected using LabVIEW and the following National Instrument data acquisition devices which were all connected to the same cDAQ chassis (see Figure 29):

- **NI 9213** - Used for thermocouple sensors.
- **NI 9219** - Used for actuating pressure-sensor.
- **NI 9215** - Used for the front FF sensors.
- **NI 9215BNC** - Used for the rear FF sensors.

The motor speed measurements and resulting torque measurements were collected using a Vector CANcaseXL (see Figure 26) as CAN-messages and sent to the PC through a USB-port.

Figure 26: Vector CANcaseXL.

The OP-amp used (MCP6004) provides 4 channels (See Figure 27), meaning that only two of these integrated circuits (IC's) were needed for the 8 FF sensors. The electronics and data acquisition setup can be seen in Figure 29. Note that only the two IC's on the left breadboard were used during testing (the third was brought only for validation purposes and was not used during testing). The flow of data can be seen in Figure 28.

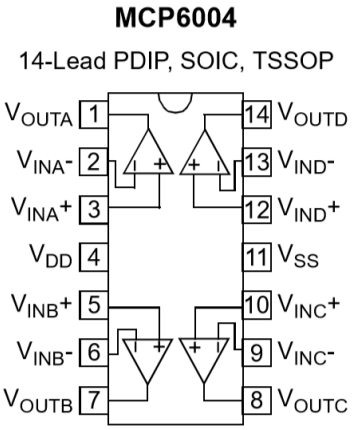

Figure 27: 4 channel OP-amp MCP6004.

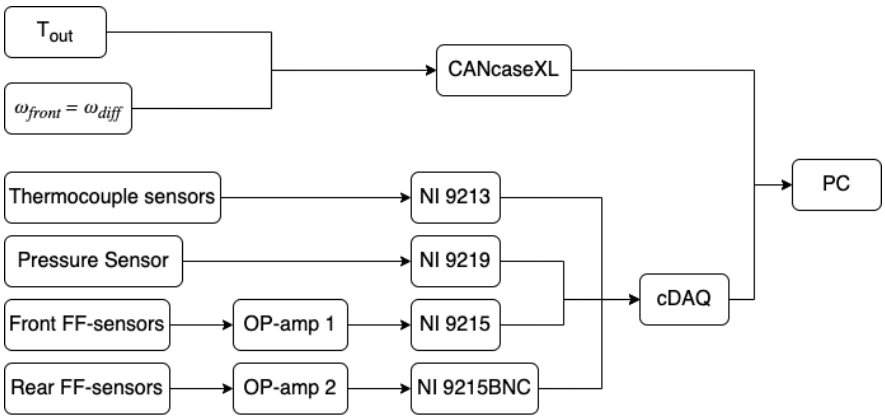

Figure 28: Data Flow.

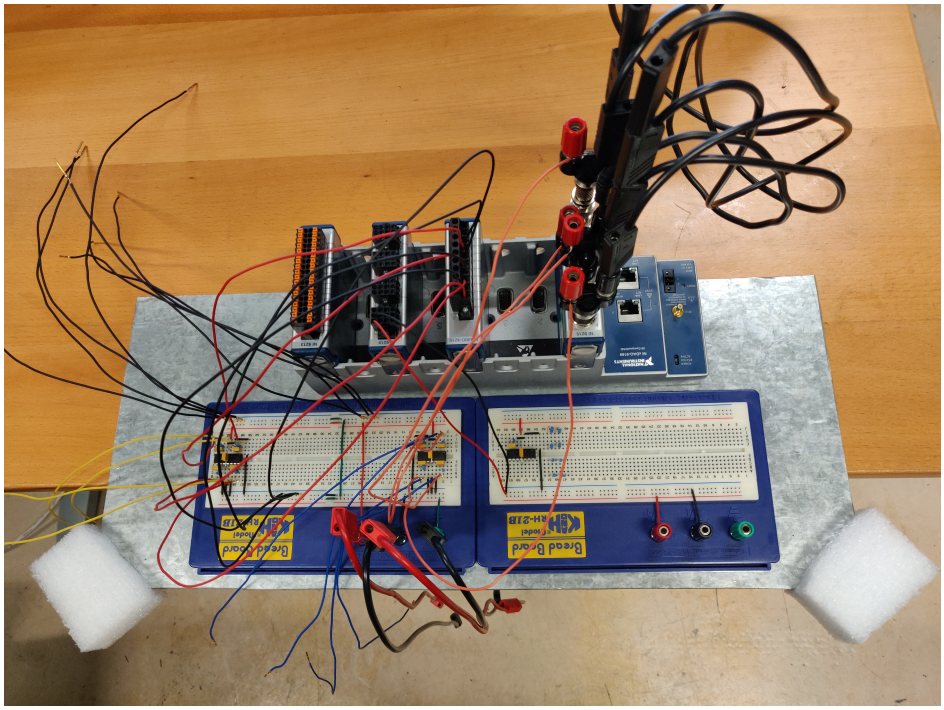

Figure 29: Electronics, wire harness and data acquisition setup.

The data acquisition software was set up using LabVIEW and a custom-written virtual instrument (see Figure 30) where the lamella temp, oil temp as well as actuating pressure were monitored in real-time. This was done in order to guarantee a lamella temperature of approximately 35°C before tests and to confirm functioning measurements during tests.

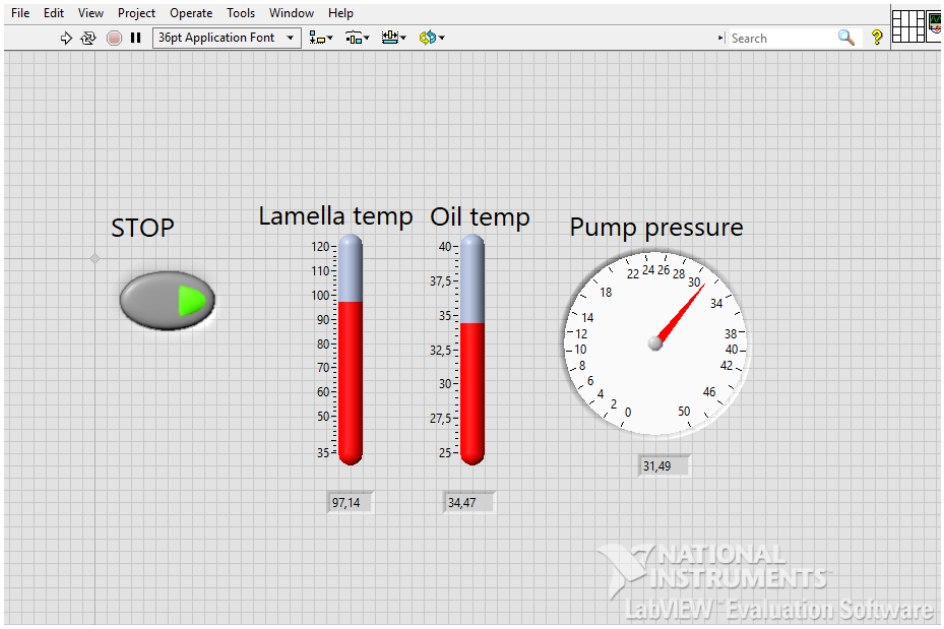

Figure 30: LabVIEW Virtual Instrument used.

4.3 Test Sequence Dynamics

In order to focus tests towards the two different hypotheses from Section 3.3, two different test sessions were planned. Note that in both tests, the clutch was controlled in terms of actuating pressure and not torque. The idea was not primarily to test the Torque Accuracy (since a reference was not set), but rather to see how the response of the FF sensors and torque could be related to ω_{diff} and the dynamics of applied pressure. This was done by making standardized test sequences of applied pressure which were all run with some different sets of ω_{diff}.

4.3.1 Test Session 1

Since Hypothesis 1 (spline friction losses) presented in Section 3.3 is dependent on the relative speed ω_{diff} as well as the speed and direction of clutch pack compression, some test sequences where these variables are varying were planned. In these tests the shafts were forced to a relative speed ω_{diff}, after which an actuating pressure was applied to the clutch pack. These are all called Delta Before Pressure (DBP) runs. The test sequences can be seen in Table 3. Note that:

- The test sequences were repeated for relative speeds of $\omega_{diff} = 10$, 30 and 50 rpm respectively. These speeds were chosen as they are representative for applications in a vehicle, typical in BorgWarner tests and believed to give a good basis for comparative analyses.
- Both positive and negative steps were run in the same sequence and that the lamella temp was cooled to approximately 35°C before initiating the next sequence.
- For all sequences the time indicates the total time from requesting the pressure increase until requesting 0 bar again.
- The test sequences can be thought of to be numerated in decreasing speeds, i.e. sequence 1 has the fastest dynamics of applied pressure, and 5 has the slowest.

Table 3: Test session 1.

Sequence	**Description**	**Actuating Pressure [bar]**	**Force Dynamics**	ω_{diff} **[rpm]**	**Lamella Temp [°C]**	**Time [s]**
1	Step	0 - 40, 40 - 0	DBP, 2 steps	10, 30, 50	35	10
2	Inc step	0 - 40, 40 - 0	DBP, 8 steps	10, 30, 50	35	24
3	Ramp 4 sec	0 - 40, 40 - 0	DBP, Ramp	10, 30, 50	35	4
4	Ramp 12 sec	0 - 40, 40 - 0	DBP, Ramp	10, 30, 50	35	12
5	Ramp 24 sec	0 - 40, 40 - 0	DBP, Ramp	10, 30, 50	35	24

The pressure request sequences used in Test session 1 are for clarification purposes illustrated in figure 31.

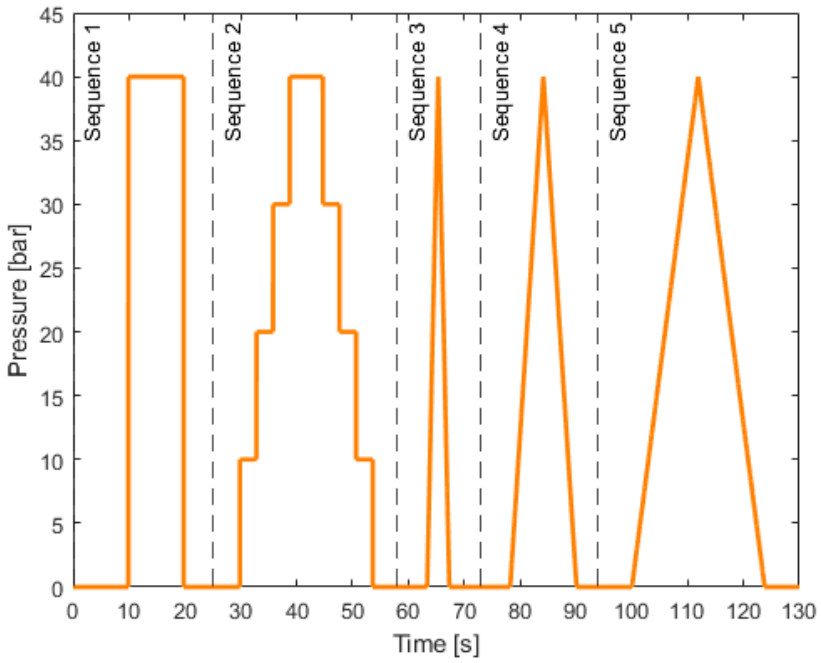

Figure 31: Test session 1 pressure request sequences.

4.3.2 Test Session 2

Similarly, since Hypothesis 2 (oil film reduction) as presented in Section 3.3 is dependent on whether the actuating pressure is applied before (PBD) or after (DBP) the clutch experiences a Diff-Omega, some PBD-tests were planned to allow the comparison of these cases. Here, it was decided to only perform tests where the actuating pressure was applied in one step, since this is the only comparable sequence when considering DBP vs PBD. Initially, tests with actuating pressures of 10, 20, 30 and 40 bar respectively, with relative speeds of $\omega_{diff} = 10$, 30 and 50 rpm were planned. However, after performing test session 1 it was decided to only consider cases of 40 bar since these were considered to be the most illustrative cases. It was also decided to only consider relative speeds of 10 and 30 rpm due to power limitations of the rig motor. Instead it was decided to perform the same tests but with two different starting lamella temperatures of approximately 35°C and 60°C. Test session 2 can be seen in Table 4. To clarify, all sequences were performed by applying both positive and negative steps in speed during a constant pressure of approximately 40 bar.

Table 4: Test session 2.

Sequence	**Actuating Pressure** [**bar**]	**Force Dynamics**	ω_{diff} [**rpm**]	**Lamella Temp** [**°C**]	**Time** [**s**]
1	40	PBD, 2 steps	10	35	10
2	40	PBD, 2 steps	10	60	10
3	40	PBD, 2 steps	30	35	10
4	40	PBD, 2 steps	30	60	10

4.3.3 Pump Control

As mentioned above, the clutch was controlled in terms of applied pressure. This was done by sending custom written CAN pressure requests to the pump ECU using the Vector CANcaseXL, as described in Section 4.2. These messages were sent from a PC to the CANcaseXL through a USB-port through which the CANcaseXL also received its power.

4.4 Test Rig

BorgWarner possesses several types of clutch rigs with different features at their test department. Ultimately, choosing one was a matter of *Technical Requirements* and *Test Specific Limitations*.

4.4.1 Technical Requirements

Some technical requirements were considered in towards choosing a test rig. These were of varying importance; some were considered necessary and some were considered desirable. These are discussed below:

- **Controlling Omega diff** - At least one motor was necessary to control ω_{diff} speed. With a one motor rig, the incoming shaft is driven and the outgoing shaft is locked. Such a rig can be seen in Figure 32. There are also rigs with motors at both incoming- and outgoing shafts, such as seen in Figure 13. This type of rig better represents the conditions in a vehicle where both the rear and front axle rotates. The drawback of a locked outgoing is that the oil circulation functionality could decrease in performance as described in Section 2.1.1. The requirement of rpm control is based on the test specifications where the clutch actuating pressure should be controlled at a specific rpm.

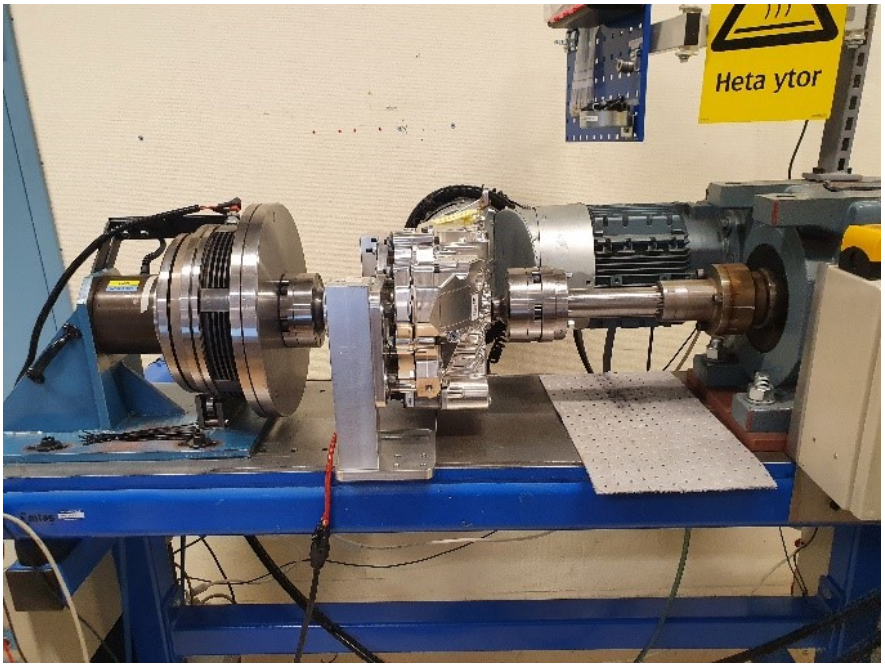

Figure 32: One motor test rig.

- **Integrated torque and rpm measurement sensors** - All rigs considered were equipped with integrated torque and rpm measurement sensors. However, these types of measurements could also have been implemented externally.
- **Integrated communication software** - A software tool to control the rig motor and sample rig states such as torque and rpm. BorgWarner uses both CANalyzer and Diadem software to communicate with the rigs through CANbus.
- **Two driveshafts with different elasticity** - In line with the hypothesis of a correlation between driveshaft elasticity and torque inaccuracies, a rig with at least two different elasticity driveshafts was considered desirable. This was deemed optimal but not critical.

4.4.2 Test Specific Limitations

On top of the technical requirements, there were also some practical limitations to be considered. These were:

- **Wire harness** - The choice of using FF HT201- and thermocouple sensors inside the clutch resulted in implications on wire harness possibilities. The sensors had to be placed either on the lamellas or steel discs to catch the correct dynamics. The lamellas are rotationally locked to the incoming shaft while the same goes for the steel discs to the outgoing shaft. Thus, if sensors were to be mounted on a disc connected to a rotating shaft, the harness would have to be exited through the shaft and connected to a telemetry logging system. This would therefore be a must in a two motor rig, while in a one motor rig, the sensors could be mounted on the braked steel discs and exited through the rear housing.
- **Availability** - The utilization of test rigs were high at BorgWarner's test facilities and during the time of this thesis most rigs were already booked by other projects.

4.4.3 Choice of Test Rig

Considering the hypotheses presented in Section 3.3, Hypothesis 1 was deemed more suitable to be tested in a test rig with a locked outgoing shaft. This was due to the fact that the FF sensors were deemed crucial for this type of test but that its wire harness would introduce complications if choosing a rig with a rotating outgoing shaft. Performing these measurements in this kind of rig would require major modifications on the clutch and shafts. At the same time, Hypothesis 2 was deemed more suitable to be tested in a rig with a rotating outgoing shaft due to the fact that this rig allows for a better oil flow and control of oil film.

As a result, the testing phase was divided into two separate testing occasions; one for each test session. Since all rigs with two rotating shafts were unavailable in the weeks to follow at the time, the plan was made to perform test session 1 in a rig with a locked outgoing shaft, then analyze gathered data and make further planning towards test session 2 based on drawn conclusions as well as practical testing experience and rig availability further along.

In the end, after performing test session 1 it was decided to perform test session 2 on the same rig with a locked outgoing shaft. This decision ultimately came down to insufficient rig availability of the rig with a rotating outgoing shaft within a reasonable time frame of the project.

4.5 Test Setup and Execution

As it was decided to use a rig with a locked outgoing shaft, the FF- and thermocouple sensors would not rotate in relation to the clutch drum and housing and it was therefore possible to exit them between the front and rear housing, see Figure 33. In order for the FF sensors not to get cut or bent between the front and rear housing, all edges near the sensors were filed down. Since the thermocouple sensors were very thin and fragile they were exited through small holes which were drilled, see Figure 33a. This picture was taken after the tests and one can see that the sensors held up well without any damage or excessive bending here. During assembly, the FF sensors were taped to the sides in a manner which left some slack within the clutch, see Figure 33b. This was done in order to avoid tensioning them during the axial displacement of the steel discs during clutch engagement.

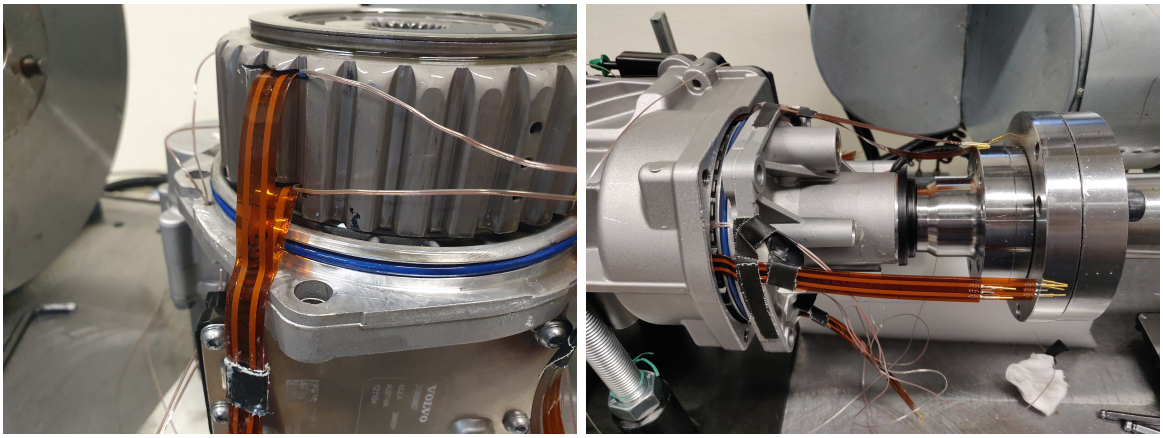

(a) Slots in drum and holes in clutch. (b) Exiting sensors.

Figure 33: Sensors in clutch.

The complete test setup can be seen in Figure 34.

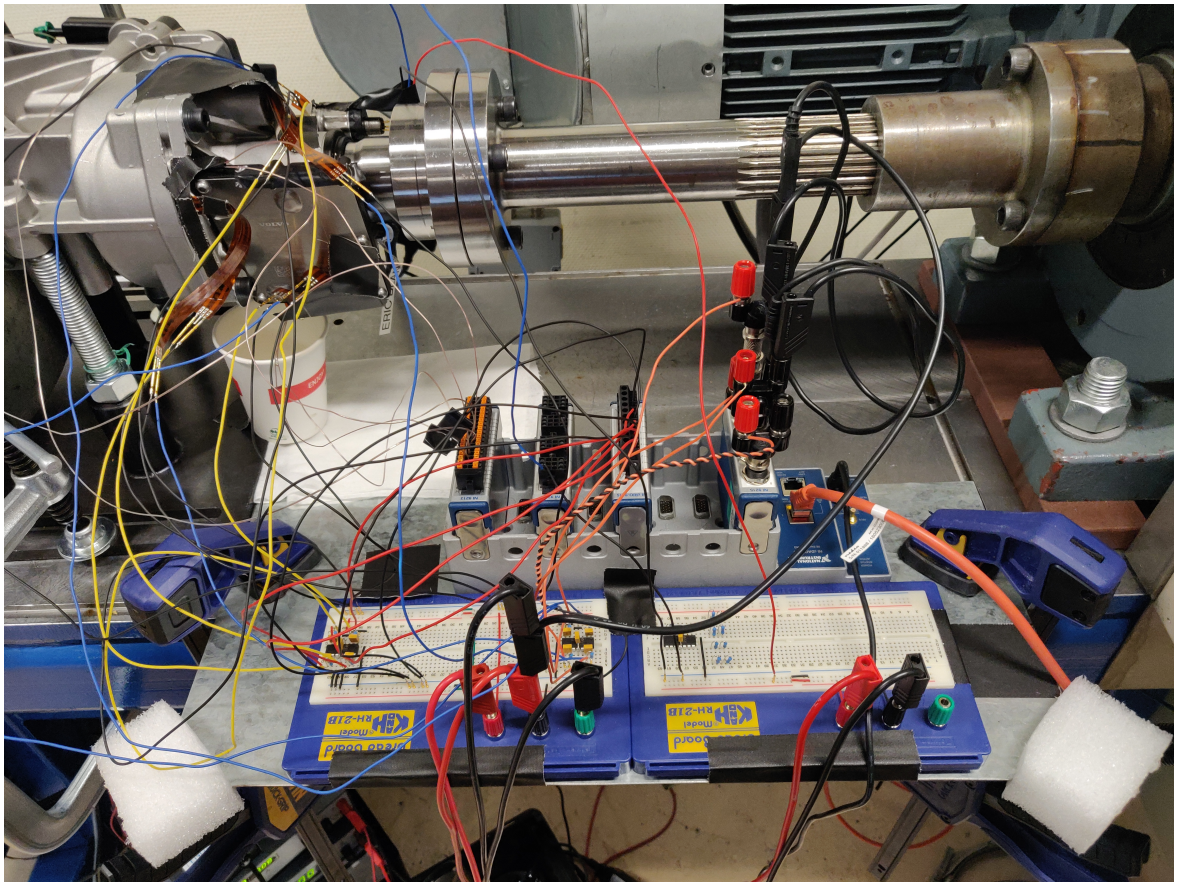

Figure 34: Complete Test Setup.

In the figure, note:

- The cup used to catch leaking oil due to filed edges and drilled holes. Even though holes were drilled and some material was filed down, there was not a significant leakage.
- The one pair of twisted orange and black wire used to check whether this had a noticeable effect on disturbance rejection in the cables. This was not the case and therefore not implemented on the rest of the cables.
- The power supplies at the bottom of the image supplying 1V and 6V for the FF-circuit, 12V for the ECU controlling the pump and 18V for the pump itself. The DAQ-devices are connected directly to a power outlet.

5 Test Results and Analysis

As described in Section 4.4, the test session 1 was performed first. The analysis of test session 1 was partly done before starting test session 2.

During the testing phase it was noticed that only one of the four lamella thermocouple sensors were working. As these were expected to give a similar output anyways, this was not considered an issue. For all lamella temperature readings presented below, these were taken from that one sensor. The rest of the measurements worked as intended, except partly the FF-measurements (which is discussed further below). Because of this, all of the FF sensor data was critically analyzed and considerations were made whether the output is more plausible to be explained by sensor behavior or behavior in the clutch. It also means that some of their data cannot be trusted with 100% certainty. Therefore, all data was used as a indication towards clutch dynamics rather than absolute truths. These indications were then to be used as guidelines for the modeling phase and partly to be judged by validation of the models produced. The possibility of major changes in clutch dynamics due to the presence of FF sensors mounted inside the clutch was considered small and thus neglected in the analysis and interpretation of data.

5.1 Test Session 1

5.1.1 Individual FF sensor analysis

As test session 1 (see Section 4.3.1 for explanation) mainly focused on the variation of force measurements depending on which sequence was run, the variation of force measurements between these sequences were primarily analyzed. The output voltage measurements from each amplifier circuit and FF sensor were plotted and compared. See Figure 35 for those voltages from the front sensors, i.e. the sensors closest to the pump piston. Similarly, the voltages from the rear sensors can be seen in Figure 36. In the plots, the voltages outputs for each sensor can be seen on the left y-axis and the applied pressure can be seen on the right y-axis.

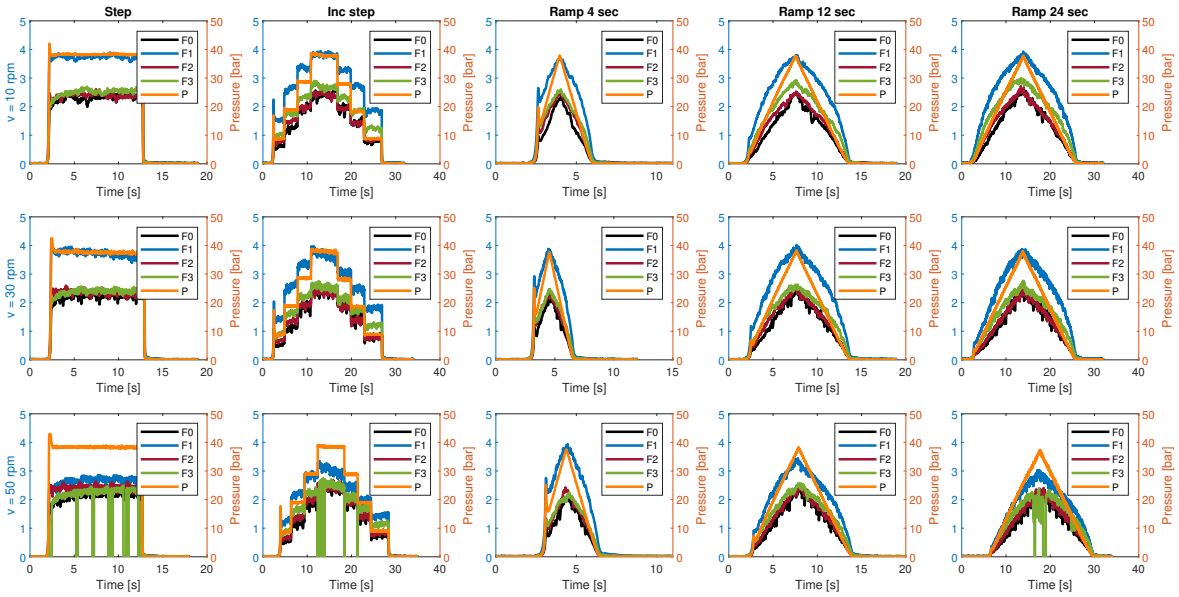

Figure 35: Voltages front.

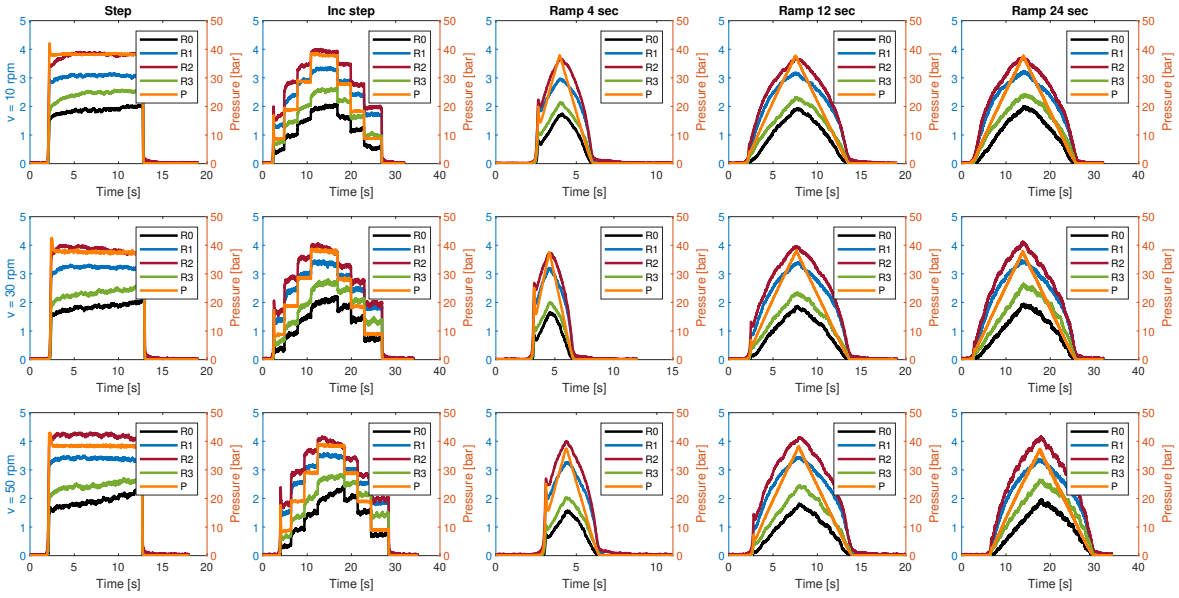

Figure 36: Voltages rear.

Conclusions from these tests are the following:

- No sensor bottomed at maximum available output voltage from the OP-amp of 6.0 V. The resistance and voltage outputs of the sensors were therefore all within the expected ranges.
- The pressure can be seen to show somewhat of a spike in the fast and positive parts of the pressure requests. This is due to the fact that when performing a pressure request of the pump, it is programmed to give a "kick" in pressure in order to compensate for the slower mechanical response of the clutch and to reach a desired state of compression faster. This kick can also be noted in the output response from the FF sensors, which is an indication of good responsiveness.
- The front sensors seem to experience higher amounts of noises.
- As discussed in Section 4.1.1, the sensors were highly stressed in relation to the recommended usage according to [20]. Therefore, the quality and consistency of the sensor responses were evaluated continuously during the testing phase. Here, it was noticed that the sensor F3 seemed to loose connection in the 50 rpm-runs Step (subplot 11), Inc step (12) and ramp 24 second (15). Apart from this, its measurements seemed to be coherent with its other outputs.
- Also, when considering the runs in subplot 11 and 15, the FF sensor F1 shows a significantly dropped output voltage compared to previous runs. This indicates that this sensor seem to have taken some significant damage, probably due to the high stresses on the sensors. Interestingly, it is worth noting that the other tests had been made on a Friday and that these runs were made on the Monday after the weekend. In other words, this sensor seem to have taken some damage while resting over the weekend.

5.1.2 Summed FF sensor analysis

As the total force from each set of FF sensors on each lamella is ultimately what is of importance, the sum of voltages for both the front and rear lamellas were also compared. These can be seen in Figure 37. One should note however, that since the correlation between applied force and output voltage for each sensor is highly non-linear (see Figure 23), comparing the summed voltages for the front and rear lamella is not a direct indication of the force applied. To exemplify, according to Figure 23, the summed voltage of two sensors taking 2500 N each is about $3.5 + 3.5 = 7.0$ V, whereas the summed voltage of one sensor taking 5000 N and the another taking 0 N is about 4.0 V even though the total force is the same. However, this plot was still gave valuable information in the sense of noting if any irregular sensor behavior had occurred. As stated in Section 4.1.1, the sensors were expected to share the total lamella force fairly evenly and fairly similar sensor outputs were expected from the same sequences but varying speeds.

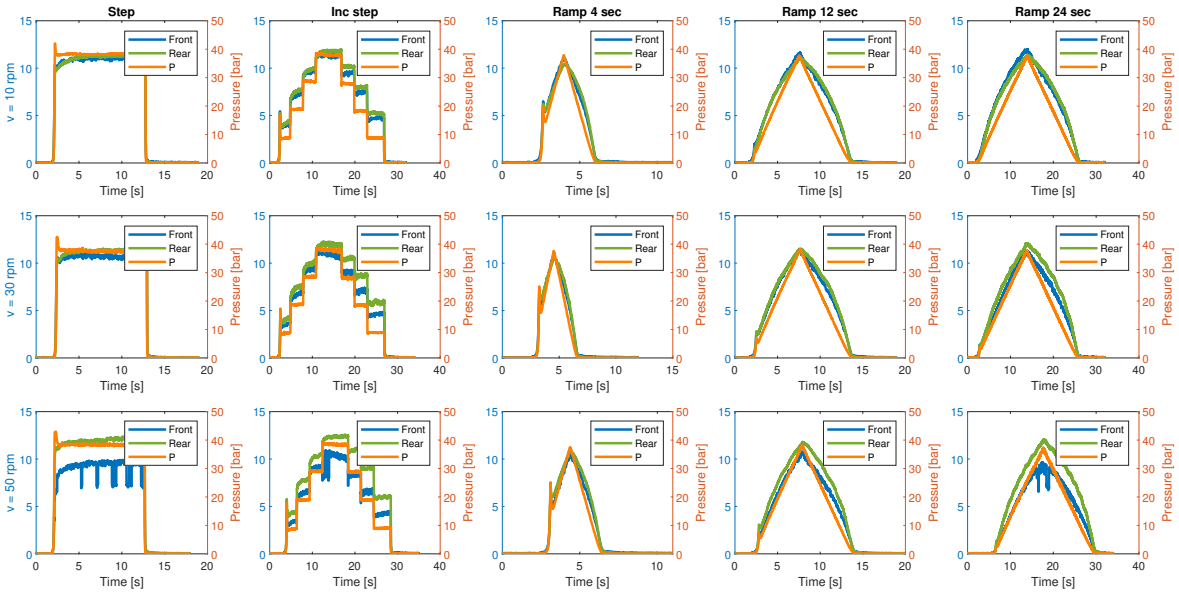

Figure 37: Voltages Front vs Rear.

Another way to illustrate the FF sensor data is in a voltage to pressure plot which can be seen in Appendix 8.2.

The main aspects noted were the following:

- There is a clear indication that the front sensors had a failure at the 50 rpm test sessions in subplot 11, 12 and 15 (not referring to the lost connection for sensor F3 as mentioned above). This confirms the suspicion that the decreased output from the front sensor F1 is significant. As a result, the front sensor measurements of these runs are neglected in the analysis.
- When comparing the increasing (compression) and decreasing (rebound) parts of the sequences, there seem to be a hysteresis in normal force acting on the lamella (this is illustrated more clearly in the figures in the Appendix). However, due to the nonlinear voltage to force relationship and due to the increase of temperature during the runs, no such conclusion can confidently be drawn based on this data alone.
- The front voltages seem to be decreasing with increased rpm while the rear voltages are increasing with increased rpm. While rpm could be a factor that influence friction losses and thus would affect the lamella forces it cannot be ruled out that this trend could be a result of sensor drift over time since the test was performed in the order of increased rpm. Also, while the rear sensor voltage differences between different velocity sessions theoretically could be explained by clutch pack friction losses, the same explanation would seem implausible for the front sensors due to their close mounting to the actuator. For this reason, it seems more plausible that the changes in voltages is a result of sensor drift. For this reason, it was deemed that a sensor calibration for each sensor and for each speed was necessary. This conclusion erases possibilities for comparative analyzes in absolute values between different velocity sessions.

5.2 Test Session 2

As test session 2 in the end was executed in the same rig as in session 1, the front sensor problems were inherited. Thus, although the front lamella sensor measurements from session 2 are presented in the result, they are neglected for the analysis of clutch dynamics. An overview of the results from test session 2 is presented in Figure 38.

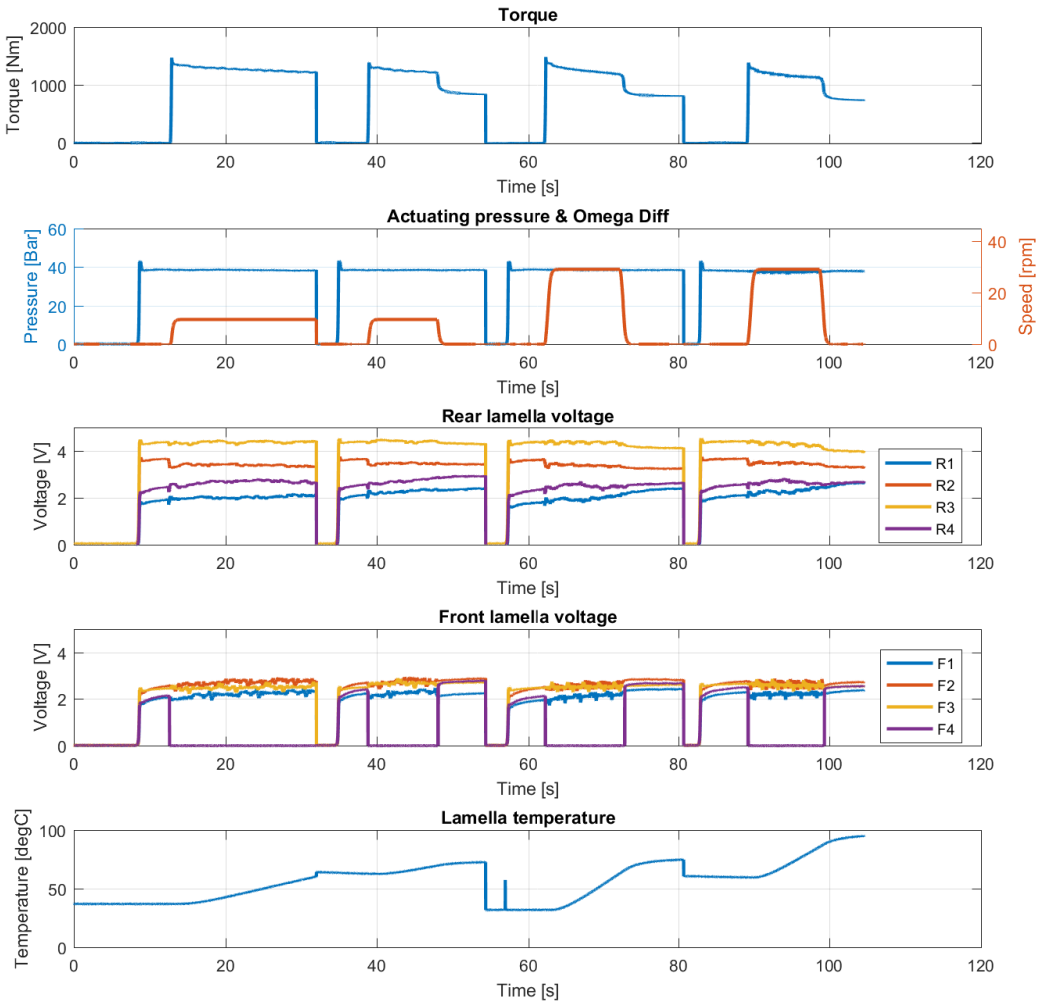

Figure 38: Overview of session 2 data.

The main aspects noted were the following:

- The rear lamella voltage shows similar values and proportions for all four runs which indicates a deterministic behavior of the rear sensors.
- A force redistribution between the sensors seem to occur when ω_{diff} is applied (R2 drops and R4 rises). It is believed that this is due to tensions in the rig and housing that offsets the clutch from its angle at rest.

- The front lamella voltage is low in comparison to previous runs and there are connection issues with sensor F4 which drops to zero several times.
- The torque measurement does not go to zero when ω_{diff} is reduced. This is due to rest tensions between the brake and the in going motor as the actuating pressure still on.

5.2.1 FF temperature sensitivity

In Table 2 each sensor is stated to have a temperature sensitivity of $0.36\%/^{\circ}C$ based on Tekscan datasheet. During the PBD runs (such as can be seen in figure 38), the normal force on each lamella is kept relatively constant during the entire run since no transients in actuating pressure is applied. The PBD data thus serves as the best data from the test session to evaluate the sensors temperature sensitivity. Within this session, no noticeable difference in voltage during temperature rise can be concluded. During the temperature rise interval, both a small rise and fall in voltage could be noticed. This could be a result of other factors such as changed normal force distribution. A low temperature sensitivity can also be noticed in Figure 46. As will be shown, the conclusions drawn from the FF data are based on comparisons between front and rear sensor values at equal time instants which consequently minimises the need of temperature mapping since the temperature is similar at front and rear lamella at each time instant. The temperature sensitivity of FF sensors is thus neglected in the data treatment.

5.3 FF Sensor Deterioration

As mentioned, it was noted that there seemed to be a change in FF Sensor behavior over time as they were used and resting in the clutch. In order to investigate this change, a plot was made over how their peak voltages changed between different dates. This can be seen in Figure 39. Here, the runs in test session 1 were performed during the 13/11 and the 17/11. The other tests in the plot are from coming tests in test session 2 and after. All these tests were performed with a peak pressure of 40 bar.

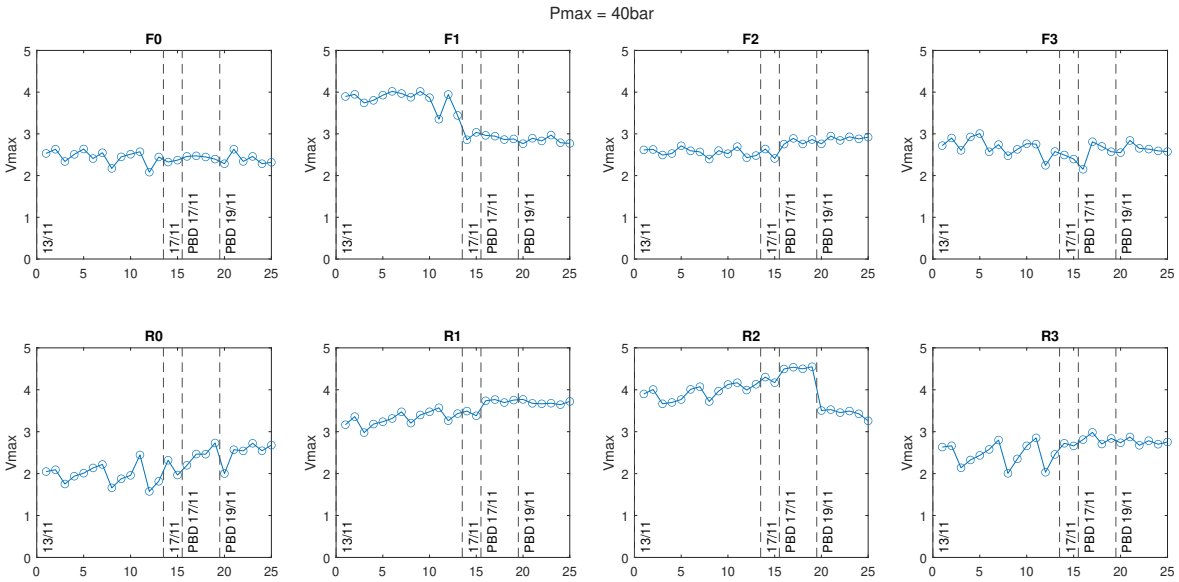

Figure 39: FF Sensor deterioration.

From the figure, one can clearly see that FF sensor F1 had deteriorated in performance between the dates 13/11 and 17/11. Similarly, sensor B2 had deteriorated between the dates 17/11 and 19/11. This was believed to be a consequence of oil leaking into the sensors during resting between the dates after performing tests with the high loads present. Based on this, it was concluded that the data from the front sensors was valid for tests on the 13/11 and the data for the rear sensors through the 17/11. I.e. all FF-data was believed good for test session 1 and the FF-data for the rear sensors was also good through half of test session 2.

Apart from that, one can note some patterns of performance. For example, consider the values of the rear sensors for the tests performed on the 13/11. As different sessions differentiate in absolute peak pressure due to different dynamic scenarios it is expected that the peak pressure varies a bit from run to run, but that all four sensors follows the same trend. The fact that they all (especially R0 and R3) show a similar type of pattern between the tests suggests that (at least) those results are likely to be reliable as they are coherent over time.

5.4 Sensor Calibration

In order to convert the calculated sensor voltages to their equivalent forces, a sensor calibration was necessary. As stated in Section 4.1.1, since the force to voltage output is expected to vary highly from sensor to sensor, an individual calibration of each sensor was needed. Optimally, the sensors would be calibrated with an accurate force measurement device that could apply at least 5 kN. However, nothing that met the requirements was available within the scope of test time. Therefore it was decided to use the mounting in the clutch itself as a calibration rig and apply a force in form of a pressure from the actuator. The issue with this method (as will be discussed more further on in the report) is that it is not possible to distinguish between sensor-to-sensor variations and force distributions between sensors on the same lamella. Thus

some assumptions had to be done during the treatment of data as will be described in Section 5.5.

After the rig tests were performed it was discovered that the department of solid mechanics at LTH possessed a machine meeting the calibration requirements. This was used to perform a post calibration. With the help from Jonas Engqvist at LTH, the machine was programmed to apply a load in the form of two slow ramp with short rests at the peak of 8000 N. A picture of the sensor mounted in the machine is shown in Figure 40. The test sequences including sensor output and the fitting of a second degree polynomial can be seen in Figure 41. For reference, an unused sensor was tested as well which is shown in the bottom right.

Figure 40: Calibrating.

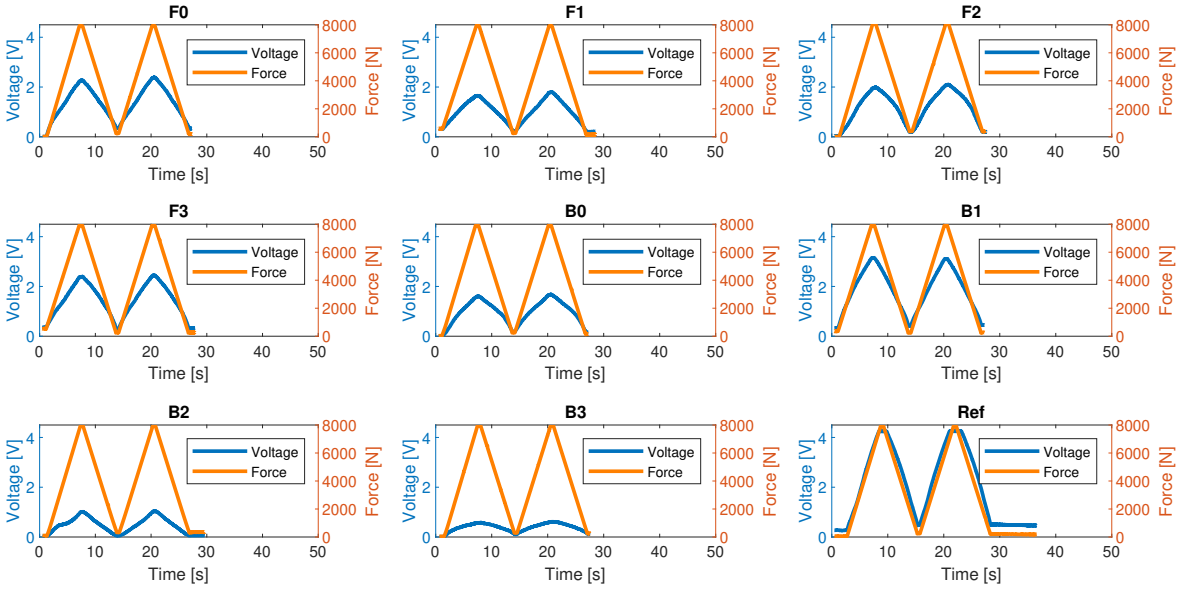

Figure 41: Calibration runs.

It should also be noted that two other unused reference sensors (ref1 and ref2) were also tested in a similar fashion, as can be seen in a figure in the Appendix, Section 8.3. These also showed unexpected behavior of lower outputted voltages, similar to the used sensors. This confirms the assumed big sensor-to-sensor variation and support the fact that an individual calibration is needed. It also disproves that any "low" (in comparison to expected according to Figure 23) outputted voltages for the sensors must be due to sensor deterioration.

To illustrate the voltage vs force - relationship based on the calibration, Figure 42 was made. Here it can clearly be seen that the output voltages differ greatly between sensors for a given force. It can also be seen that second degree polynomials are a good fit and that they cross the x-axis near the origin, as expected.

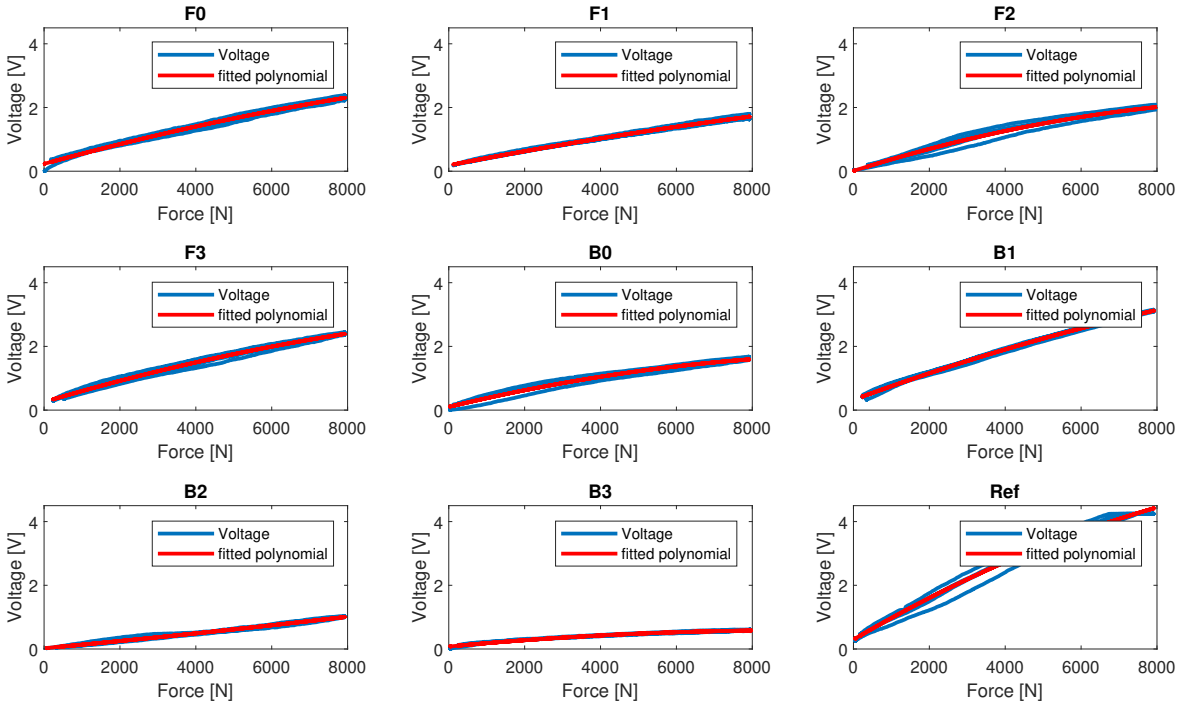

Figure 42: Calibration V vs F.

When comparing these results with voltage output levels from previous runs, such as can be seen in Figures 35, 36 and 39, it can clearly be seen that all sensors (except possibly sensor B1 which reaches an output of approximately 4V as expected) have deteriorated greatly, between the last run and the calibration session. Oddly though, the reference sensor also showed unexpected results of an output of only about 2 V at a load of 8000 N.

The reason for these changes in behavior can likely be explained by considering the states of the sensors after the tests. As can be seen in Figure 43, which is taken during disassembly, for several sensors the glue between the sensor and the steel disc had came off. Furthermore, the glue between the plastic films for several sensors had also loosened, meaning that the sensor had opened and the active sensing area was exposed. As mentioned previously, it is therefore believed that oil has leaked into the active sensing area and caused damage to the sensors during or after disassembly.

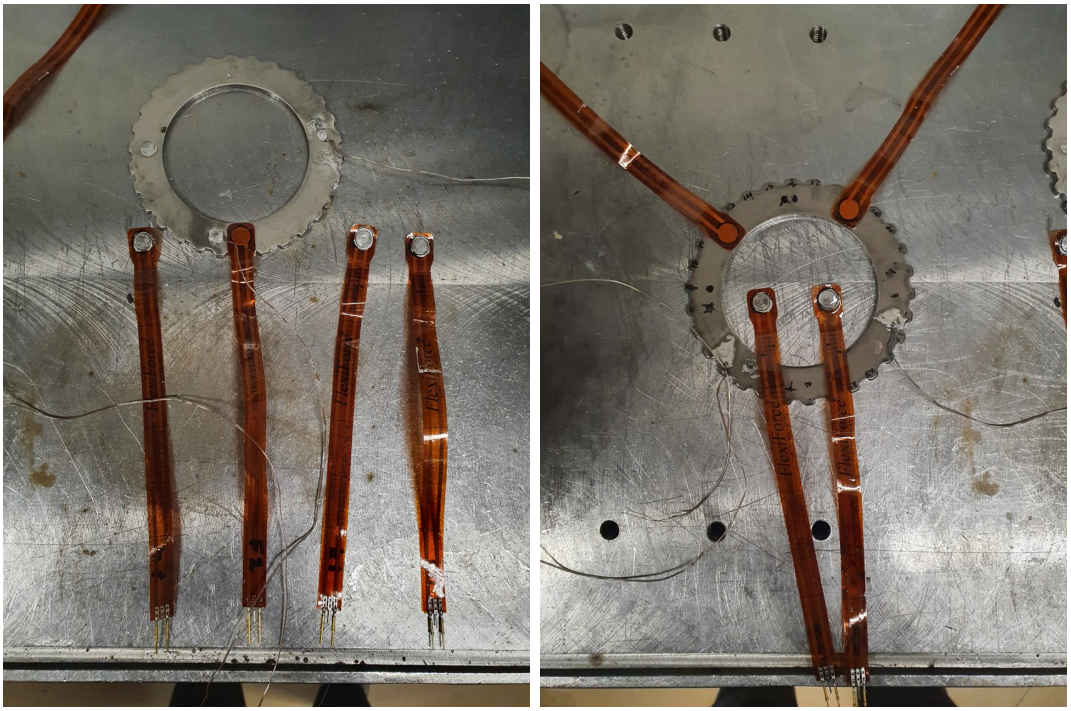

(a) Front FF sensors during disassembly. (b) Rear FF sensors during disassembly.

Figure 43: FF sensors during disassembly.

The calculated total forces on the front and rear sensors based on the calibration was therefore unsuccessful, which could clearly be seen by the exceeding large resulting forces. the total forces front and rear based on the calibration can be seen in the Appendix, Section 8.3.

The reason for the exceedingly high resulting forces based on the calibration is because the sensors all reduced in outputted voltages during the calibration session. The resulting force to voltage - relationship as seen in Figure 42 therefore results in much larger forces when the curves are used for the testing data (this conclusion is illustrated further by a curve presented in the Appendix, Section 8.3 of calibrated force as a function of voltage). The reason for these high forces is believed to be a consequence of sensor deterioration during the testing but also mainly when disassembling the clutch considering the large differences between the final run and the calibration. As the physical calibration was clearly unsuccessful, it was decided to perform force estimations based on motivated assumptions.

5.5 Force Estimation

In the lack of appropriate calibration it was decided to perform two different force estimations based on sensor measurements during operation. Motivated by the approximate relation of voltage vs force according to the FF datasheet ([21]) as shown in Figure 23 and fitted polynomial to calibrated data as seen in Figure 42 it was believed that the voltage to force - response of the FF sensors could be well estimated by a second degree polynomial through origin. By minimizing the squared difference

between the total estimated force and the actuating force this type of calibration could be computed in Matlab in two different ways based on two different assumptions:

1. **Same Force** - All sensors split the total force equally but are calibrated differently. With this assumption it follows that the difference in sampled voltage from sensor to sensor is due to sensor variations. This assumption can mathematically be described as:

$$\frac{F_{actuating}}{4} = a_1 v_1^2 + b_1 v_1 \tag{6}$$

$$\frac{F_{actuating}}{4} = a_2 v_2^2 + b_2 v_2 \tag{7}$$

$$\frac{F_{actuating}}{4} = a_3 v_3^2 + b_3 v_3 \tag{8}$$

$$\frac{F_{actuating}}{4} = a_4 v_4^2 + b_4 v_4 \tag{9}$$

   where v_n is the measured FF sensor voltage for sensor n and $[a_n, b_n]$ are fitted constants for sensor n.

2. **Same Sensor** - All sensors are calibrated equally but take different amounts of force. This can mathematically be described as:

$$F_{actuating} = av_1^2 + bv_1 + av_2^2 + bv_2 + av_3^2 + bv_3 + av_4^2 + bv_4 \tag{10}$$

   where v_n is the measured FF sensor voltage for sensor n and $[a, b]$ are fitted constants.

It should be noted that these calibration methods both have their limitations which need to be addressed. First of all, it is assumed that the rear sensors are reaching the same force levels as the front sensors, which implies that all losses along the pack have disappeared over time. Whether this is true or not is unknown. Thus, conclusions of absolute values and comparisons of front to rear absolute values cannot be done with confidence. Secondly, the most likely case in reality is that the sensors both take different loads and have a sensor to sensor variation, i.e. both assumptions partly being true. It is therefore of interest to compare the result of the two estimation methods. If the measurements are sensitive to calibration method, a more conservative approach towards the result should be done. If not, the result can be trusted to a higher degree.

For a good fit, data that covers the whole bandwidth of forces and different kinds of dynamics is preferable as fitting data. The incremented step session covers both ramp and step dynamics and also holds at maximum pressure and was thus deemed most suitable. As stated in Section 5.1, due to potential sensor drift, one calibration per ω_{diff}-session was computed. However, as the PBD sessions only contained data of maximum actuating pressure, which did not serve well as fitting data, the calibration of $\omega_{diff} = 50$ rpm was used on the PBD data.

Figure 44 shows the result of the estimated voltage to force (proportional to pressure) for each ω_{diff} of both methods.

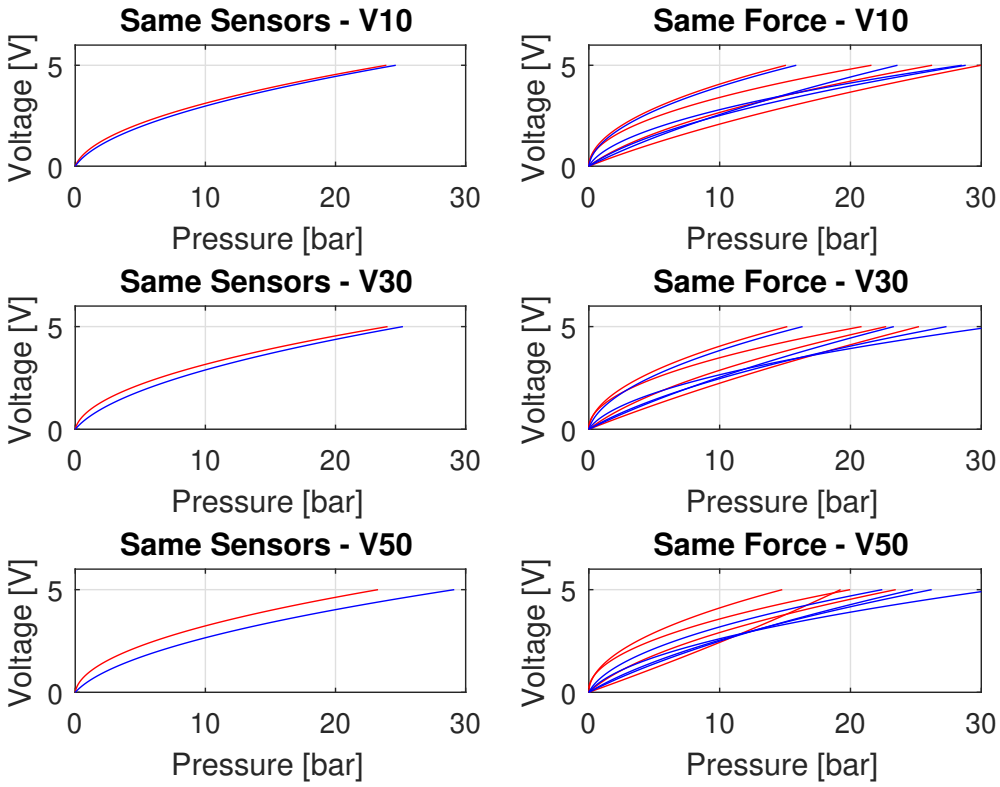

Figure 44: Calibration of sensors, fitted on the incremented step session data. Rear sensor(s) in red and front sensor(s) in blue.

In the left column (same sensor estimation) the front sensor estimation drifts for increased ω_{diff} while the rear sensor estimation is durable. This once again indicates that the front sensors took more damage and deteriorated over time. A similar trend can be noticed in the right column (same force estimation) where the front sensor estimations changes in behaviour for increased ω_{diff}.

Both methods result in similar pressure outputs and pressure dynamics which indicates that the result is not sensitive to estimation method. This can for example be seen in Figure 45 where the "Same Sensors"-estimation is plotted in the left column and the "Same Force"-estimation is plotted in the right column. Similar plots for all sequences can be found in Appendix.

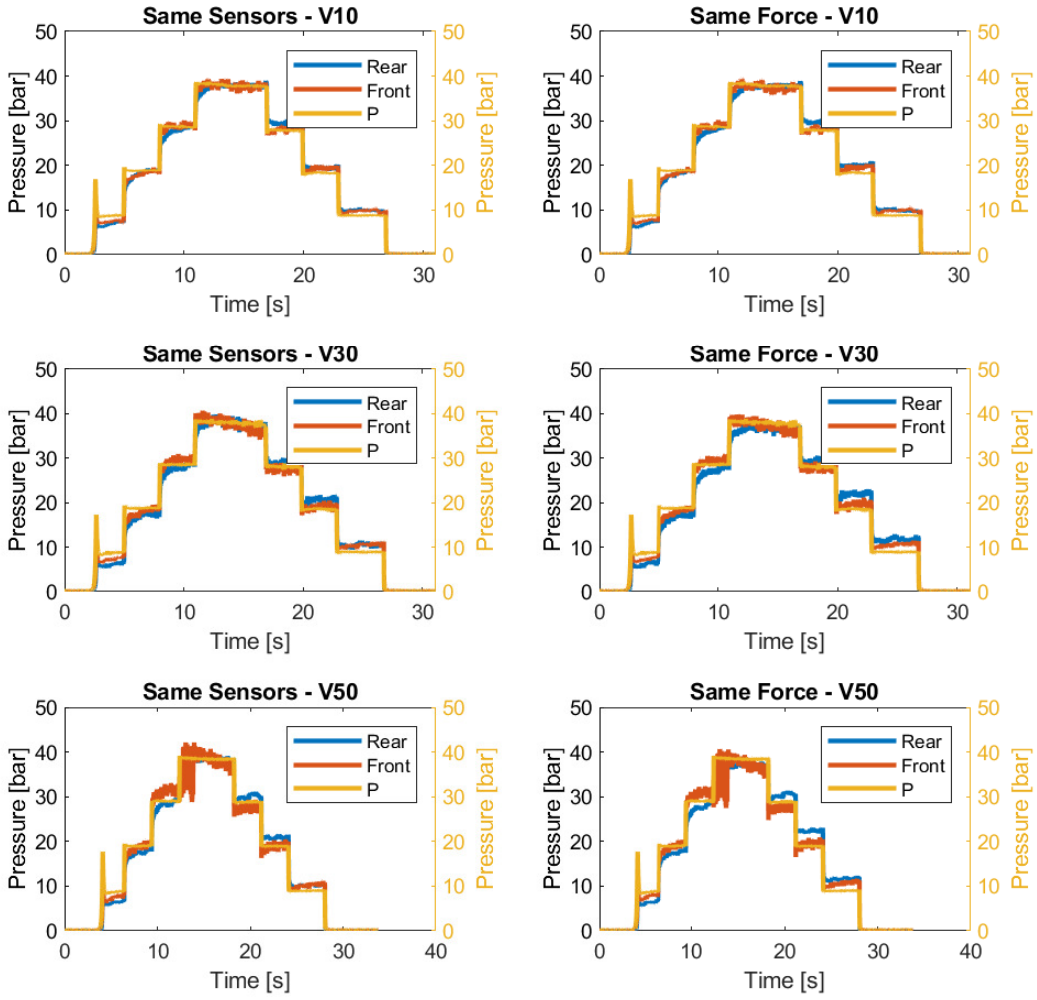

Figure 45: Estimated pressures at front and rear lamella with two different estimation methods; "Same Sensor"-estimation in the left column and "Same Force"-estimation in the right column.

5.6 Hypothesis Analysis

In this section focus will be on finding arguments for or against hypotheses presented in Section 3.3. Note that the measured lamella forces presented are computed according to the estimations in previous chapter. For convenience, when comparing data to the actuating pressure, lamella force estimations are presented in equivalent pressure units. The 50 rpm runs have been neglected in the analysis due to FF sensor failure during these runs. Finally, the fact that the steady state value of the rear lamella pressure plot is lower for DBP than for PBD is not conclusive since the PBD pressure were computed based on $\omega_{diff} = 50$ rpm force estimation. The absolute value should thus be neglected. It is more likely that the rear pressure is similar regardless of run during steady state conditions due to the similar torque output.

5.6.1 Step Input Analysis

In this subsection, the step dynamics of the tested clutch will be investigated in the form of steps in both pressure and ω_{diff}. According to the hypothesis presented in Section 3.3, the following types of behavior are expected:

- According to Hypothesis 1 related to spline friction losses, the compression and rebound dynamics are dependent on the order and the magnitude in which ω_{diff} and actuating pressure are applied which could result in variations of torque.
- According to Hypothesis 2 related to oil film reduction, the PBD runs are expected to result in higher torque due to increased friction in these scenarios. As the test was performed with stiff driveshafts which implies that a ω_{diff} is initiated fast, these effects are expected to be small and active during a short initial time after rotation of incoming shaft is initiated.

In Figure 46, cold runs of DBP and PBD are compared for ω_{diff} values of 10 and 30 rpm. It should be noted that the drop in torque over time is due to increased lamella temperature, i.e. the data is not normalized after temperature. The FF data in this figure were calibrated with the "Same Sensor"-calibration method.

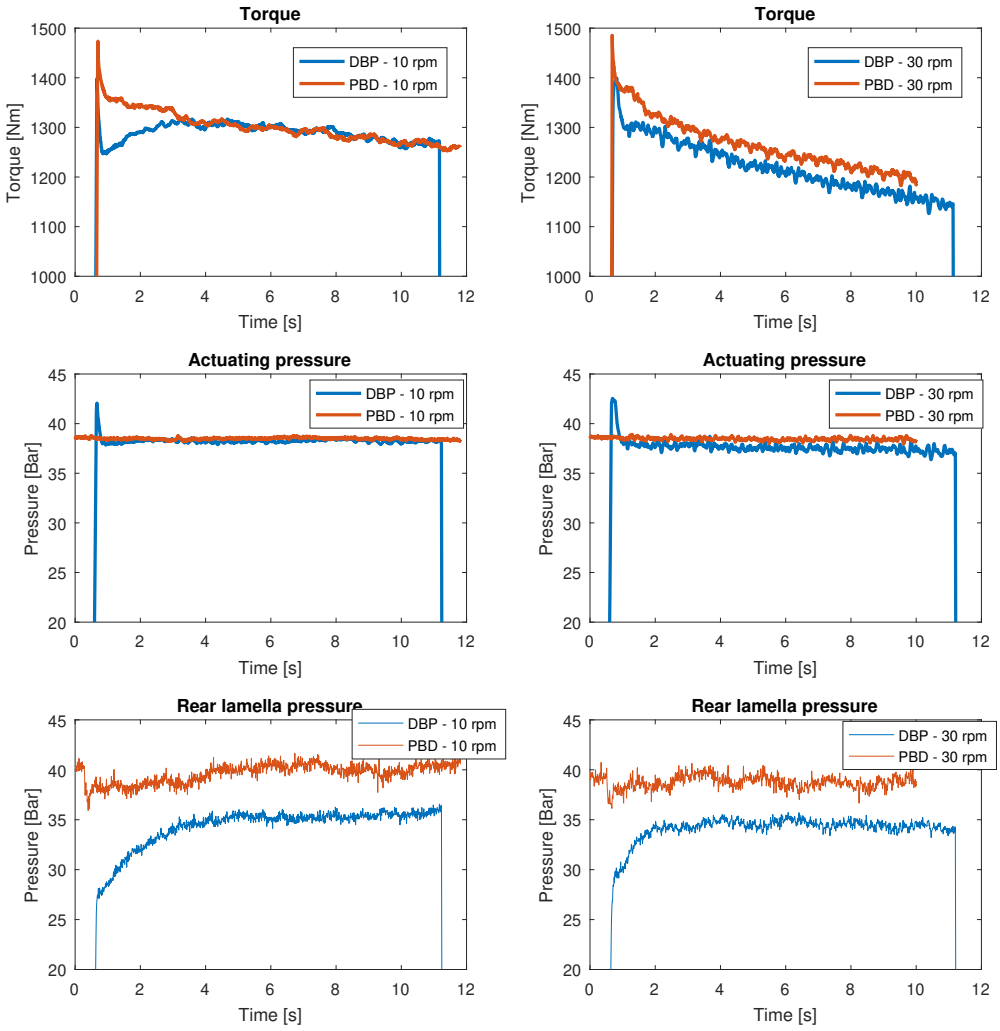

Figure 46: Comparison of DBP and PBD run.

Based on the result in Figure 46 the following indications of Hypothesis 1 can be made:

- Both the DBP and PBD runs output similar torque after the initial rise in torque. The offset in torque for the 30 rpm run is due to actuating pressure differences (same pressure was requested to the ECU but the result shows variations in actual pressure). Regarding Hypothesis 1, it can thus not be concluded that PBD would result in a higher steady state torque output than DBP in the scope of the tested time period.
- There is a significant difference in dynamic behavior during torque rise in the initial seconds of the step. For PBD, the rear lamella pressure is in steady state during the whole run. This is not true for DBP where the pressure rises for the first couple of seconds. This type of dynamic behavior was expected according to Hypothesis 1. The difference is also reflected in torque.

- According to Hypothesis 1(a) and 1(b) it was suspected that DBP-sessions during low ω_{diff} would result in a quicker compression and thereby higher torque than during a high ω_{diff}. However, the result indicates the opposite. To understand why, the Hypothesis should be clarified further. The theory was based on differences in rise time of torque for different ω_{diff}. The differences in rise time was obvious in studies of earlier tests, for instance as can be seen in Figure 14. For a low ω_{diff}, the torque would increase slowly which would allow for compression of lamellas before spline friction forces builds up and the opposite would be true for a high ω_{diff}. However, the root cause of differences in rise time is elastic driveshafts. As our tests showed, with the usage of a stiff driveshaft, the torque rise time is close to independent of ω_{diff} in relation to other factors such as actuating pressure rise time. A comparison of torque response in Figure 14 and Figure 46 illustrates the difference. Thus it cannot be expected that Hypothesis 1(a) and 1(b) would be true for our tests. Neither can the fact that the opposite (high ω_{diff} results in faster compression of lamellas) was true be considered confirmed due to low amount of repeated runs and uncertainties in sensor measurements. However, if the result reflects the reality over repeated runs, one suggestion of explanation could be that a higher ω_{diff} would induce more vibrations and therefore enhance the compression abilities.

Based on the result in Figure 46 the following indications of Hypothesis 2 can be made:

- The torque seems to spike/overshoot heavily for the PBD run even though neither the actuating pressure nor ω_{diff} induces any such characteristics. The rear lamella pressure for PBD indicates that no large pressure differences occur and therefor the torque spike can not be linked to an increased normal force in the friction contact surface area. It is thus believed that this is due to oil film reduction or dry friction according to Hypothesis 2.

In Figure 47, estimated P_{diff} is shown for step inputs (sequence 1) performed in test session 1. The sensor voltage to pressure conversion is based on the force estimation methods presented in Section 5.5. Both force estimation methods are only based on 10 and 30 rpm runs (the data from the 50 rpm test were ignored due to sensor failure).

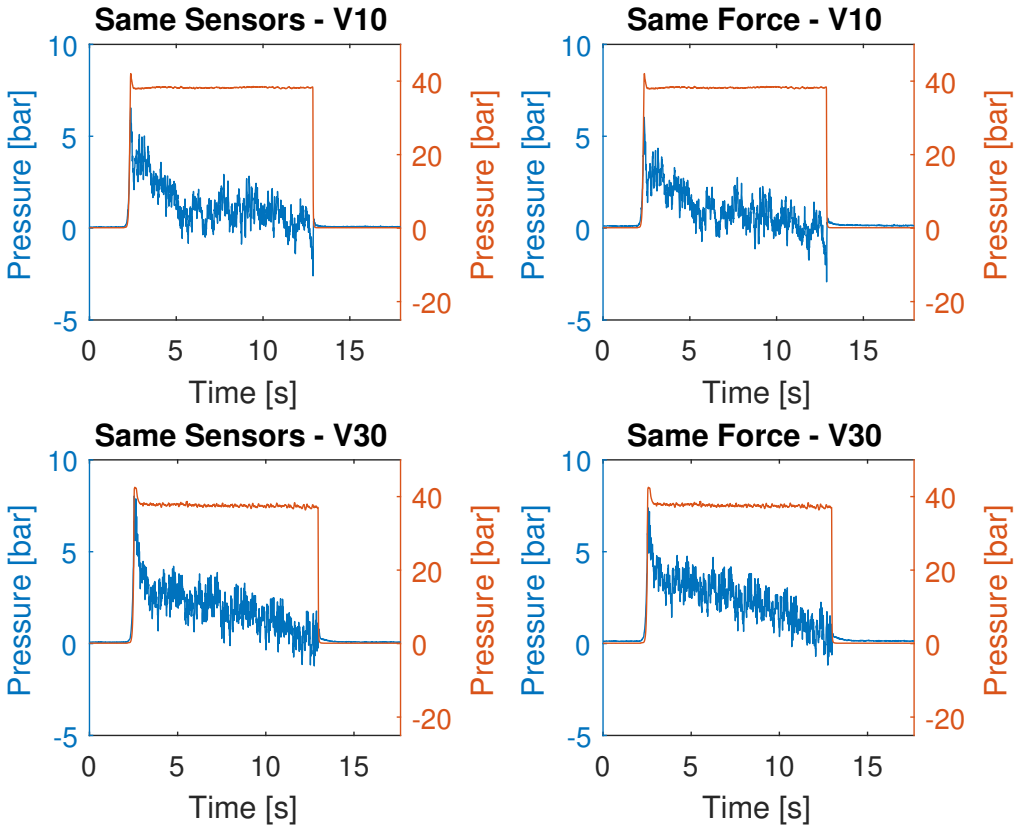

Figure 47: Estimated P_{diff} (left axis) for step pressure responses (right axis).

The measurements indicate that a pressure loss is present, which is initially high but decays over time. This suggests that the lamellas creep towards steady state over time as the actuating pressure is kept constant. According to Hypothesis 1(c) it was expected that the rear lamella would "get stuck" in a compressed state at negative pressure transients. However, this is not supported by the data as there is no remaining P_{diff} when the actuating pressure is reduced to zero.

5.6.2 Incremented Step Analysis

While the step analysis covered a discussion of both hypotheses, in center of discussion of the incremented step analysis is instead only Hypothesis 1. In line with the hypotheses the following behavior are expected:

- According to Hypothesis 1(a-b) a positive pressure difference is expected when the pressure is incremented. As the losses are expected to be a function of torque (which changes with applied pressure in the steps), the increasing torque magnitude at the time when the actuating pressure is increased should lead to an increase in P_{diff}.
- According to Hypothesis 1(c) a negative pressure difference is expected when the pressure is decremented. Using the same logic as above, the pressure differences should vary in magnitude depending on torque state.

In Figure 48, the estimated P_{diff} (by both estimation methods) based on FF sensor measurements for incremented step responses (sequence 2 in Test Session 1) is presented.

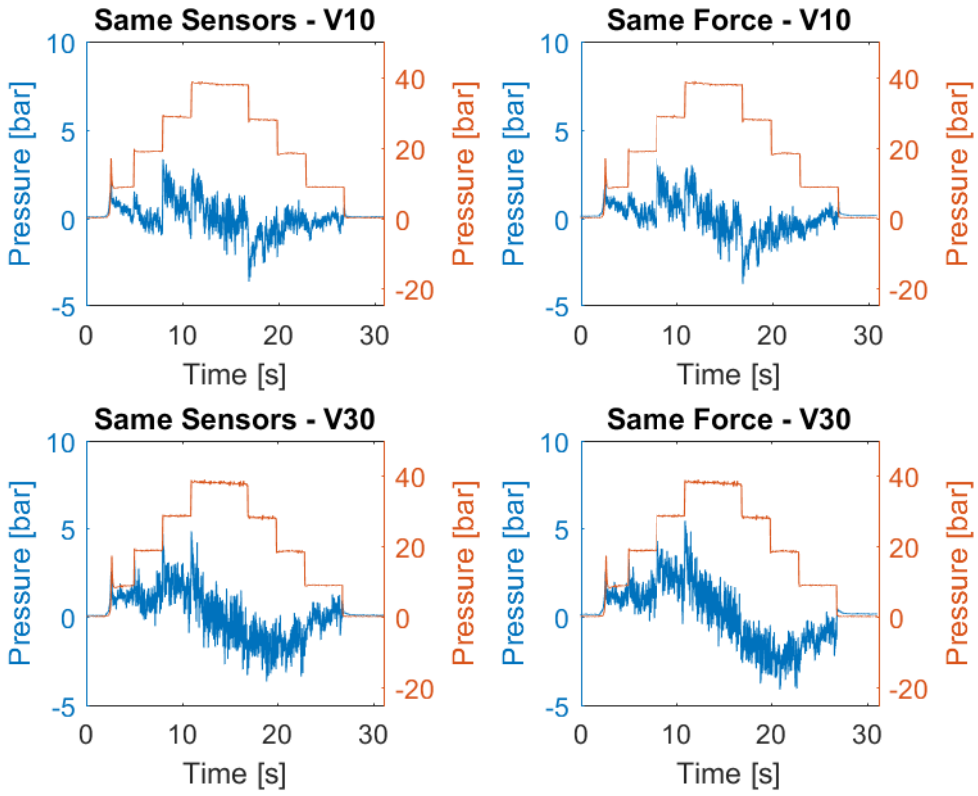

Figure 48: Estimated P_{diff} (left axis) for incremented pressure step responses (right axis).

According to the result, arguments can be made that the dynamic behavior of Hypothesis 1 is likely confirmed. At positive increments of actuating pressure, a positive P_{diff} is present while the opposite is true for decremented steps. It is also noticeable how the losses are greater at high torque states. To truly confirm Hypothesis 1 the pressure losses must also be linked to a difference in torque. More specifically it should be confirmed that a higher torque is measured for the decremented steps than for the incremented steps. The complications of this comparison is that the friction coefficient (and thus torque) is temperature dependent and that the temperature is significantly higher during the time of decrements than increments due to the coherent run. It was also noticed that even though the pressure request levels for decrements and increments were equal, the measured actuating pressure differentiated. For those two reasons, the torque data was normalized against the temperature and the measured actuating pressure (by assuming a proportional relationship between torque and pressure). The result is presented in Table 5 as a percentage of increase in mean torque level at matching decremented vs incremented step levels.

Table 5: Percentage of increase in torque for decremented vs incremented step levels (Torque data normalized against temperature and actuating pressure).

Session	Pressure level 1	Pressure level 2	Pressure level 3
10 rpm	1.1%	0.15%	1.8%
30 rpm	5.7%	4.8%	3.5%

5.6.3 Ramp Analysis

Just as for the incremented step analysis, the ramp analysis will mainly focus on Hypothesis 1 with the same behavior of lamella pressure losses expected. The measured P_{diff} for FF sensor ramp responses (sequences 3-5) is presented in Figure 49.

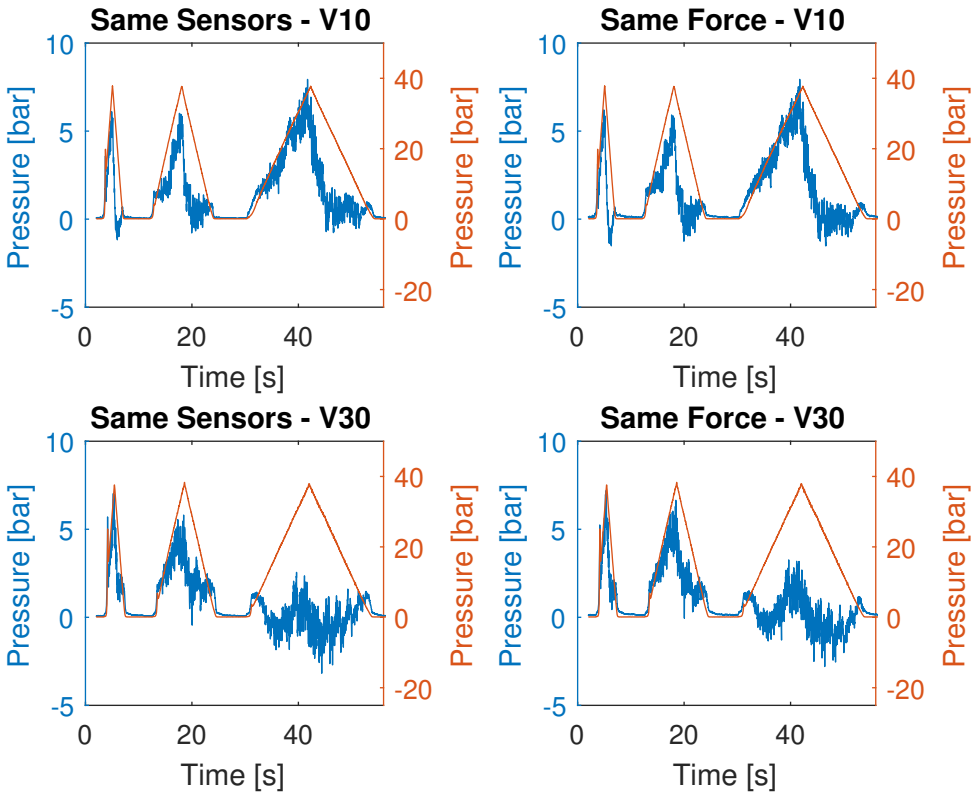

Figure 49: Estimated P_{diff} (left axis) for ramp pressure responses (right axis).

The data shows the similarities with the incremented step data, but also differences. First of all, an increased positive pressure difference can be noticed during the actuating pressure rise time for most runs. This dynamic behavior was also recorded for the incremented step runs and expected according to Hypothesis 1(a-b). During decreasing actuating pressures, the front and rear pressure differences drop down close to zero for most runs. Worth noting is that few negative pressure differences were measured. This demonstrates a difference in lamella pack dynamics when the actuating pressure drops from a steady state value as a step as in previous section compared to when

the actuating pressure goes from a positive ramp to a negative ramp instantly. The data suggests that during a ramp drop, the lamella does not tend to get stuck in a compressed state as suggested by Hypothesis 1(c).

Table 6: Percentage of increase in torque of negative vs positive ramp dynamics (Torque data normalized against to temperature and actuating pressure).

Session	4 second ramp	12 second ramp	24 second ramp
10 rpm	5.8%	3.4%	11.4%
30 rpm	2.75%	0.14%	8.9%

5.6.4 Hypothesis Analysis Conclusions

To conclude the results presented in the above sections and in Figures 47, 48, 49 and Tables 5 and 6 they speak towards Hypothesis 1 being true since there is a noticeable correlation between P_{diff} and torque. Secondly, they also indicate that a larger pressure difference appears for the 30 rpm- than for the 10 rpm runs which in line with the hypothesis should result in greater torque differences for the 30 rpm run. As the result shows, this is also the case.

Since there were not as many conclusions drawn towards (for or against) Hypothesis 2 based on the tests conducted in this thesis, the model proposal in the next chapter is only based on Hypothesis 1. It is believed that the main reasons for limited conclusions towards (for or against) Hypothesis 2 is the two following reasons:

1. First of the fact that the novel measurement technique performed in this thesis, namely the FF sensors, introduced a method towards measuring dynamics of forces within the lamella pack, which was strongly related to Hypothesis 1. The indications of Hypothesis 2 were considered harder to measure.
2. Secondly, since factors affecting the oil film were harder to isolate. This was largely due to limitations in the used testing rig, since its locked outgoing shaft was believed to make the oil flow and quality of the oil film difficult to control. See Section 4.4 for motivation of chosen test rig.

6 Model Proposal

6.1 Mathematical description

The proposed model is based on a combination of physical modeling and identification techniques. The fundamental properties are illustrated in Figure 50, where $F_{act} = P_{act} \cdot Area$ is the actuating force, z_n, k_n, c_n and F_{fn} is the displacement, spring constant, damping coefficient and spline frictional force respectively, for lamella n.

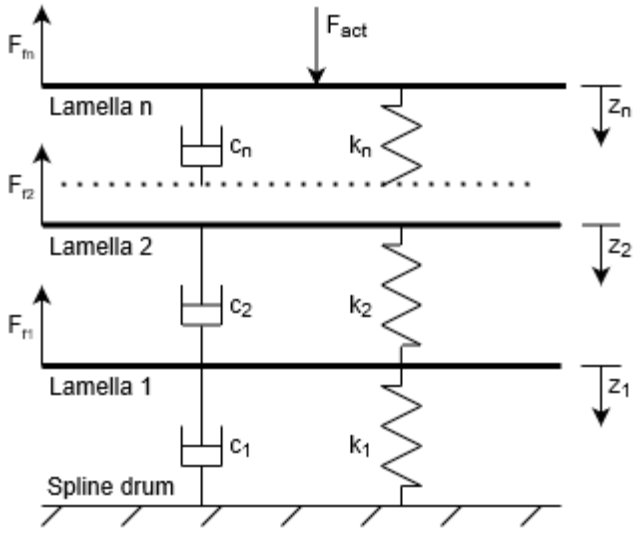

Figure 50: Free body diagram of lamella pack.

Each lamella is assumed to have a spring force, a damping force and a spline friction force acting on its body. The lamellas are enumerated from the rearmost lamella and forward. Thus, the actuating pump pressure is applied on lamella n. The test performed during the thesis will serve as data input to the model fitting. As all lamellas in theory are identical in terms of physcal properties, as goes for the oil between each lamella to disc interface; the spring constant, lamella mass and damping coefficient is assumed equal through the entire lamella pack.

Due to the large number of states in a 8 lamella clutch, the following state space example is presented for a 3 lamella clutch. Since lamella $z_2 \rightarrow z_{n-1}$ share the same principles of dynamic physical description, the 3 lamella model can easily be derived to an 8 lamella model.

$$m\ddot{z_1} = k(z_2 - z_1) + c(\dot{z_2} - \dot{z_1}) - F_{f1} - kz_1 - c\dot{z_1} \tag{11}$$
$$m\ddot{z_2} = k(z_3 - z_2) + c(\dot{z_3} - \dot{z_2}) - F_{f2} - k(z_2 - z_1) - c(\dot{z_2} - \dot{z_1}) \tag{12}$$
$$m\ddot{z_3} = F_{act} - F_{f3} - k(z_3 - z_2) - c(\dot{z_3} - \dot{z_2}) \tag{13}$$

By a change of variables according to Equation 21:

$$x_1 = z_1 \tag{14}$$
$$x_2 = \dot{z_1} \tag{15}$$
$$x_3 = z_2 \tag{16}$$
$$x_4 = \dot{z_2} \tag{17}$$
$$x_5 = z_3 \tag{18}$$
$$x_6 = \dot{z_3} \tag{19}$$
$$u_1 = F_{act} \tag{20}$$
$$u_2 = F_{fn} \tag{21}$$

Equation 11, 12 and 13 can instead be represented in state space form:

$$\dot{x} = Ax + Bu \tag{22}$$
$$y = Cx \tag{23}$$

where:

$$A = \begin{bmatrix} 0 & 1 & 0 & 0 & 0 & 0 \\ -k/m & -c/m & k/m & c/m & 0 & 0 \\ 0 & 0 & 0 & 1 & 0 & 0 \\ k/m & c/m & -2k/m & -2c/m & k/m & c/m \\ 0 & 0 & 0 & 0 & 0 & 1 \\ 0 & 0 & k/m & c/m & -2k/m & -2c/m \end{bmatrix} \tag{24}$$

$$B = \begin{bmatrix} 0 & 0 \\ 1/m & -1/m \\ 0 & 0 \\ 0 & -1/m \\ 0 & 0 \\ 0 & -1/m \end{bmatrix} \tag{25}$$

$$C = \begin{bmatrix} 1 & 0 & 0 & 0 & 0 & 0 \\ 0 & 1 & 0 & 0 & 0 & 0 \\ 0 & 0 & 1 & 0 & 0 & 0 \\ 0 & 0 & 0 & 1 & 0 & 0 \\ 0 & 0 & 0 & 0 & 1 & 0 \\ 0 & 0 & 0 & 0 & 0 & 1 \end{bmatrix} \tag{26}$$

6.2 Friction Model

Based on Section 2.1.1 about friction theory and Section 2.2 about the current Borg-Warner model, it is known that the friction coefficient is a function of several parameters. For the clutch setup tested during this thesis, the two following parameters could be noticed of having an effect on the friction coefficient:

- **Temperature dependence** - The temperature dependence of the friction coefficient is assumed to decay linearly as described in Section 2.1.1 based on data inherited from BorgWarner.
- **Normal force** - As presented in Section 2.1.1, the normal force generally has a low influence on friction, and if any the friction coefficient is generally increasing with normal force. The test session performed during this thesis suggests the opposite with an decrease of friction of approximately 5% at 40 bar of actuating pressure. A linear scaling of the friction coefficient is thus used in the model with a frictional loss of 0% at 0 bar and 5% loss at 40 bar.

6.3 Computation of Torque

What is considered affecting torque from the model is the spring force acting on each lamella. The damping force is considered a pure loss since it is believed to mainly be a consequence of oil viscous effects. As described in Section 2.1.1, the oil can transfer torque through viscous drag but within the scope of the model this factor is neglected. With this assumption the torque can be computed according to Equation 27 where μ is the frictional coefficient, R_e is the effective radius and N is the number of lamellas. The multiplication of 2 comes from each lamella having two friction surfaces.

$$T_{out} = 2\mu R_e \sum_{n=1}^{N} (k(z_n - z_{n-1})) \tag{27}$$

Unlike Equation 1 which describes the torque from a one unit lamella pack, Equation 27 sums the frictional forces from each lamella individually.

6.4 Fitting of Dynamic Parameters

6.4.1 Spring Constant

As described in Section 2.1.2, an increased axial spring constant for increased compression is expected from a lamella pack. The linear state space model requires linear representation of state variables i.e the system characteristics are independent of state values [23]. Therefore, the spring constant must be linearized. This is done around the high actuating pressure area since this is where the dynamics mainly are studied. However, it should be noted that a linear assumption of this kind also makes the model invalid for low actuating pressures.

The data of axial spring force is received from a 10 lamella pack. Since the proposed model assumes one equal spring constant per lamella, with the springs connected in a series, the data of the 10 lamella pack is transposed to single lamella spring constant according the Equation 28.

$$k_{lamella} = 10 \cdot k_{lamellapack} \tag{28}$$

6.4.2 Damping Coefficient

As stated in Section 2.1.2, no data of a damping coefficient c was inherited nor gathered during the thesis. For this reason, the damping coefficient is entirely based on estimations from sampled data of the clutch.

Assuming no frictional forces acting on the lamellas and a spring force in the magnitude of measures referred to in previous section, it can be shown that the damping coefficient has a minor effect on the difference in normal force from lamella to lamella for the studied frequency bandwidth. This indicates that the result presented in Section 5.6 cannot simply be explained through damping effects. The damping coefficient is however affecting the time constant of the torque output (assuming the earlier stated assumption that only spring forces affect torque). Therefore, the estimation of the damping coefficient is done by analysing the torque time constant at step inputs. As the spline friction losses also affect the time constant of the torque response, fitting of the damping coefficient is done coherently with the spline friction losses fitting.

6.4.3 Spline Friction Losses

In Section 5.6, it was discussed how the pressure differences between the front and rear lamella could be a source of torque hysteresis. It could be seen that during positive P_{diff} a lower torque was measured than during negative P_{diff} for the same actuating pressure. This was also what Hypothesis 1 expected. As described in the previous section, the damping effects of the system have minor effects on lamella normal force losses from lamella to lamella. This indicates that the measured P_{diff} is a result of other types of losses, or as suggested: losses from spline friction. The main philosophy of the spline friction model is thus to utilize the dynamic properties of the measured P_{diff} and transform it to a force acting on individual lamellas. The gathered data of P_{diff} is thus also used as fitting data for the loss functions.

Two kinds of models of the spline friction losses are considered:

1. A torque dynamic friction function fitted to P_{diff} with Gaussian-Newton optimization.
2. A viscous friction function fitted manually to P_{diff} through iterative simulation.

Since the spline losses are expected to be physically related to transmitted torque, both functions uses torque as an input. Further explanation of each function are:

1. **Torque dynamic friction function** (also referred to as F_f-T)

   The data of pressure losses are presented in Figure 47, 48 and 49. From this data, noticeable dynamics were:

   (a) Asymptotic stability: $P_{diff} \to 0$ when $t \to \infty$.
   (b) First order dynamics: Single exponential decay of P_{diff}.

A transfer function fulfilling these criteria and thus proposed are.

$$F_f = (\frac{\tau s}{\tau s + 1})\kappa T = (1 - \frac{1}{\tau s + 1})\kappa T \tag{29}$$

A block diagram representation of Equation 29 can be seen in Figure 51.

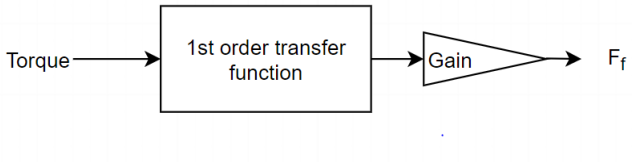

Figure 51: Block diagram illustration of F_f-T.

Equation 29 is a first order transfer function with one pole ($= -\frac{1}{\tau}$) and one zero ($= 0$). The variable τ sets the bandwidth which in general determines how quickly the system responds to input changes [19]. Thus τ can be interpreted as of how quickly P_{diff} decays over time. This is illustrated in Figure 52 where Equation 29 is plotted for $\tau = 1$ and $\tau = 3$.

The gain of Function 29 is determined by κ which also can be considered as a conversion from pressure to force. By fitting Equation 29 to the dynamics of P_{diff}, not only the dynamics will be caught, but also the magnitude. The proposed model is built on the principle that a force F_f is affecting single lamellas. The pressure difference P_{diff} is however a measurement of the total pressure loss from front to rear lamella. It is unknown if the pressure transient in between the front and rear lamella is linear or nonlinear. Thus an assumption must be made and for this model it is assumed that the pressure transient is linear. Ultimately, it is then also assumed that the force loss transient is linear and thus F_f can be viewed as a proportional function to the fitted function, scaled by κ.

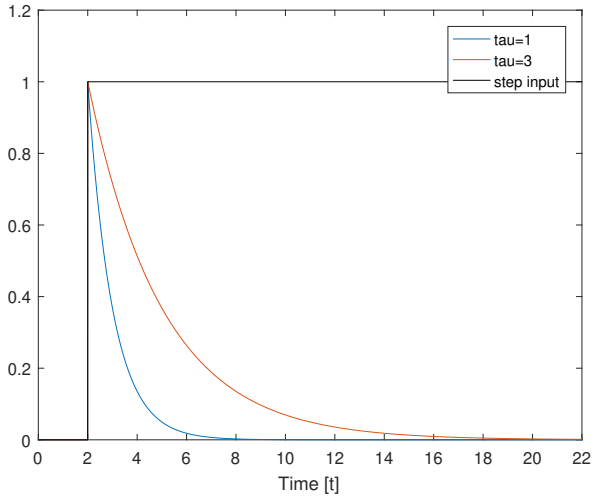

Figure 52: The step response of Equation 29 for two different values of tau.

The fitting process of Equation 29 is done with P_{diff} as fitting data. With the help of the Matlab System Identification toolbox, an estimation of the parameters could be done. The toolbox uses Gaussian-Newton optimization to optimize a transfer function of specified order to data [24]. This was done for Equation 29.

2. **Viscous friction function** (also referred to as F_f-V)

The viscous friction function is based on the friction modeling theory presented in Section 2.2.3 and assumes that the frictional force is a function of lamella to spline drum interface velocity and is linearly scaled with torque as torque in theory is proportional to the contact normal force. The function uses individual lamella velocity and thus takes into account the lamella states unlike F_f-T that is a pure transfer function of torque. The force acting on each lamella can mathematically be described according to the Equation 30.

$$F_{fn} = T\kappa \frac{1}{\tau s + 1} \dot{z_n} \tag{30}$$

The transfer function in Equation 30 is a low pass filter that is used to fit the time constant of the function to match measured P_{diff} and to filter high frequencies of $\dot{z_n}$. κ is used to scale the frictional force and τ sets the bandwidth of the transfer function, similar as for F_f-T. To illustrate, a block diagram of Equation 30 can be seen in Figure 53.

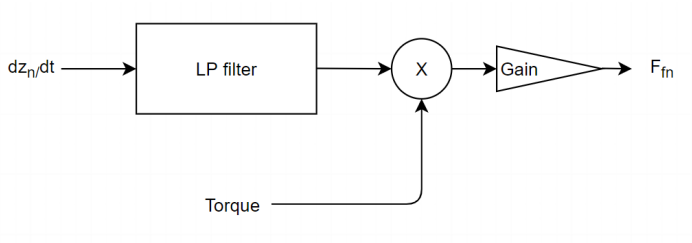

Figure 53: Block diagram illustration of F_f-V.

With similar reasoning as when choosing fitting data for the FF-estimation (fitting data that covers all dynamic properties of the system are desirable), the incremented step (test Sequence 2) data was chosen as fitting data. One fit each was done for the 10- and 30 rpm sessions with the purpose of catching potential ω_{diff}-dependent dynamics.

6.5 Validation of Model

The models are validated toward the same pressure inputs as used in test session 1. As models based on identification methods in general tend to have a bias towards fitted data, validation is generally done on data not used in the fitting process. In Figure 54 the fitted spline force models are compared to both fitting data (incremented step) and validation data (step and ramps). As expected, the models also seem to be biased toward sequence 2 data. As this was used as fitting data, this was expected. Notice that this plot only illustrates the fit of the spline friction loss-models to the measured pressure losses, not the fit of the torque model to torque measurements. It is thus of interest to validate not only the overall fit of the torque model to data, but also compare how the spline friction loss-models is translated into accuracy of the torque model for biased versus non-biased data. If the overall philosophy of the models are correct, a good fit of spline friction losses should translate to a good fit of torque.

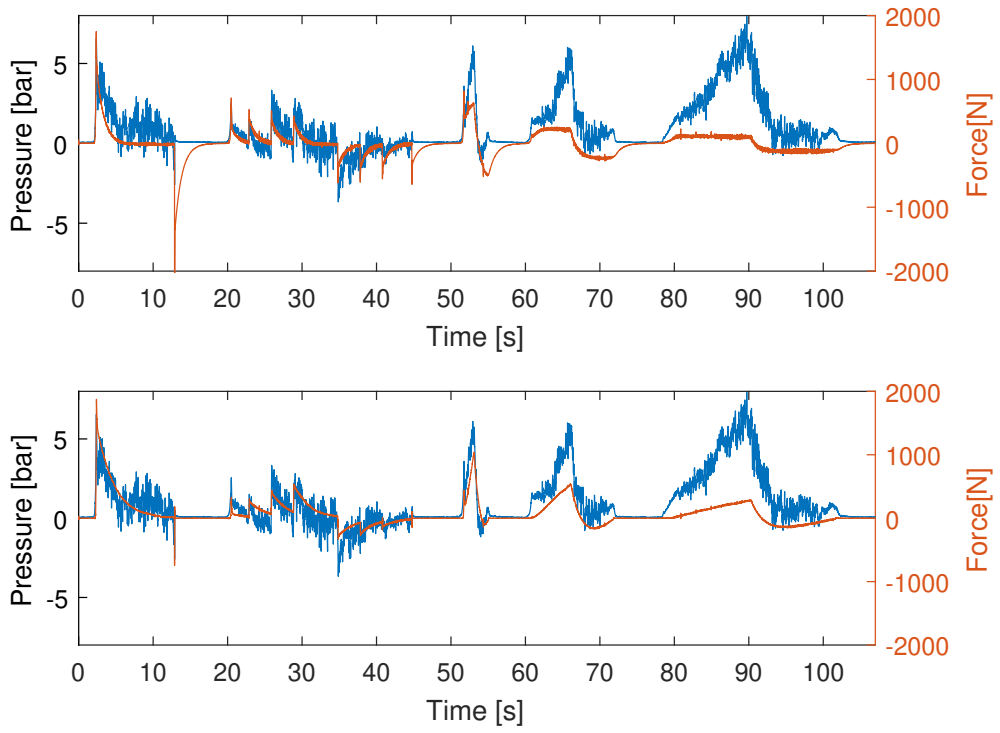

Figure 54: Lamella force difference based on F_f and lamella pressure difference (P_{diff}) for a ω_{diff} of 10 rpm. Top plot: F_f-T model, bottom plot: F_f-V model.

Similar results of the fitted models as for the 10 rpm session is seen in the 30 rpm session, which can be seen in the Appendix, Section 8.5. By comparing the two models presented, it can be concluded there is a difference in dynamic behavior. This is especially noted during rebound. A summary of the main aspects of notation from Figure 54 are:

- **Step** - The overall dynamics of both loss functions and P_{diff} fit well at the actuating step input and during the actuating pressure hold time. It can be noted at the end of the step input (during the instant drop of actuating pressure) that, F_f-T is inaccurate in its estimation losses. F_f-T estimates large losses while P_{diff} diminish to zero instantly. The dynamic properties of the F_f-T transfer function, simply does not handle transients to zero torque well. F_f-V does however handle this type of dynamics better. This is due to the proportional scaling of F_f-V against torque. As torque decreases to zero, the estimated forces therefore quickly diminish to zero as well.
- **Incremented step** - It is obvious that the dynamics of the friction force models fits the incremented step session best, as expected (since this was used as fitting data). F_f-T misses an adjustment factor that regulates the losses according to torque level. It can be noticed in the P_{diff}-data that higher losses occur during transients from high torque states. This is not reflected for F_f-T. It can be seen that F_f-V covers this type of dynamics; once again due to the proportional scaling against torque.

- **Ramp** - The simulated F_f-losses of ramps clearly illustrate the main differences between the two models. During a ramp, the actuating pressure quickly goes from a positive- to a negative transient. Thus, the lamellas are in constant movement i.e in transient states during the whole ramp. As F_f-T is a pure transfer function of torque, it does not take lamella states into account when modelling friction forces. This is an essential miss of dynamics since a frictional force needs to be initiated by some other force or motion. F_f-V uses the lamella states as an input to the frictional force estimation and does thus also estimates the dynamics of the losses during transient lamella states better.

  A weakness of both models seems to be the magnitude of loss estimation for slow transient dynamics. This is obvious for the slow ramp where none of the models are close to reach the measured loss magnitude. In section 2.2.3, models that assume a large breakaway frictional force were presented. A model of this kind would estimate larger forces for the low speeds than F_f-T and F_f-V and could therefore be an alternative to cover these dynamics better.

In Table 7 the fitted parameters for each F_f model can be seen.

Table 7: Fitted parameters for F_f-T and F_f-V.

Parameter	F_f-T 10 rpm	F_f-V 10 rpm	F_f-T 30 rpm	F_f-V 30 rpm
κ	0.3786	2	0.3705	2
τ	0.9434	2	1.9384	2.5

In terms of caught dynamics of losses, it can from the result above be concluded that F_f-V is the better alternative in comparison to F_f-T. This conclusion is entirely based on FF data which needs to be taken into consideration due to insecurities in sampling. Subsequently, the torque model is next tested for the different loss functions and evaluated through Torque Accuracy. The result of the models in terms of Torque Accuracy is shown in Figures 55 and 56.

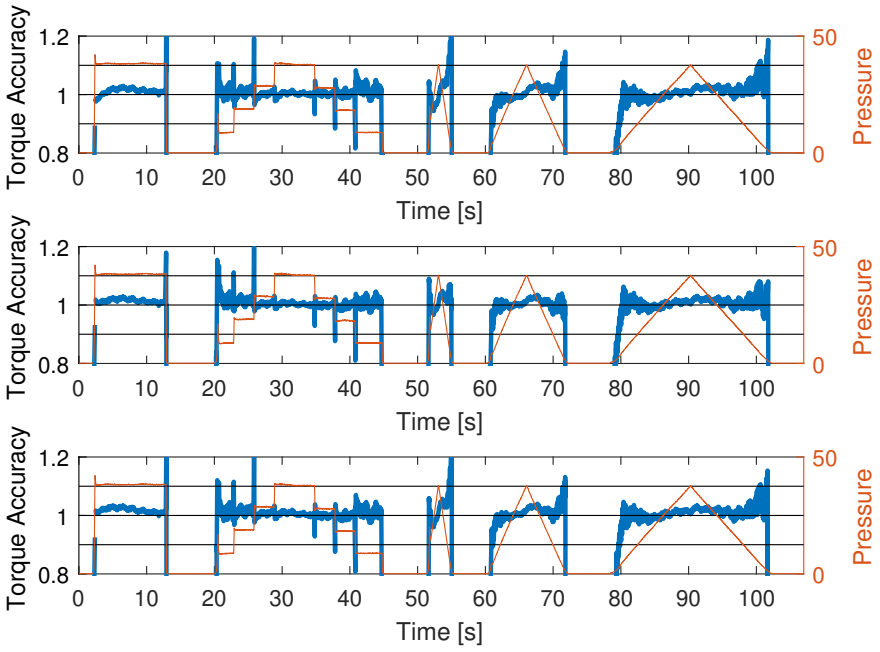

Figure 55: Torque Accuracy of reference (steady-state) model (top plot), F_f-T - model (middle plot) and F_f-V - model (bottom plot) for 10 rpm data.

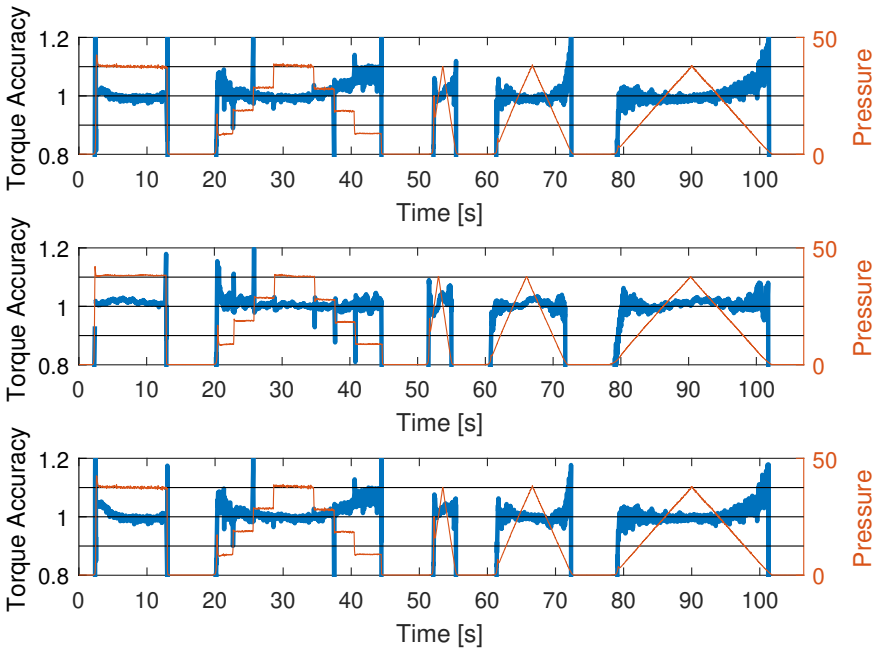

Figure 56: Torque Accuracy of reference (steady-state) model (top plot), F_f-T - model (middle plot) and F_f-V - model (bottom plot) for 30 rpm data.

In Figure 57 the RMSE values for each sequence is displayed, where the error is calculated as $T_{measured} - T_{model}$. As a reference, the RMSE value for a model assuming

no frictional spline forces is used. The RMSE values are important to study since it gives a quantitative measurement of the result. The torque accuracy plots can give a visual hint of performance but is however more sensitive for errors during low- than for high torque levels which may portray a skewed visualization of performance if not examined critically.

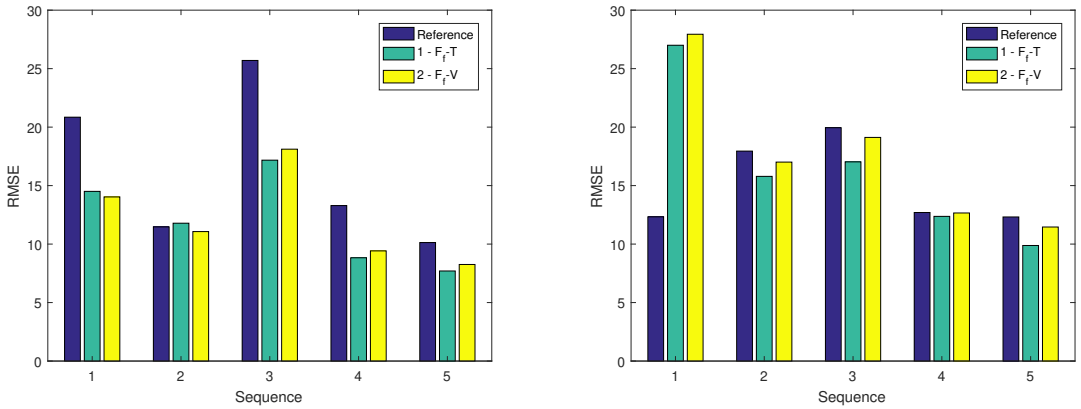

(a) RMSE values for sequences during ω_{diff} 10 rpm.

(b) RMSE values for sequences during ω_{diff} 30 rpm.

Figure 57: RMSE values.

Overall, a decrease in RMSE values can be noticed for F_f-T and F_f-V in comparison to the reference model. This is an indication that there is a correlation between Hypothesis 1 and dynamic properties of the torque transfer. One exception is sequence 1 for the 30 rpm run where the reference model has a significant lower RMSE value. For this specific run, the torque response was close to proportional to the actuating pressure while for all other runs, the torque response had a significant degree of time dynamics. This can also be noticed in Figure 46 in Section 5.6. An overall trend of decreased time dynamic properties could be noticed for higher rpm runs which also is shown in the RMSE values. The physical explanation to this trend cannot be confirmed but it is suspected that higher rpm runs impose more power, vibrations and higher temperatures which are believed to both raise the degree of stochasticity (due to vibrations of two frictional contact surfaces) and introduce dynamics which are not accounted for in the models presented in this thesis.

A contradictory result in comparison to the loss function validation is that the F_f-T model have a better torque accuracy and lower RMSE value than F_f-V, even though F_f-V is considered to have a higher correlation to P_{diff} in dynamic properties. The difference can mainly be noticed in Figures 55 and 56 for the ramp data, where the rebound dynamics are better caught for the F_f-T model. The difference between the models during the ramps, as can be seen in Figure 54, is that F_f-T estimates larger negative frictional losses during rebound. This type of losses could not be seen in the P_{diff} data. A similar trend can be seen at the rebound for the incremented steps where F_f-T better estimates the torque due to higher negative losses.

To conclude, as stated above, it is believed that F_f-V has a better correlation towards P_{diff} based on desired dynamics according to Hypothesis 1 than F_f-T. At the same time, F_f-T results in a better Torque Accuracy, which seems contradictory. The reason for this is believed to be that neither F_f-T nor F_f-V are good enough models to describe the frictional force dynamics in general. The results presented above are therefore not enough to draw any conclusions regarding the validity of one model versus another. This also means that although we could see some improvements in torque accuracy, we cannot conclude that they are better models in general compared to a steady-state model. However, as stated, the purpose of these models were not to be comprehensive for all driving scenarios, but rather to investigate the correlation between hypotheses and data, which was done to some degree. Subsequently, it is believed that the models are good enough to support Hypothesis 1 and to motivate the continuation of modeling these dynamics.

7 Discussion

7.1 Sources of Error

There are several possible sources of error in this study. Some of the most noteworthy are:

1. As the FF sensors were damaged and the calibration unsuccessful, no absolute force measurements could be made. Although some clear errors in the data was found and discarded, it is still unknown if- and in that case how much the sensors have altered in behavior during the tests resulting in the kept data. Although the mathematical estimation methods used based on two separate assumptions were shown to render similar results and believed to be good enough in terms of indicating clutch dynamics, these tests should be remade with a successful calibration to ensure the conclusion of Hypothesis 1.
2. As stated in Section 4.1.1, the FF sensors were not recommended to be immersed in any liquids or oils, due to internal venting channels. This, on top of the fact that the FF sensors were stressed outside of their rated force range has likely caused their variation in performance. As there are custom sensor designs with internal venting available to seal the sensor from harsh environments, these might be interesting to try. Another solution may be to calibrate the sensors towards temperature and/or oil exposure.
3. Another possible source of error is the possible introduction of new dynamics by installing the FF sensor. This could be tested by performing the same tests without the sensors installed and comparing the test results in terms of torque output.
4. As discussed in Section 4.4 and 5.6.4, the usage of FF sensors limited the usage of rig setup to a locked outgoing shaft which had an influence on oil circulation and lubrication of lamellas and steel plates. I.e. it is certain that the rig is not fully descriptive of real driving scenarios in the intended application of an AWD vehicle. No results presented in this thesis are confirmed for vehicle applications, which they would need to be in order to be concluded with certainty.

7.2 Conclusions

As mentioned in Section 2.1.1, clutches are complex and difficult to model since there are several colliding fields such as solid mechanics, contact mechanics, fluid mechanics, thermodynamics, chemistry, material sciences, physics and more. It is clear that there are several factors which affect the torque output of the clutch, both individually and by cross-correlations, and it is therefore likely not one single aspect which has a negative effect on the Torque Accuracy, but rather a combination of several factors. One must also remember that in practice, there is no such a thing as a perfect model. It is however believed that the Torque Accuracy can be improved by these kinds grey-box modeling techniques in this case, but to what extent is unknown.

Referring to Section 1.2, the stated goals of this thesis (**in bold**) and underneath our results, conclusions and achieved degree of fulfillment regarding these goals are:

1. **The first goal was to identify the dynamic behavior of the lamella pack and its correlation towards the torque output of the clutch. This was the primary goal of the thesis as it would lead to a greater understanding of the product at a mechanical degree.**

   Hypothesis 1 related to spline friction losses is a cause to certain torque dynamics. It is however not believed to be the only cause accounting for the Torque inaccuracies. For example, it is believed to be the main explanation for Torque inaccuracies in Test A, but not in Test B.

   Hypothesis 2 related to oil film reduction is believed to hold at least some truth. It is however believed that, based on the tests conducted in this thesis, Hypothesis 2 is not believed to be a cause for torque inaccuracies as long there is any ω_{diff} in the clutch, above a certain degree. This conclusion is mainly based on analysis based on previous tests as few notations regarding this hypothesis could be made from tests performed within this thesis.

   As there are Torque inaccuracies still remaining, it cannot be ruled out that there are other dynamics present than discussed in this thesis.

2. **The second goal was to propose a model which based on physical characteristics describes the found dynamics of the clutch. This was considered a desired but not critical goal since modeling is a work process which takes time to tune and incorporate in the product software in a desirable manner.**

   Two versions of a mathematical model assuming each lamella to be affected by a spring force, a damping force and a spline friction force acting on its body was suggested. One of these versions was shown to increase torque accuracy on tested data.

3. **The third goal was to implement the model in the control algorithm and validate it in car and rig. This was the final goal which was considered very ambitious and unlikely to be realized due to the time constraints of the project.**

   This goal was never approached, mainly due to time constraints.

7.3 Future Improvements and Recommendations

Even though no absolute force measurements could be guaranteed in this thesis, the authors believe that these should be possible to obtain with accurate and confident values using the FF sensors. To further investigate the dynamic properties of the lamella pack, it is therefore recommended to keep using the FF sensors in these applications. Although the relative P_{diff}-values are believed to be good enough in terms of being used as a basis to prove Hypothesis 1, they are not believed to be good enough in terms of being used as the sole data used for model fitting. More data (especially from in-vehicle tests) should be used to validate any model and used as a basis for model fitting before implementing in a commercial software.

For anyone interested in re-creating these tests, utilizing FF sensors in these (or similar) applications, or to further investigate the dynamic properties of a wet lamella clutch pack, the main improvements and recommendations from this thesis are to:

1. If a viable option for force-measuring sensors using chord-less telemetry is found, this should be used in a rig using two rotating axles as well as for in-vehicle tests.
2. Calibrate the sensors before the tests (as well as after). This way, even if a sensor starts to change in output, the data up until that point is safe. It also becomes easier to see if, when or how much they have deteriorated in performance. The reason why the calibration was not performed until after the tests in this thesis was simply because the machine used was not known to exist by the authors until after the tests had been performed and because no machine fulfilling requirements was found at BorgWarner.
3. Investigate improved attachment of sensor surfaces inside the clutch, such as other types of glue/epoxy for instance.
4. Pull out sensors straight out through rear clutch housing in order to reduce the tugging/pulling of the sensors during jerky movements during fast actuating and high Diff Omega - speeds.
5. Use Tekscans new custom-made pucks found using the following **link**. One might also want to try drilling out slots for the pucks in the thicker front- and rearmost lamellas to ensure better fastening.
6. Use clutches with more lamellas for increased variations of forces within the lamella pack. This way, the prevalence of spline friction forces should be higher and it may be possible to apply less forces (being less stressful for the FF sensors) while still experiencing the dynamic tendencies.
7. Perform the same (or similar) test sessions using voltage control of the actuating pump rather than pressure control. This would remove the pressure "kick" which may facilitate the drawing of conclusions.
8. Stop at top of pressure ramps for a few seconds, when testing. this way, steady-state values can be reached for the both positive and negative parts of the ramps which may facilitate the analysis.

9. Test Hypothesis 2 and oil film reduction in a rig-setup with 2 motors. Here, one could test the material permeability of oil in PBD scenario with both axles rotating but with 0 Diff Omega. This should then be compare to torque outputs from equivalent PBD-tests (possibly those from this thesis). It might be interesting to perform launched starts with a locked clutch to test Hypothesis 2. As it would be difficult to include the used FF sensors in this type of rig, these should either be replaced by other force-measuring sensors, or simply removed. These tests should also be repeated for driveshafts of different elasticity. One should also measure the axle-speeds close to clutch in these tests as a means to isolate the speed of the clutch as well as to further investigate the Diff Omega filtering.

8 Appendix

8.1 Test B

This section of the Appendix supplements Figures 18 and 19 in Section 3.2.

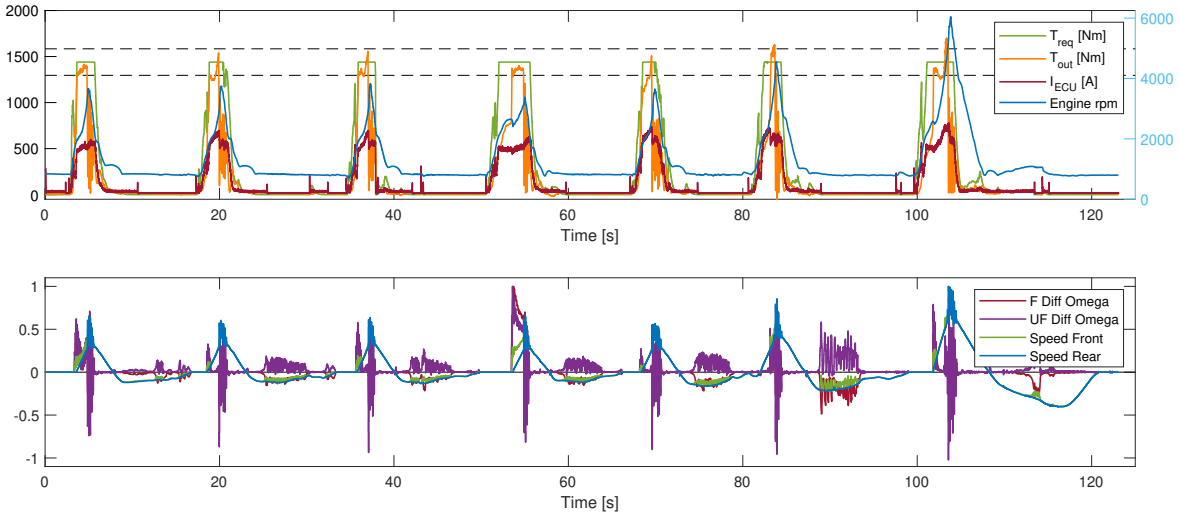

Figure 58: Test B - all data.

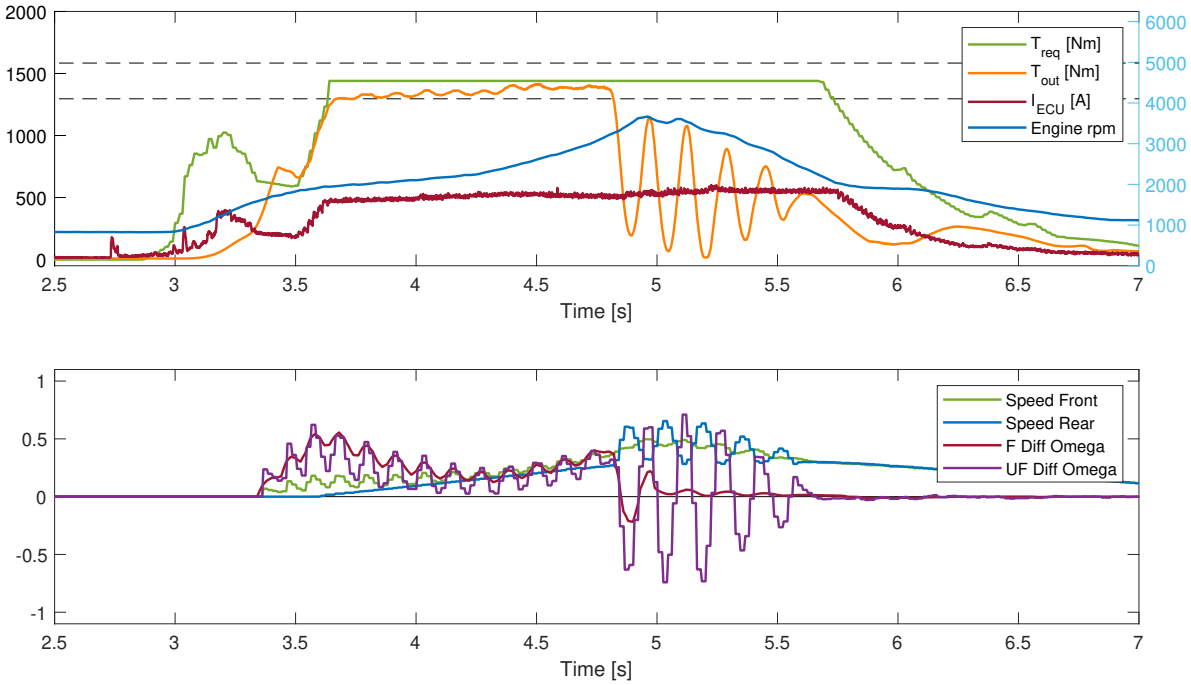

Figure 59: Test B - run 1.

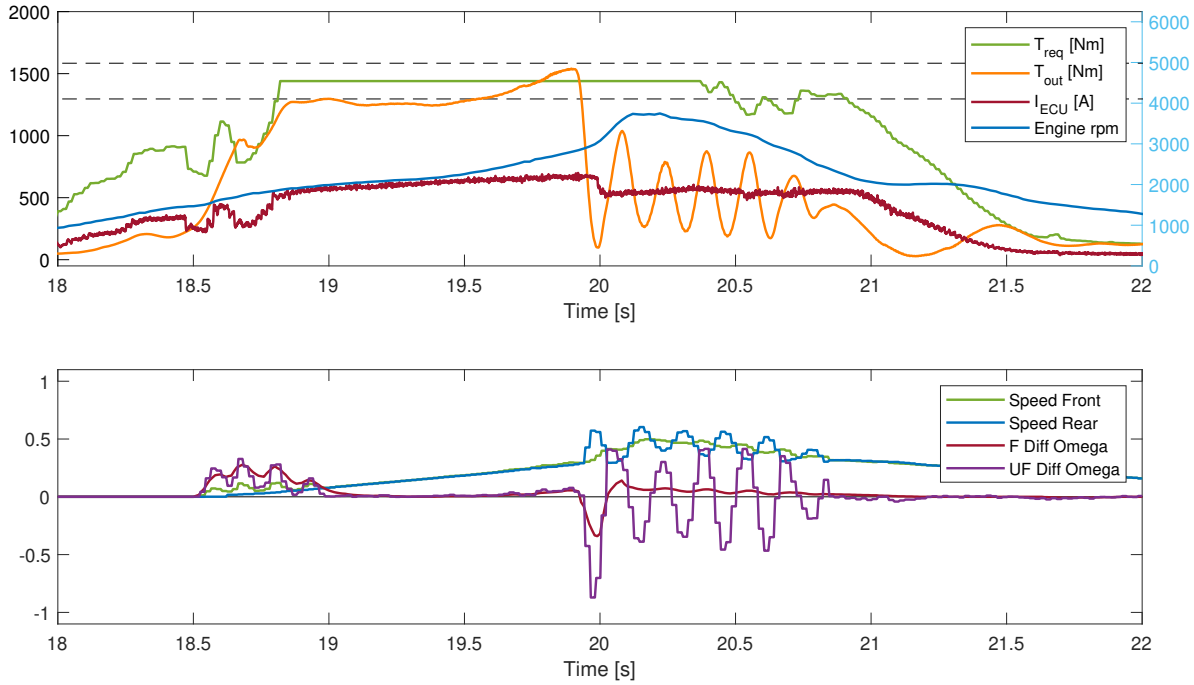

Figure 60: Test B - run 2.

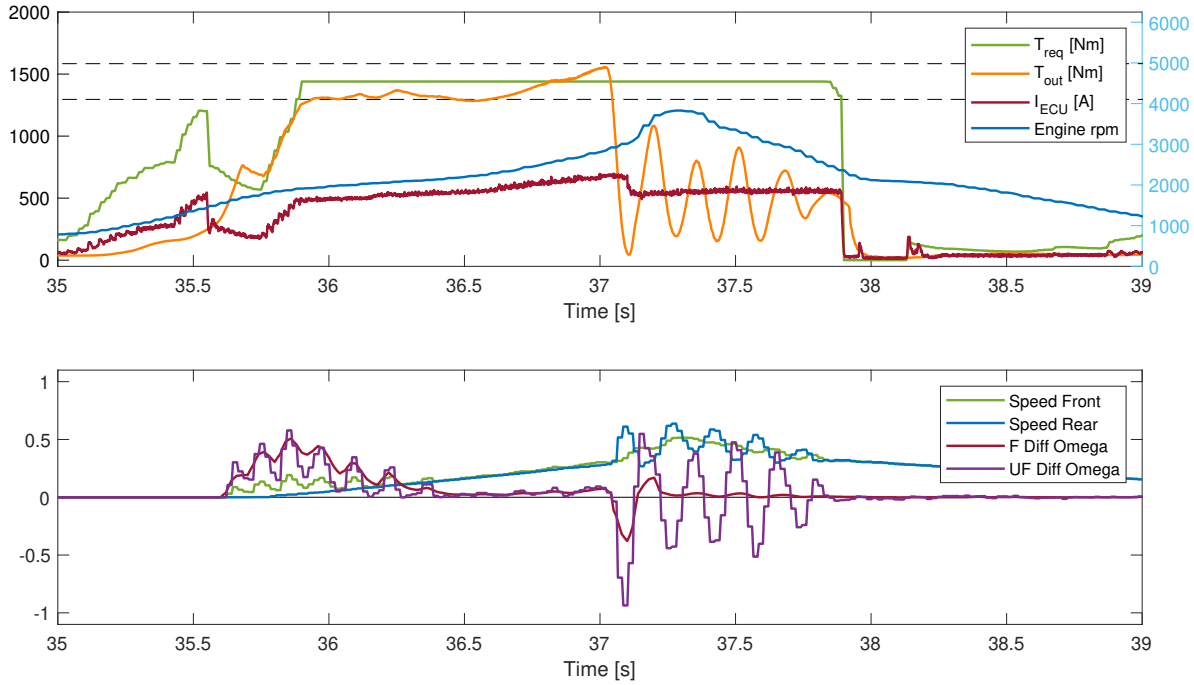

Figure 61: Test B - run 3.

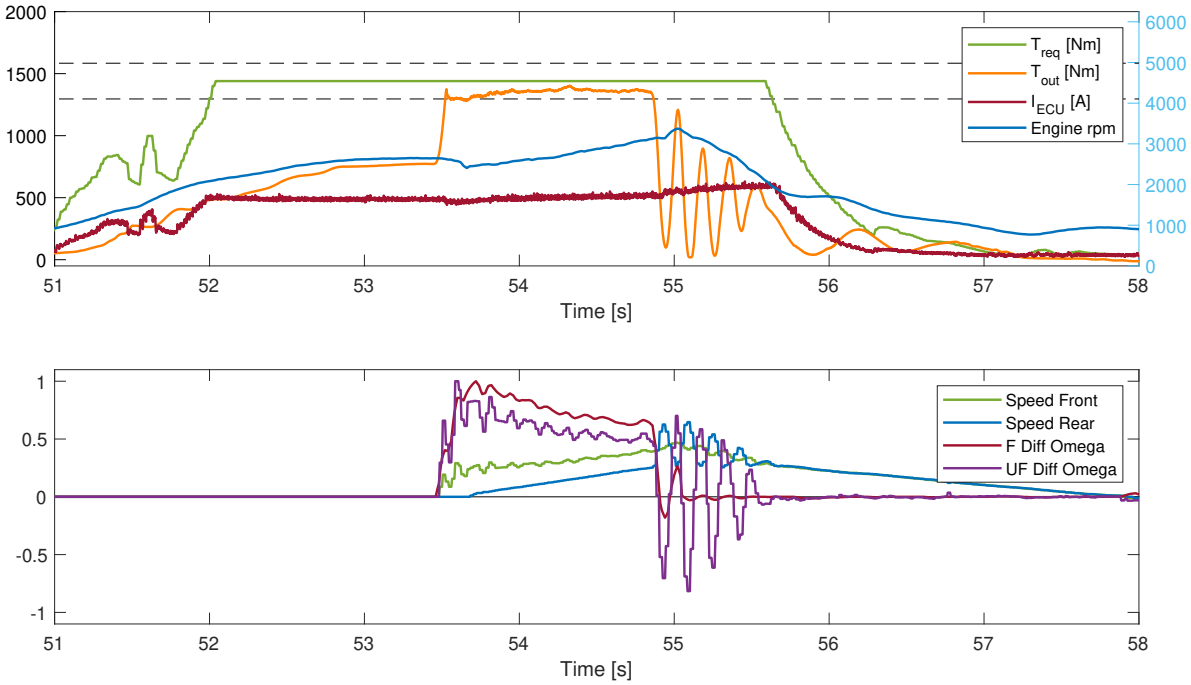

Figure 62: Test B - run 4.

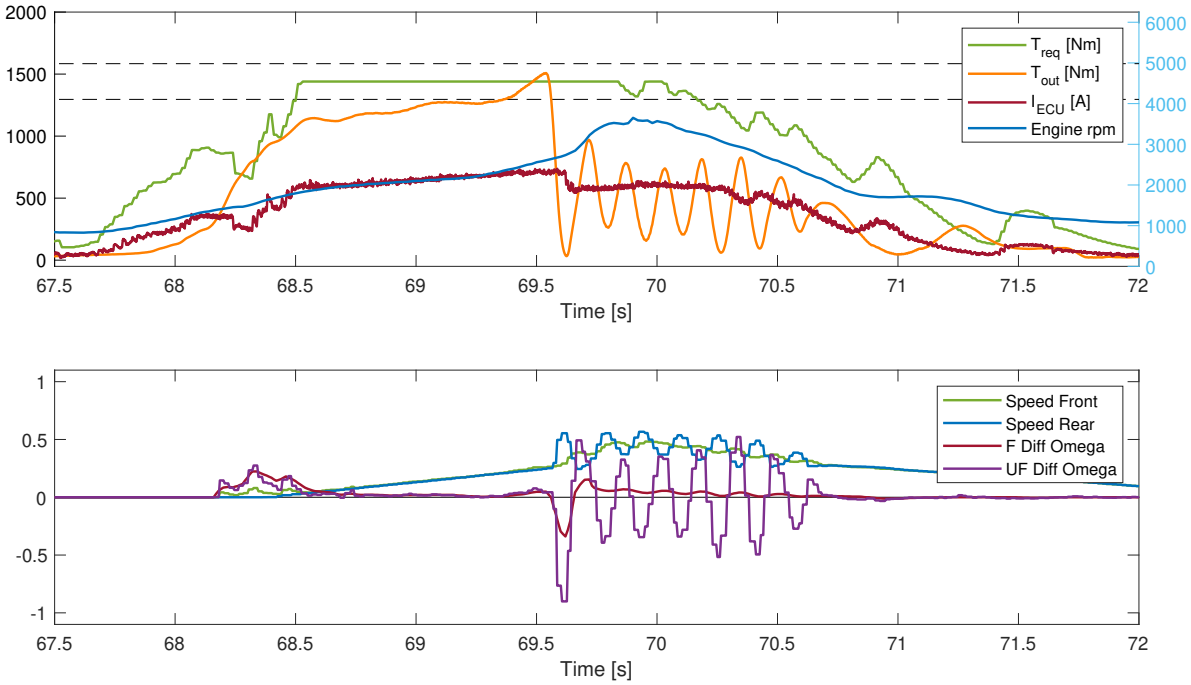

Figure 63: Test B - run 5.

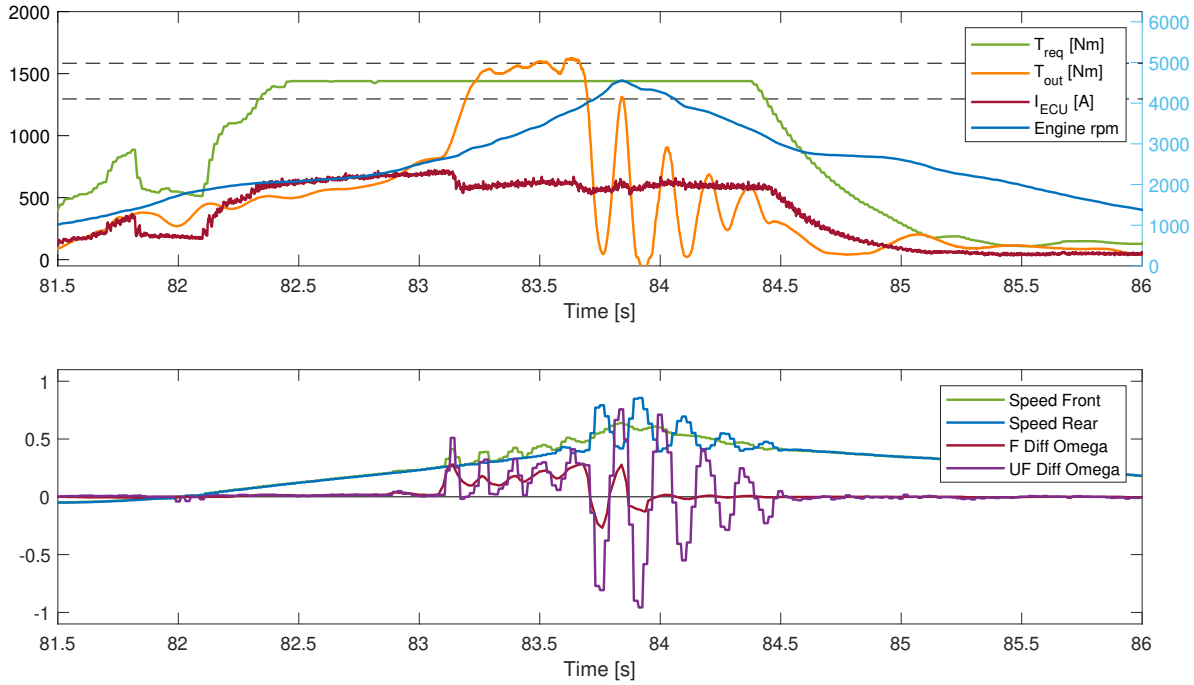

Figure 64: Test B - run 6.

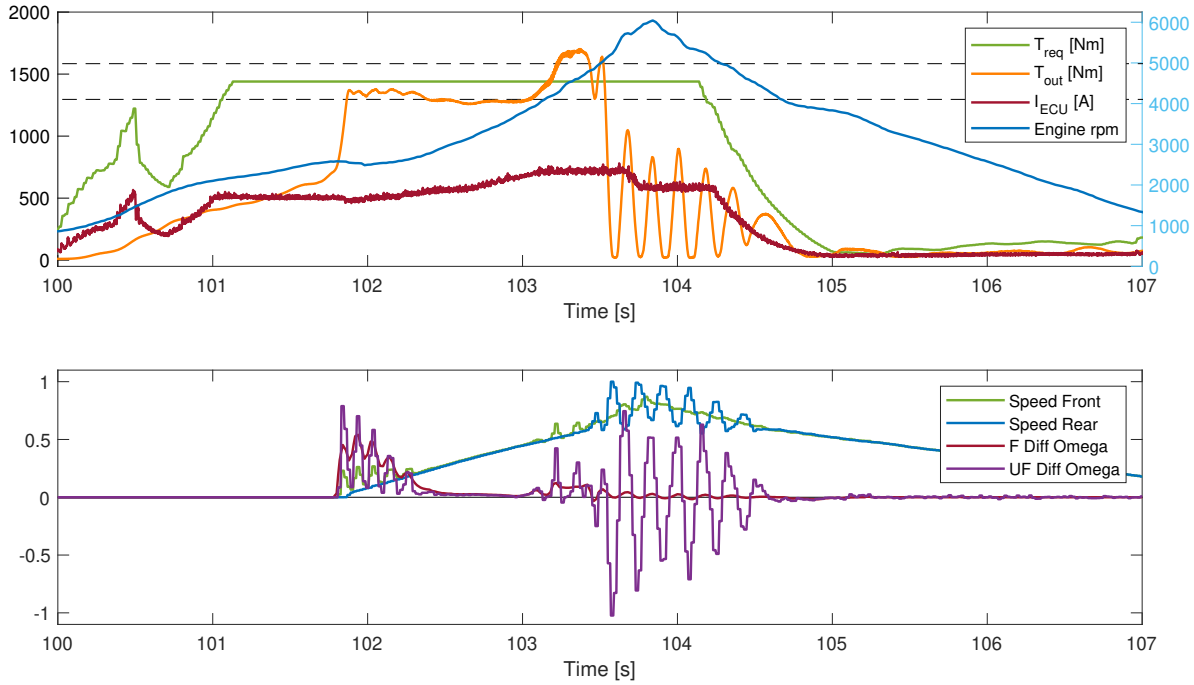

Figure 65: Test B - run 7.

8.2 Hysteresis

This section of the Appendix supplements Figure 37 in Section 5.1.

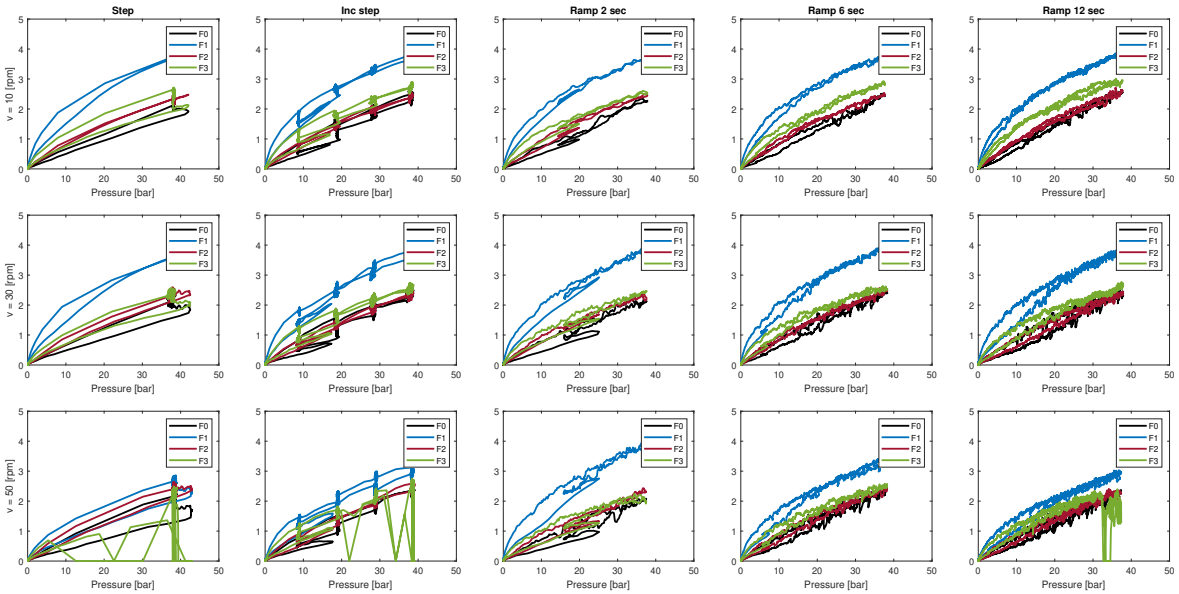

Figure 66: Hysteresis - Front.

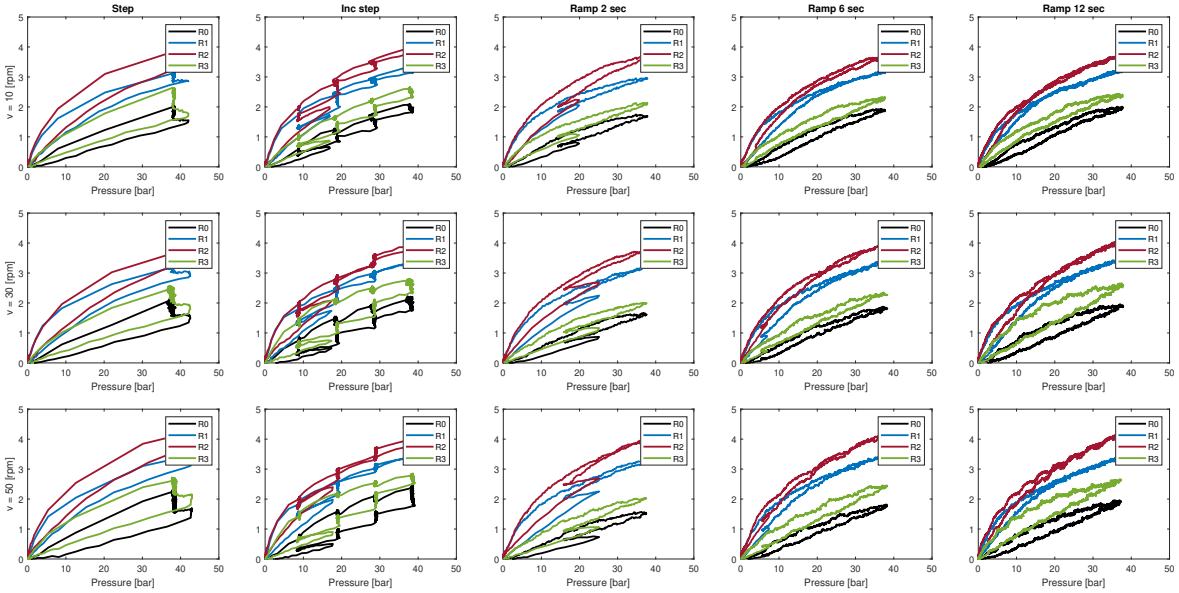

Figure 67: Hysteresis - Rear.

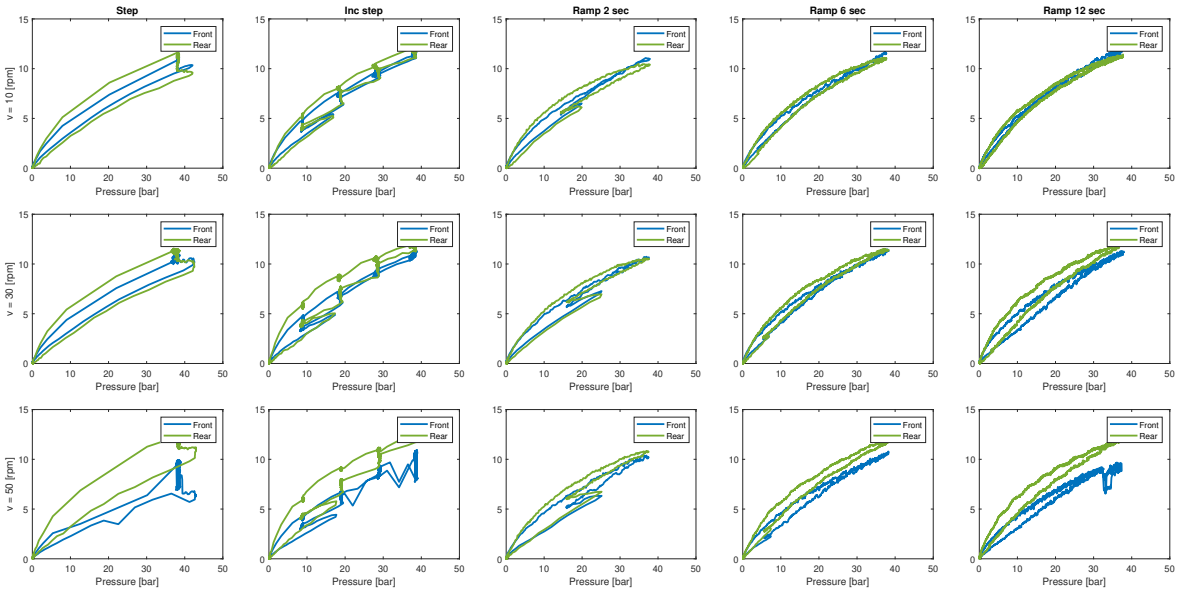

Figure 68: Hysteresis for Front vs Rear sensors.

8.3 Calibration

This section of the Appendix supplements Figures 41 and 42 in Section 5.4.

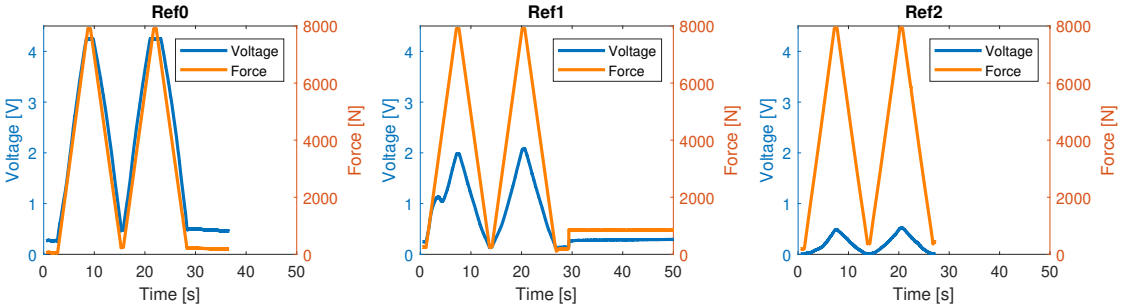

Figure 69: Reference sensor calibration.

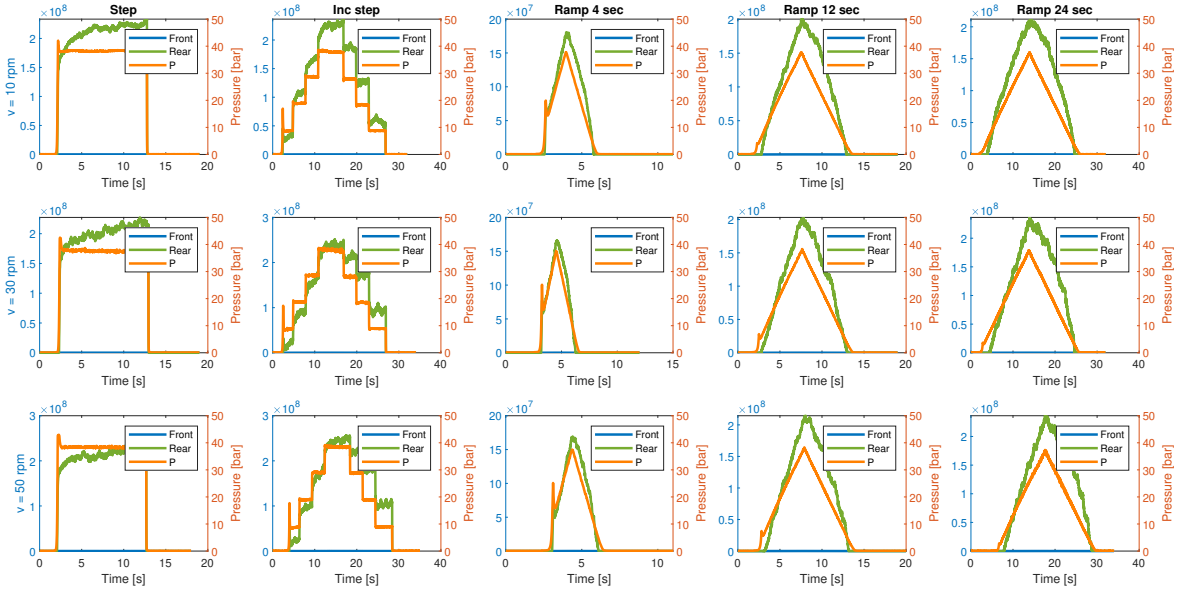

Figure 70: Front and rear forces based on calibration.

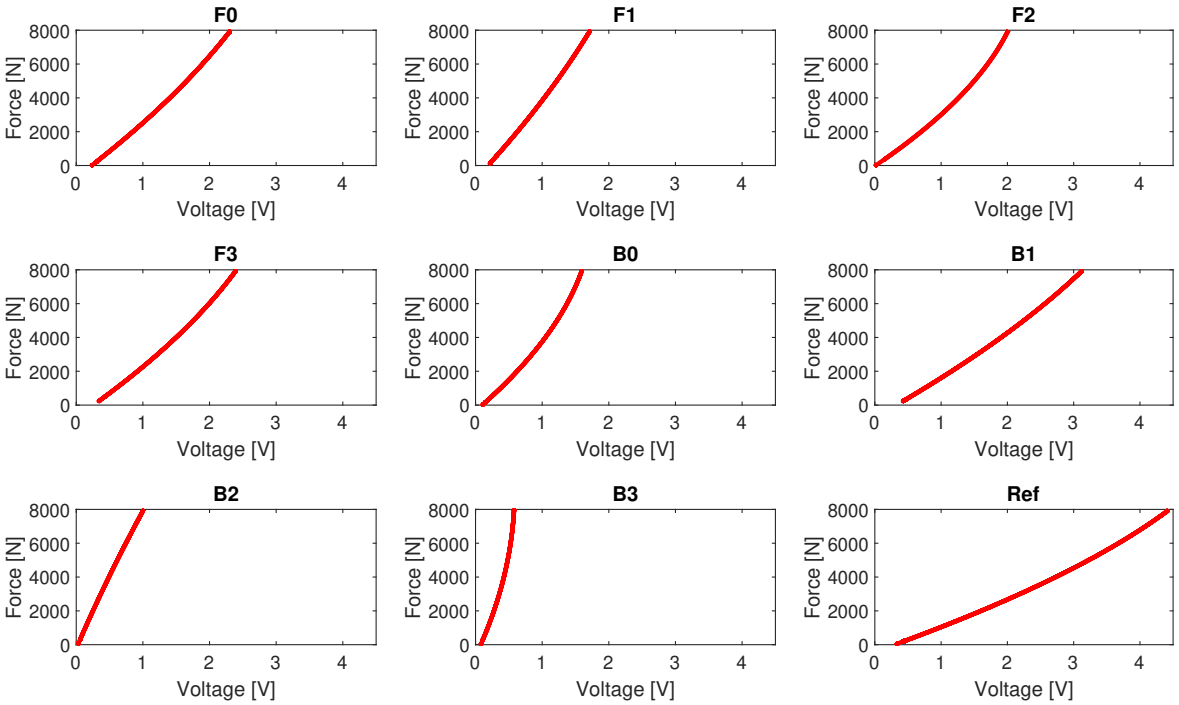

Figure 71: Calibration F vs V.

8.4 Force Estimation

This section of the Appendix supplements Figure 45 in Section 5.5.

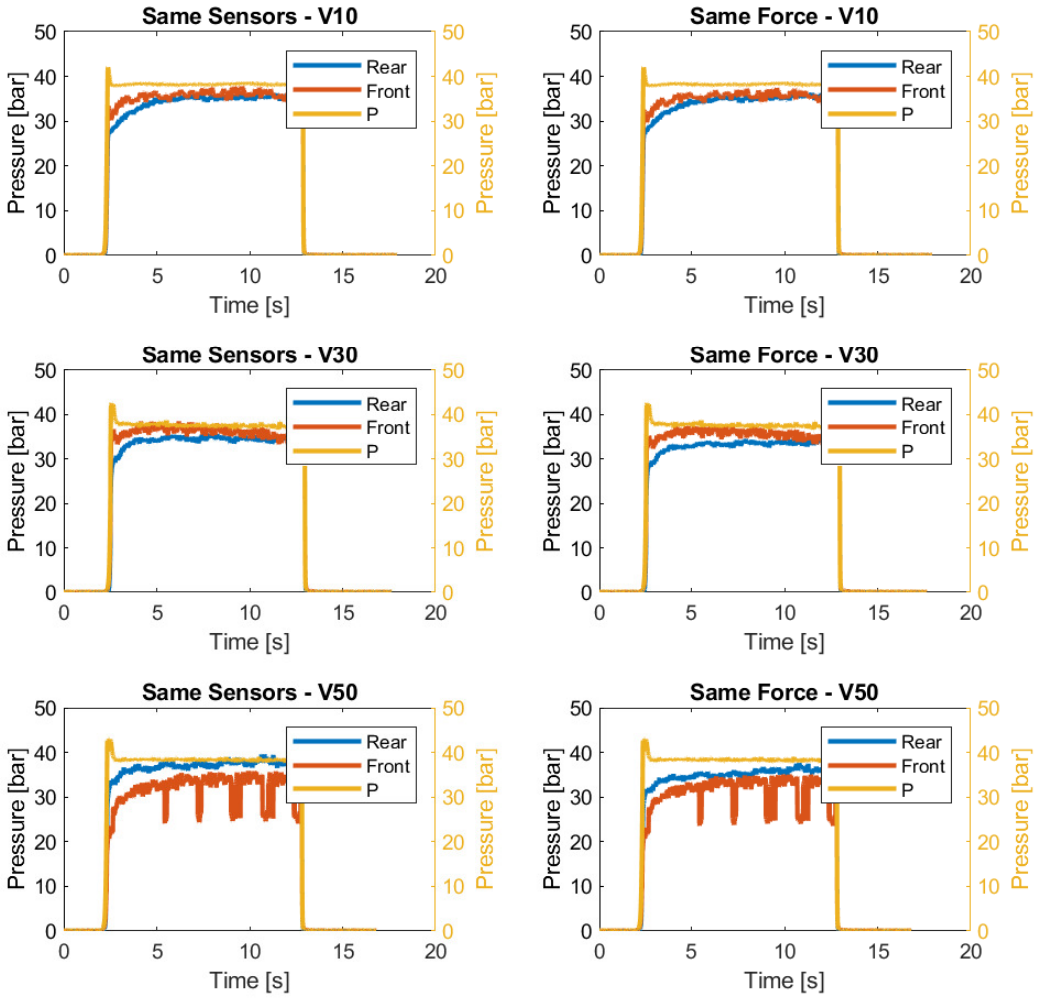

Figure 72: Estimated Pressures for Sequence 1.

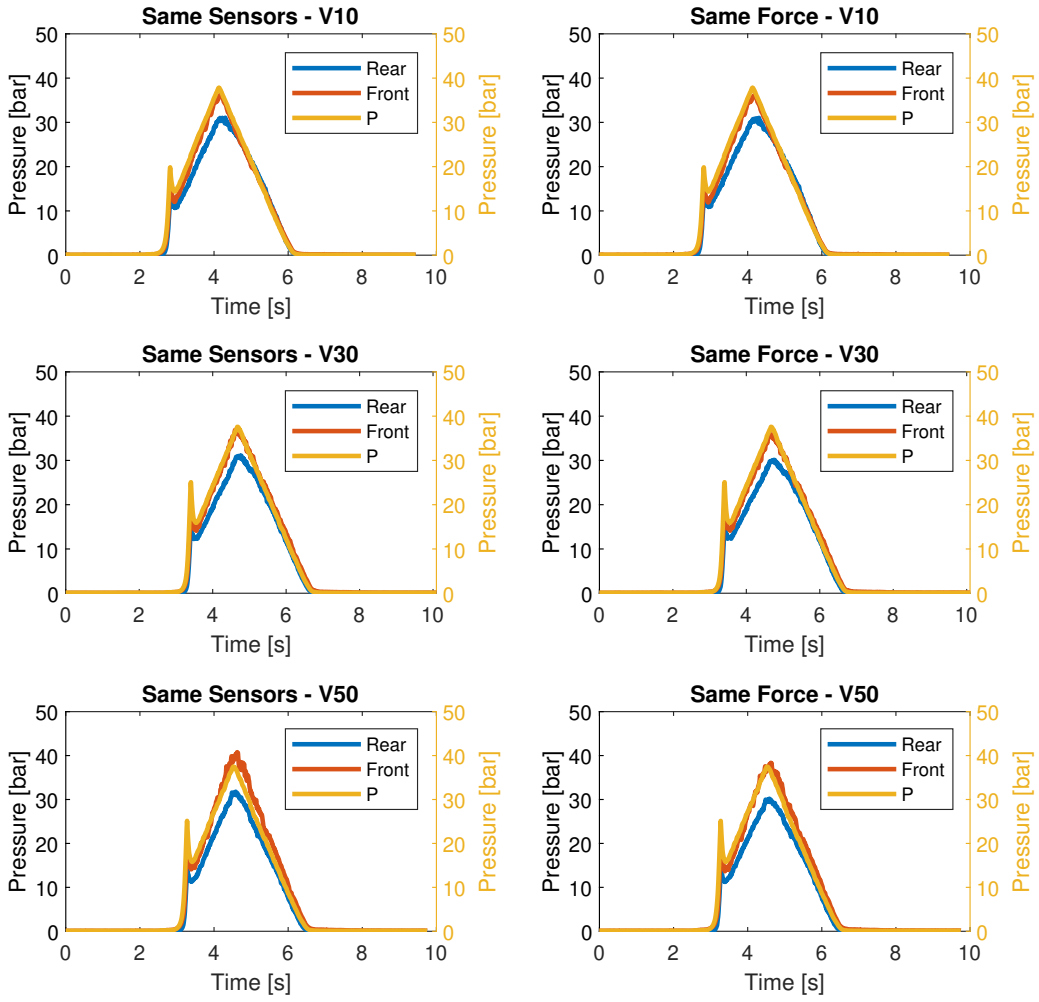

Figure 73: Estimated Pressures for Sequence 3.

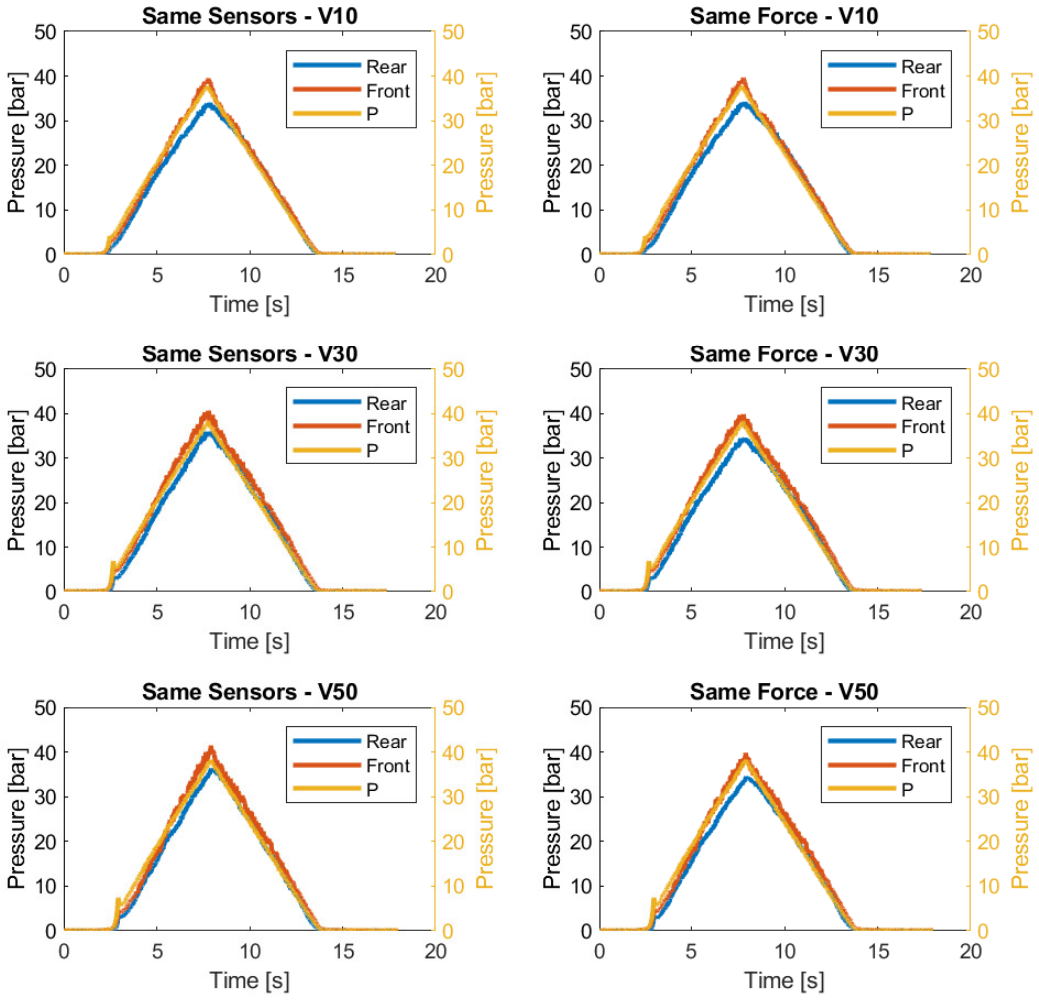

Figure 74: Estimated Pressures for Sequence 4.

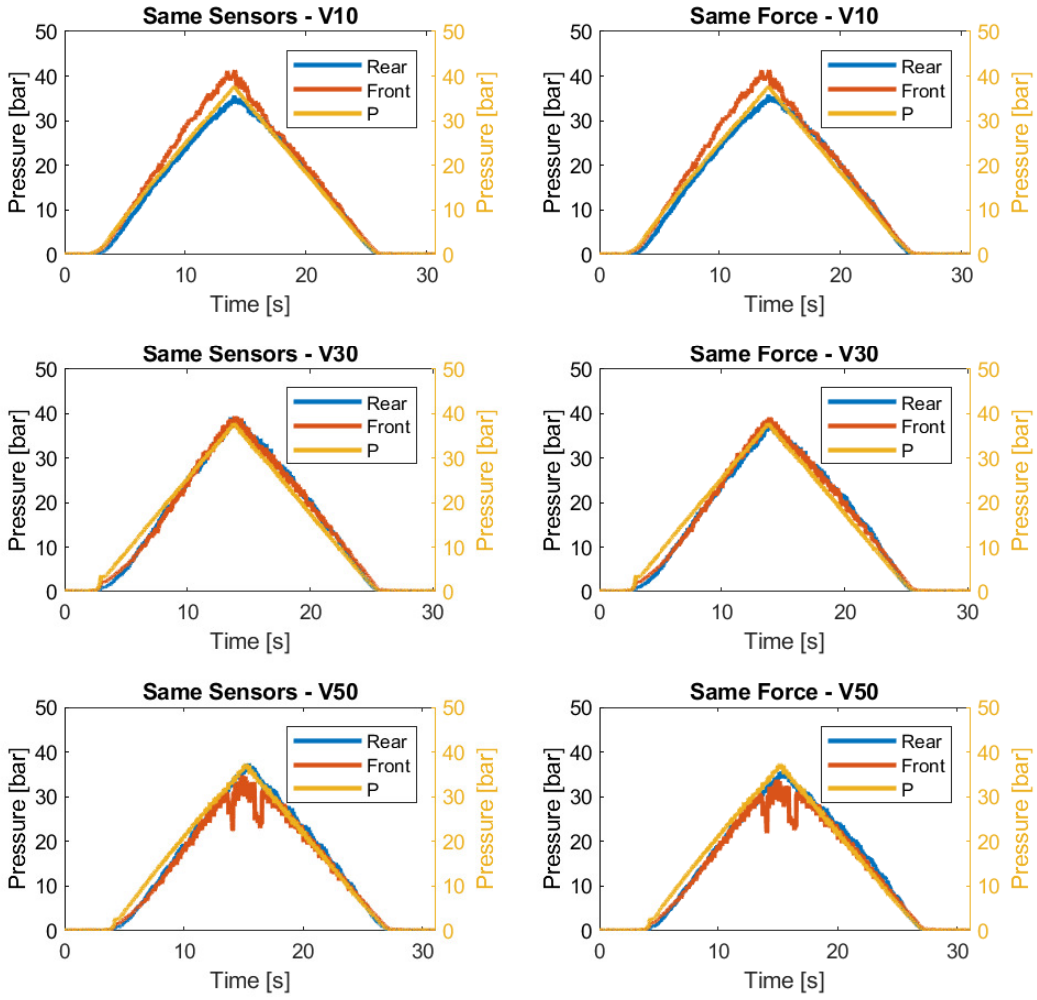

Figure 75: Estimated Pressures for Sequence 5.

8.5 Validation of Model

This section of the Appendix supplements Figure 54 in Section 6.5.

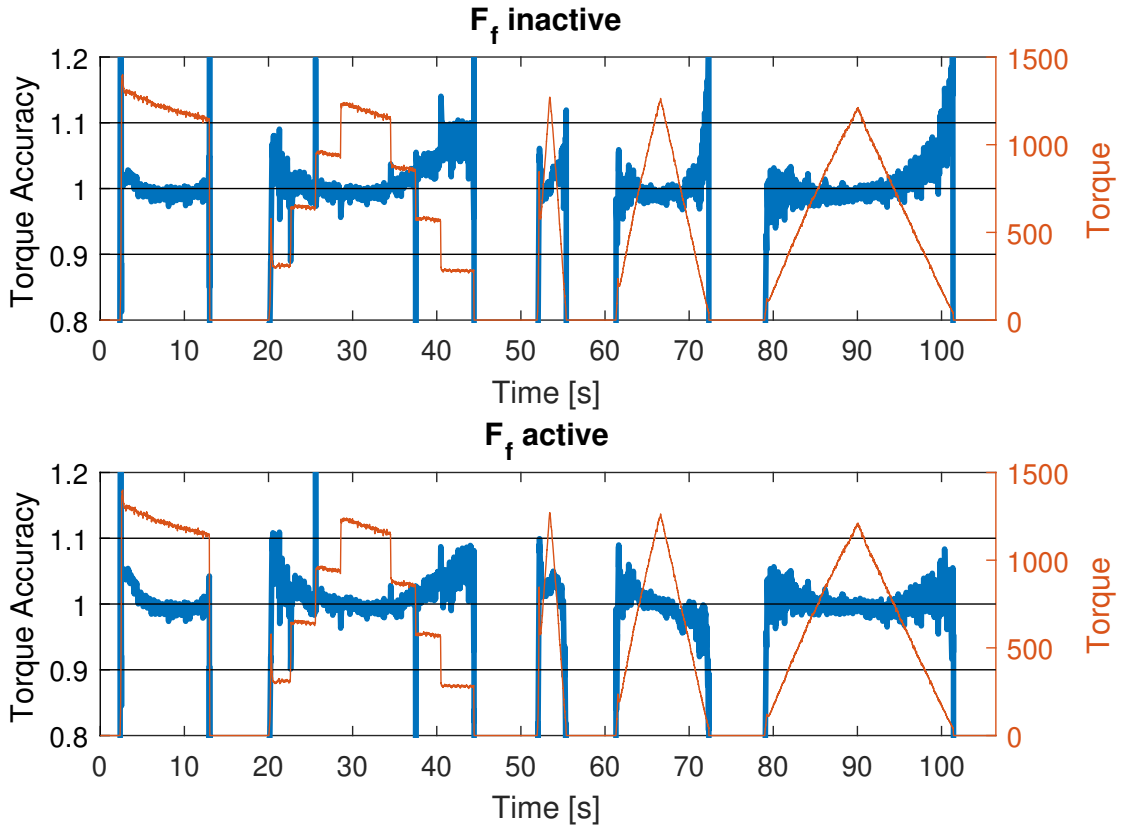

Figure 76: Torque Accuracy of model with and without friction losses activated for 30 rpm data.

References

[1] Rikard Mäki. *Wet Clutch Tribology.* Luleå University of Technology, 2005.

[2] R. Kikuuwe, N. Takesue, A. Sano, H. Mochiyama, and H. Fujimoto. Fixed-step friction simulation: from classical coulomb model to modern continuous models. pages 1009–1016, 2005.

[3] B. Cena et al. *Main steps in the Experimental Tuning Process of a 4WD Vehicle.* SAE Technical Papers, 1990.

[4] M. Hoeck and C. Gasch. *The Influence of Various 4WD Driveline Configurations on Handling and Traction of Low-Friction Surfaces.* SAE Technical Papers, 1999.

[5] G. Naito et al. *New Electornically Controlled Torque Split 4WD Systemfor Improving Cornering Performance.* SAE Technical Papers, 1990.

[6] S.K Mohan and B.V. Ramarao. *A comprehensive study of self-induced torque amplification in rotary viscous couplings.* Journal of Tribology, 2003.

[7] Pär Marklund. *Wet clutch tribological performance optimization methods.* Luleå University of Technology, 2008.

[8] B. Ganemi et al. *Durability and friction characteristics of a novel high performance four wheel drive automotive transmission fluid.* SAE Technical Papers, 2000.

[9] Pär Marklund et al. *Modeling and Simulation of thermal effects in wet clutches operating under boundary lubrication conditions.* Luleå University of Technology, Division of Machine Elements, 2008.

[10] Kristian Bengtsson. *Origin of stick-slip in a wet disc clutch.* Institution of Machine Elements, Faculty of Engineering, Lund University, 1995.

[11] S. Andersson, A. Söderberg, A. Sano, and S. Björklund. Friction models for sliding dry, boundary and mixed lubricated contacts. 2006.

[12] Rikard Mäki. *New demands driving new technology; A literature review of research into the behaviour and performance of wet clutches.* Luleå University of Technology, 2005.

[13] C.D Tipton and E.A Schifer. *Fundamental Studies on ATF Friction I.* SAE Technical Papers, 1997.

[14] Torkel Glad Lennart Ljung. *Modeling of Dynamic Systems.* Prentince Hall PTR, 1994.

[15] Isaac Newton. *Philosophiæ Naturalis Principia Mathematica.* Benjamin Motte, 1687.

[16] Georg Ohm. *Die galvanische Kette.* Bei T.H. Riemann, 1827.

[17] George E. P. Box. Science and statistics. *Journal of the American Statistical Association*, 71(356):791–799, 1976.

[18] Lennart Ljung. *System Identification - Theory for the User (2nd edition)*. Prentince Hall PTR, 2007.

[19] Sigurd Skogestad and Ian Postlethwaite. *Multivariable Feedback Control - Analysis and design*. John Wiley Sons, 2005.

[20] Tekscan. Flexiforce design integration guide, best practices in mechanical integration, best practices in electrical integration, . URL `https://www.tekscan.com/flexiforce-integration-guides`.

[21] Tekscan. Flexiforce ht201 datasheet, . URL `https://www.tekscan.com/products-solutions/force-sensors/ht201`.

[22] Mouser. Mcp6004 datasheet. URL `https://ww1.microchip.com/downloads/en/DeviceDoc/MCP6001-1R-1U-2-4-1-MHz-Low-Power-Op-Amp-DS20001733L.pdf`.

[23] Tore Hägglund. *Reglerteknik AK Föreläsningar*. Automatic Control Faculty of Engineering LTH, 2000.

[24] The MathWorks. System identification toolbox. URL `https://www.mathworks.com/help/ident/ug/how-to-estimate-transfer-function-mod-els-in-the-system-identification-app.html`.